

الجمهورية الجزائرية الديمقراطية الشعبية
People's Democratic Republic of Algeria
وزارة التعليم العالي و البحث العلمي
Ministry of Higher Education and Scientific Research

University Mohamed Khider of Biskra

Faculty of Sciences and Technology

Department: Mechanical Engineering

Ref :.....



جامعة محمد خيضر بسكرة

كلية العلوم و التكنولوجيا

قسم: الهندسة الميكانيكية

المرجع:.....

Thesis submitted for obtaining the degree of
Doctorate in: Mechanical Engineering
Specialty (Option): Energetic

**Study of sorption cooling systems adapted to hot climates: use of available
energy resources in the Saharan regions**

Presented by:

KHEIREDDINE Mohamed-Abdelbassit

Thesis defended publicly on: 14/02/2024

The jury members :

Adel BENCHABANE	Professor	Supervisor	University of Biskra
Noureddine BELGHAR	Professor	Examiner	University of Biskra
Toufik ARRIF	Professor	Examiner	URAER-CDER of Ghardaïa
Adnane LABED	Professor	President	University of Biskra

Université Mohamed Khider – Biskra

Faculté des Sciences et de la
technologie

Département : Génie Mécanique

Réf :



جامعة محمد خيضر بسكرة

كلية العلوم و التكنولوجيا

قسم: الهندسة الميكانيكية

المرجع:.....

Thèse présentée en vue de l'obtention

Du diplôme de

Doctorat en : Génie Mécanique

Spécialité (Option) : Energétique

**Étude des systèmes de refroidissement par sorption adaptés au climat chaud :
utilisation des ressources énergétiques disponibles dans les régions sahariennes**

Présentée par :

KHEIREDDINE Mohamed-Abdelbassit

Soutenue publiquement le : 14/02/2024

Devant le jury composé de :

Adel BENCHABANE	Professeur	Superviseur	Université de Biskra
Noureddine BELGHAR	Professeur	Examineur	Université de Biskra
Toufik ARRIF	Professeur	Examineur	URAER-CDER de Ghardaïa
Adnane LABED	Professeur	President	Université de Biskra

ACKNOWLEDGMENT

I must first of all thank **Allah** for having given me the health and strength to accomplish this work.

My sincere thanks go to my advisor, Prof. Dr. **Adel BENCHABANE** for his patience, noble guidance, and support in accomplishing this work. He has been encouraging me and giving valuable suggestions for the past five years. Thank you very much, Prof. Dr. **Adel BENCHABANE**.

I want to acknowledge the rest of my thesis committee members

for their discussions, comments and ideas. I am extremely grateful for your valuable contributions in my thesis.

I would like to express my special thanks to **Dr. Chawki MAHBOUB** and everyone in **Turkish team in Yildiz Technical University, Istanbul, Turkey** for their wonderful help to get and complete the scholarship February 2020, for one month. It was a valuable experience. I will never forget your great help.

Last but not least, I would like to thank and dedicate this research paper to my beloved parents, my whole family, my friends and my colleagues in university of Biskra.

ABSTRACT

In this work, we propose three configurations for the cooling tower, including one suggested as a technical solution to enhance the thermal performance of the solar sorption cooling system during scorching outdoor air temperatures. These configurations are based on a combination of the dry cooling tower (DCT) with one or more sorption systems, where these systems are defined as a spray water system (SWS), a direct evaporative cooler (DEC), and a ground heat exchanger (GHE). The combined system may incorporate more than one sorption system in the same configuration. A case study is presented concerning an adsorption device primarily driven by solar energy in the dry and hot climate of Biskra, Algeria. The developed methodology was validated, and a good agreement was found between numerical simulations and experimental results obtained from the literature. It was concluded that the coupling of the cooling tower with one or more sorption systems is an effective solution in hot and arid regions.

Keywords: Solar adsorption, cooling tower, spray water, direct evaporative cooler, ground heat exchanger.

RESUME

Dans ce travail, nous proposons trois configurations pour la tour de refroidissement, dont une suggérée comme solution technique pour améliorer les performances thermiques du système de refroidissement par sorption solaire lors de températures torrides de l'air extérieur. Ces configurations sont basées sur une combinaison de la tour de refroidissement sèche (DCT) avec un ou plusieurs systèmes de sorption, ces systèmes étant définis comme un système d'eau pulvérisée (SWS), un refroidisseur par évaporation directe (DEC) et un échangeur de chaleur géothermique (GHE). Le système combiné peut incorporer plus d'un système de sorption dans la même configuration. Une étude de cas est présentée concernant un dispositif d'adsorption principalement alimenté par l'énergie solaire dans le climat sec et chaud de Biskra, en Algérie. La méthodologie développée a été validée et un bon accord a été trouvé entre les simulations numériques et les résultats expérimentaux obtenus à partir de la littérature. Il a été conclu que le couplage de la tour de refroidissement avec un ou plusieurs systèmes de sorption constitue une solution efficace dans les régions chaudes et arides.

Mots clés : Adsorption solaire, tour de refroidissement, eau pulvérisée, refroidisseur à évaporation directe, échangeur de chaleur au sol.

ملخص :

في هذا العمل، نقترح ثلاثة تكوينات لبرج التبريد، بما في ذلك واحد مقترح كحل تقني لتعزيز الأداء الحراري لنظام التبريد بامتصاص الطاقة الشمسية أثناء درجات حرارة الهواء الخارجي الحارقة. تعتمد هذه التكوينات على مزيج من برج التبريد الجاف (DCT) مع واحد أو أكثر من أنظمة الامتصاص، حيث يتم تعريف هذه الأنظمة على أنها نظام رش الماء (SWS)، والمبرد التبخيري المباشر (DEC)، ومبادل حراري أرضي (GHE). قد يشتمل النظام المدمج على أكثر من نظام امتصاص واحد في نفس التكوين. تم تقديم دراسة حالة تتعلق بجهاز الامتزاز الذي يعمل بشكل أساسي بالطاقة الشمسية في المناخ الجاف والحار في بسكرة، الجزائر. تم التحقق من صحة المنهجية المطورة، وتم العثور على اتفاق جيد بين المحاكاة العددية والنتائج التجريبية التي تم الحصول عليها من الأدبيات. وقد تم التوصل إلى أن اقتران برج التبريد بواحد أو أكثر من أنظمة الامتصاص يعد حلاً فعالاً في المناطق الحارة والقاحلة.

الكلمات المفتاحية: الامتزاز الشمسي ، برج التبريد ، رذاذ الماء ، المبرد التبخيري المباشر ، مبادل حراري أرضي.

TABLE OF CONTENTS

I. CHAPTER I: SOLAR REFRIGERATION TECHNOLOGY	4
I.1 Introduction	4
I.2 Renewable energy	4
I.3 Energy of solar	4
I.4 Solar refrigeration technology	5
I.4.1 Solar photovoltaic cooling systems	5
I.4.2 Solar thermo-electrical cooling	6
I.4.3 Solar thermo-mechanical cooling	7
I.4.4 Solar cooling techniques using thermal energy	8
I.5 Sorption cooling systems	9
I.5.1 Desiccant Cooling Systems	11
I.5.1.1 Operating principle	12
I.5.2 Absorption process between liquid-gas.	14
I.5.2.1 Operating principle	14
I.5.3 The adsorption phenomena	15
I.5.3.1 Operating principle Closed cycles with physical adsorption	16
I.5.3.2 Physical adsorption	19
I.5.3.3 Chemical adsorption	19
I.6 Comparison adsorption versus absorption	20
I.7 Conclusion	21
II. CHAPTER II: THE TECHNIQUES USED TO SOLVE THE MALFUNCTIONING PROBLEMS OF A SOLAR ADSORPTION SYSTEM.	23
II.1 INTRODUCTION	23
II.2 Adsorption refrigerator « Intermittent cycle »	23
II.2.1 Adsorption chiller with single adsorber (Chiller)	24
II.2.2 Adsorption chiller with double adsorber (Chiller)	26
II.3 Construction principles	29

II.3.1	Coating of the adsorber heat exchangers with silica gel	29
II.3.2	Compact self-supporting construction	30
II.4	Effect of operating temperatures	30
II.5	The effect of high air temperature on the adsorption refrigeration system's operation	32
II.6	The technical solution proposed for the malfunctioning of a solar adsorption cooling system	33
II.7	Innovative solutions to improve adsorption machine function in Biskra city	36
II.8	Conclusion	43
III.	CHAPTER III: HYBRID COOLING TOWER COUPLED WITH A GEOTHERMAL HEAT EXCHANGER	44
III.1	Introduction	44
III.2	System Descriptions	45
III.2.1	Evaporative Cooling Tower	45
III.2.2	Horizontal Ground Water Heat Exchanger	47
III.3	Calculation Methodology	47
III.3.1	Governing equations of the ECT heat and mass transfer	48
III.3.1.1	Dry cooling mode	48
III.3.1.2	Wet counter-current mode	49
III.3.1.3	Wet co-current mode	51
III.3.2	Coefficient of heat transfer in the ECT	52
III.3.2.1	Smooth tube case	52
III.3.2.2	Finned tube case	53
III.3.3	Heat transfer modelling of the GWHE	53
III.3.4	Solving procedure	56
III.4	Verification and validation of the calculation methodology	58
III.4.1	Smooth tube case	58
III.4.2	Finned tube case	59
III.5	Results and discussion	60
III.5.1	Water temperature discussion	60
III.5.2	Thermal design of the GWHE	62
III.5.3	ECT-GWHE system operation	63
III.6	Conclusion	66

IV. CHAPTER IV: THERMAL ANALYSIS OF THE PERFORMANCE OF A HYBRID COOLING TOWER COUPLED WITH A GEOTHERMAL EXCHANGER	67
IV.1 Introduction	67
IV.2 System description	67
IV.2.1 Dry cooling tower (DCT)	68
IV.2.2 Direct evaporative cooler (DEC)	69
IV.2.3 Ground water heat exchanger (GWHE)	70
IV.3 Mathematical model	70
IV.4 Comparison and model validation	75
IV.5 Results and discussions	76
IV.5.1 Climatically conditions of this study	76
IV.5.2 GWHE thermal design	77
IV.6 Conclusion	82
V. CHAPTER V: NEW EVAPORATIVE HYBRID COOLING TOWER COUPLED WITH A GROUND HEAT EXCHANGER	84
V.1 Introduction	84
V.2 V.2. System Descriptions	85
V.2.1 Dry Cooling Tower (DCT)	86
V.2.2 The direct evaporative cooler (DEC)	87
V.3 Horizontal Ground Water Heat Exchanger (GWHE)	88
V.4 Calculation Methodology	89
V.4.1 Governing equations of the HCT heat and mass transfer	89
a) Finned tube heat exchanger zone	89
V.4.2 Pad zone	94
V.4.3 Heat transfer modulization of the WHE	95
V.4.4 Heat transfer modulization of the GWHE	96
V.4.5 Solving procedure	99
V.5 Comparison and validation model	100
V.5.1 DEC zone	100
V.5.2 SWS zone	102
V.6 Results and discussions	103
V.6.1 Climatically conditions of this study	103

V.6.2	GWHE thermal design	103
V.6.3	WHE thermal design	105
V.7	Conclusion	108

LIST OF FIGURES

Figure I-1 Schematic diagram of a standalone PV system [13].....	6
Figure I-2 Schematic of solar thermo-electrical cooling system [14].....	7
Figure I-3 Examining Thermo-Mechanical Cooling System Schematic Diagrams: A Comparison of Solar Rankine Cooling (a) and Solar Ejector Cooling (b) [16].	8
Figure I-4 The essential components of a solar thermal cooling system [13].	9
Figure I-5 Various thermochemical heat storage systems' mechanics [19].	10
Figure I-6 Sorption refrigeration plant [21].	10
Figure I-7 Principle of solid desiccant cooling [22].	11
Figure I-8 Schematic of solid desiccant cooling with SC [24].	13
Figure I-9 The evolution of air in the diagram of moist air [23].	14
Figure I-10 General schematic of absorption system [16].	15
Figure I-11 Diagram of a Solar-Powered Adsorption Cooling System [32].	18
Figure I-12 Basic adsorption cycle [32].....	19
Figure II-1 A diagram illustrating the adsorption cooling process utilizing CPC solar collectors [54]. ...	24
Figure II-2 Phases, heat fluxes, and a one-bed adsorption chiller setup. Adsorption and isosteric cooling (a), desorption and isosteric heating (b) [1].	24
Figure II-3 The different phases of adsorption chiller with single chiller.	25
Figure II-4 Adsorption chiller ACS 08 / ACS 15 [56].	27
Figure II-5 Crystallization process (left); alloy sponge suitable for Zeolite coating (right).....	27
Figure II-6 Working process of the adsorption chiller [56].....	29
Figure II-7 Photo of a silica gel coated tube and fin adsorbed heat exchanger [56].....	30
Figure II-8 Impact of Inlet Water Temperature on Cooling Capacity and Coefficient of Performance (COP) [52].	31
Figure II-9 Influence of the inlet temperature of cooling water on cooling capacity and performance coefficient [52].	32
Figure II-10 The ambient air temperature of Biskra city in 2020 [57].	33
Figure II-11 Scheme of the air condenser (or DCT) coupled to GAC composed by the air mixer and the EAHE [68].	37
Figure II-12 Scheme of humidified grid accessory for increasing the efficiency of air exchangers and condensers [67].	38
Figure II-13 Scheme of the ‘Adsorption chiller/geothermal air cooler’ coupling device with new elements ensuring the cooling of the adsorber [73].	40
Figure II-14 Scheme of: a) cooling tower with a ground/ (water or air) geothermal system and two direct water evaporation systems, b) cooling water basin.....	43
Figure III-1 Evaporative cooling tower (ECT) coupled with a ground-water heat exchanger (GWHE) called ECT-GWHE system: (A) in co-current and (B) in counter-current modes.....	45
Figure III-2 Fluids directions in the three operating modes of the ECT: (A) Dry mode, (B) Wet counter-current mode and (C) Wet co-current mode.	46
Figure III-3 The thermal balance of a horizontal geothermal heat exchanger (Ground/Water), GWHE..	55

Figure III-4 Flowchart diagram describing the solving procedure of the ECT-GWHE system.	57
Figure III-5 Effect of the temperature of the spray water on the process fluid temperature for different spray water temperatures, $\dot{m}_w = 0.187$ kg/s.	62
Figure III-6 Water temperature variation in the ground heat exchanger with different water inlet temperatures for a mass flow rate of $\dot{m}_w = 0.187$ kg/s.	63
Figure III-7 ECT-GWHE temperature variations in dry mode (A), without spray water circulation.	64
Figure III-8 ECT-GWHE temperature variations in counter-current mode (B), $\dot{m}_w = 0.187$ kg/s, $T_w=24$ °C.	65
Figure III-9 ECT-GWHE temperature variations in co-current mode (C), $\dot{m}_w = 0.187$ kg/s, $T_w=24$ °C.	65
Figure IV-1 Schematic description of the new DEC tower.	68
Figure IV-2 Schematic diagram of the evaporative cooling process.	74
Figure IV-3 Thermal equilibrium of the primary pipe of a GWHE.	75
Figure IV-4 The temperature and relative humidity variations of the hottest day in Biskra city in 2021.	77
Figure IV-5 Variation of water temperature along the geothermal heat exchanger with different mass flow rates.	78
Figure IV-6 a) The effect of hot air temperature on process fluid within the DCT.	79
Figure IV-7 Variation of ambient air temperature and humidity ratio for 24 hours (July 1 st 2021).	81
Figure IV-8 Evaporation water mass flow rate for 24 hours of the hot day (July 1 st 2021) in Biskra city.	82
Figure V-1 Schematic diagram of HCT-GWHE.	86
Figure V-2 Schematic diagram of evaporative cooling process.	95
Figure V-3 The thermal balance of a horizontal geothermal heat exchanger (Ground/Water), GWHE.	98
Figure V-4 flowchart of calculation program.	100
Figure V-5 The temperature and relative humidity variations of the hottest day in Biskra city in 2021.	103
Figure V-6 Variation of water temperature along the geothermal heat exchanger with different inlet water temperature, $\dot{m}_w=0.1$ kg/s.	105
Figure V-7 The effect of the DEC zone at ambient air temperature for 24 hours of a hot day in Biskra city, $T_w = 24$ °C.	106
Figure V-8 Depicts the ambient air temperature as it varies within the DEC and SWS.	107
Figure V-9 The comparison between wet and dry modes on a finned tube heat exchanger zone.	108

LIST OF TABLES

Table I-1 Comparison Between Various Solid Adsorbent Pairs.....	20
Table I-2 Comparisons of the COP and SCP values of different studies.....	21
Table II-1 The different working conditions of the adsorption cooling machine.	33
Table III-1 Geometric and thermophysical parameters of the finned tube heat exchanger of present ECT.	46
Table III-2 The geothermal characteristics of GWHE.....	47
Table III-3 Geometry and thermophysical characteristics of the heat exchanger used by Papaefthimiou et al. [86].	58
Table III-4 Comparison between calculation results of Papaefthimiou et al. [86] and present numerical results for process fluid T_f	58
Table III-5 Geometrical and thermos-physical parameters of the finned-tube heat	59
Table III-6 Comparison between predicted and experimental values of Wiksten and Assad [107] for wavy finned-tube heat exchanger temperatures.	60
Table III-7 The inlet flow temperatures of ECT.....	61
Table IV-1 Geometric and thermo-physical parameters of the FTHE of present DEC.	69
Table IV-2 Geometric characteristics of the DEC.	69
Table IV-3 Characteristics of the designed WGHE.	70
Table IV-4 Equations of thermal resistances in GWHE's system.	74
Table IV-5 Results and comparison.	75
Table V-1 Geometric and thermo-physical parameters of the finned tube heat exchanger of present HCT.	87
Table V-2 Geometric characteristics of the DEC.....	88
Table V-3 The geothermal characteristics of GWHE.	88
Table V-4 Comparisons between current results and experimental ones.....	101
Table V-5 Experimental and calculation results for SWS zone.	102
Table V-6 The different parameters of WHE.....	105

NOMENCLATURE

A	Total area of the heat exchange, m^2
C_f	Frictional factor
C_p	Specific heat capacity, $J/(kg \cdot K)$
C_d	Drag coefficient of a droplet
D	Diameter, m
C^{st}	Constant
h	Convective coefficient, $W/(m^2 \cdot K)$
l	Finned coil dimension, m
Le	Lewis number
L	Length, m
L_v	Latent heat, kJ
\dot{m}	Mass flow rate, kg/s
N	Number of rows
Nu	Nusselt number
Nu_{nc}	Squire-Eckert formulation
P	Pressure, Pa
Pd	Amplitude of waviness, m
Ph	Pitch dimension, m
Pr	Prandtl number
R	Thermal resistance, K/W
r	Radius, m
Re	Reynolds number
\mathcal{R}	Fouling resistances, m^2K/W
S	Surface per meter of length, m^2/m
S_{fin}	Fin spacing, m
T	Temperature, $^{\circ}C$
U	Overall coefficient of heat transfer, $W/m^2 \cdot K$
V	Velocity, m/s

w	Humidity, kg/kg dry of air
x	Distance, m
X_{fin}	Half wavy length, m
z	Direction

Greek symbols

ν	Kinematic viscosity, m ² /s
μ	Dynamic viscosity, Pa·s
ε	Convergence criterion
ρ	Density, kg/m ³
β	Coefficient of thermal expansion
η	Efficiency
λ	Thermal conductivity, W/m·K
Φ	Heat flux, W
ζ	Singular pressure loss coefficient, -
Λ	Linear pressure loss coefficient, -

Subscripts

a	Air
c	Water to air convection
d	Dynamic
in	Inlet
o	Outlet
e	External
g	Global
h	Hydraulic
i	Internal
$LMTD$	Logarithmic Mean Temperature Difference
f	Process fluid (water)
p	Pipe
s	Soil
t	Tube

<i>tot</i>	Total
<i>tr</i>	Transversal
<i>th</i>	Thermal
<i>v</i>	Vapor
<i>l</i>	Longitudinal
<i>w</i>	Water
<i>'</i>	Wavy

Abbreviations

DCT	Dry Cooling Tower
DEC	Direct Evaporative Cooler
ECT	Evaporative Cooling Tower
FTHE	Finned Tube Heat Exchanger
GAHE	Ground-Air Heat Exchanger
GWHE	Ground-Water Heat Exchanger
LMTD	Logarithmic Mean Temperature Difference
SWS	Spray Water System
WCT	Wet Cooling Tower
WHE	Water Heat Exchanger
WMFC	Water Mass Flow Control
GSHP	Ground-source heat pump
VGWHE	Vertical ground water heat exchanger
HGWHE	Horizontal ground water heat exchanger
EAHE	Earth-air heat exchanger
COP	Coefficient of performance
GSHP	Ground-source heat pump

GENERAL INTRODUCTION

Solar energy is generated by the sun's radiation, which can be captured and converted into electricity or thermal energy through the use of solar panels or solar collectors. The use of solar energy has numerous benefits, including reducing carbon emissions, mitigating climate change, and decreasing reliance on non-renewable energy sources.

Solar energy, a cost-effective alternative to traditional fossil fuels, is further enhanced by the integration of sorption technologies. While the initial investment in solar panels or collectors may seem high, the long-term savings are considerable, making it an economically viable choice. Governments often provide incentives and rebates to encourage the adoption of solar energy systems among homeowners and businesses. The versatility of solar energy extends beyond electricity generation; it can efficiently power homes and buildings while also serving in sorption applications. Solar energy is instrumental in heating water for both domestic use and industrial processes. Particularly in remote or off-grid areas, solar energy, coupled with sorption technologies, becomes a primary and sustainable source of electricity, overcoming limitations posed by the unavailability of traditional energy sources. This synergy aligns with the global shift towards clean and renewable energy solutions.

The primary aim of this thesis is to propose innovative technical solutions for adapting Adsorption Solar Refrigerating Machines (ASRM) to hot regions, where ambient air temperatures can exceed 45 °C, especially during summer. This requires finding effective ways to cool down the air entering the Cooling Tower (CT) to improve the performance of the ASRM. To achieve this goal, the thesis explores various approaches, including using shallow geothermal energy and cooling systems that employ direct or indirect water evaporation.

The thesis is organized into two main parts, consisting of five chapters, preceded by an introduction and followed by a conclusion. The first part focuses on the theoretical background of the ASRM and the cooling techniques used in hot regions. The second part proposes innovative solutions for adapting the ASRM to hot regions, including the use of renewable energy sources and novel cooling technologies. Overall, this thesis aims to contribute to the development of sustainable and efficient cooling systems for hot regions, which can mitigate the adverse impacts of climate change and improve the quality of life for people living in these areas.

The present thesis is divided into two main parts. The first part consists of two chapters that present a literature review of the research carried out on ad/absorption solar cooling technologies and their applicability in hot regions such as Biskra, Algeria.

Chapter I provides a comprehensive overview of the available techniques for sorption refrigeration systems. It compares different types of sorption refrigeration systems and reviews the relevant literature on the subject. The chapter highlights the advantages and disadvantages of each system and identifies the key factors that affect their performance.

Chapter II focuses on the operating principle of Adsorption Solar Refrigerating Machines (ASRM) and evaluates their applicability in hot regions. It presents a bibliographical study on the performance of ASRM in different climatic conditions, with a specific focus on Biskra, Algeria. The chapter reviews the relevant literature on the subject and highlights the challenges associated with using ASRM in hot regions.

The second part of the thesis consists of three chapters (3, 4, and 5) that propose innovative technological solutions for adapting refrigeration machines, including adsorption systems, to hot regions. The primary objective is to address the challenge of these systems malfunctioning when the ambient temperature exceeds the operating limits of the cooling heat exchangers, such as cooling towers.

Chapter III presents a parametric study of the use of shallow geothermal energy to cool the air entering the cooling tower. The chapter describes the main elements of the hybrid cooling tower and evaluates its performance in hot conditions. The latter was produced in the form of a book chapter and article entitled, respectively, "*Hybrid cooling tower for a solar adsorption cooling system: comparative study between dry and wet modes in hot working conditions*" and "*Thermal performance of evaporative cooling tower / ground-water heat exchanger system for hot and dry climates*".

Chapter IV proposes a novel approach to cooling the air using a direct evaporative cooling system and explains how to create a new coupling system that combines a direct evaporative cooler with a ground water heat exchanger. Both systems are integrated with solar adsorption cooling systems and are applicable in arid and semi-arid regions of Algeria, especially in the extreme temperatures of the summer season. A simplified mathematical model has been validated to

describe the heat and mass transfer between air and water in a direct evaporative cooler and between ground and water in a geothermal heat exchanger. The latter was produced in the form of an article entitled "*Adaptation of an Adsorption Cooling System for Hot and Dry Climates: Use of a Ground Water Heat Exchanger Coupled to a Direct Evaporative Cooling Tower*".

Chapter V studied and proposed a calculation methodology to design a hybrid cooling tower (HCT) coupled with a horizontal ground-water heat exchanger (GWHE). The HCT-GWHE system is proposed as a technical solution to enhance the thermal performance of the HCT by taking the case study of an adsorption device driven mainly by solar energy in the dry and hot climate of Biskra (Algeria). Four operation levels of the HCT-GWHE system are investigated, namely: GWHE, direct evaporative cooler DEC, spray water system (SWS), and finned tube heat exchanger. The latter was produced in the form of a patent entitled "*Dispositif d'amélioration de l'efficacité des échangeurs de chaleur à air avec nouveaux éléments couplant trois systèmes de refroidissement basés sur l'évaporation directe de l'eau et la géothermie*".

I. CHAPTER I: Solar refrigeration technology

I.1 Introduction

In recent years, the efficient utilization of renewable resources has become increasingly important due to their potential for stimulating economic growth and reducing atmospheric pollution. One key strategy for achieving this is the replacement of traditional energy sources, such as hydrocarbons, with renewable energy sources such as wind, solar, geothermal, biomass, and hydropower. These renewable energy sources are being used for cooling and heating purposes in a variety of settings, including domestic, commercial, and industrial. The present chapter is focused on the study of sorption cooling systems, which represent absorption and adsorption technologies that use renewable resources. Specifically, the research aims to investigate the adaptation of a solar adsorption air conditioner in the hot and arid climate region of Biskra, Algeria.

I.2 Renewable energy

Renewable energy is a type of energy that is derived from natural resources that are inexhaustible over time and have the ability to naturally renew themselves. This category of energy includes sources such as wind, solar, geothermal, biomass, and hydraulic energy [1, 2]. Numerous developed nations have implemented a range of renewable energy technologies. In recent times, wind energy has gained increasing popularity [3]. For instance, wind turbines are being used to generate power in the Netherlands, China, USA, Germany, Malaysia, Spain, and India [4, 5]. In Iceland, seventy percent (70%) of their manufacturers use geothermal energy for industrial reasons, while in northwest Iran, geothermal energy is produced using mineral elements [6]. Solar energy has gained considerable attention from scientists in recent years, as there has been a surge in demand for its utilization in a range of applications, including heating of water, building heating and cooling, cooking, power generation, and refrigeration [7].

I.3 Energy of solar

Solar energy is a renewable and abundant source of clean energy that is captured from the sun through photovoltaic cells, which convert sunlight into electricity. Solar power is widely

available, affordable, and environmentally friendly, making it a sustainable solution to the world's energy needs. The use of solar energy has increased in recent years due to technological advancements and a growing awareness of the need to reduce greenhouse gas emissions. Solar panels can be installed on residential and commercial buildings, as well as in large-scale solar power plants, to generate electricity for daily use. By harnessing the power of the sun, we can create a cleaner, healthier, and more sustainable future for generations to come [8].

In both commercial and residential buildings, the demand for AC increases during the summer months. This is especially true in developing countries where there is inadequate electricity and storage to support high-energy consumption systems such as refrigeration and cooling. One way to tackle this problem is by utilizing solar cooling techniques to mitigate the environmental impact and the problems consumption of energy associated with conventional refrigeration and AC systems [9].

I.4 Solar refrigeration technology

Solar energy plays a critical role in solar refrigeration systems for cooling purposes. The use of solar energy for cooling and refrigeration applications is not only cost-effective but also pollution-free worldwide. The implementation of solar-powered cooling systems can help Mediterranean countries reduce their energy costs by up to 50% [10].

Additionally, certain sub-Saharan nations with substantial solar potential can employ solar refrigeration to maintain medicines and vaccines at lower temperatures, and these systems can be designed to be portable if required, as they rely on solar energy as their power source [11, 12].

I.4.1 Solar photovoltaic cooling systems

Figure I.1 portrays the four essential components of a solar electric system: PV modules, inverters, batteries, and vapor compression cooling systems. PV cells convert solar energy into DC electrical energy, which is stored in batteries when there is sunlight and released when there is none. The charge regulator is responsible for preventing the battery from being overcharged. The inverter generates AC electrical power that powers the vapor compression AC unit, a conventional cooling or refrigeration system. The inverter transforms DC electrical power into AC and powers AC loads with electrical energy [13].

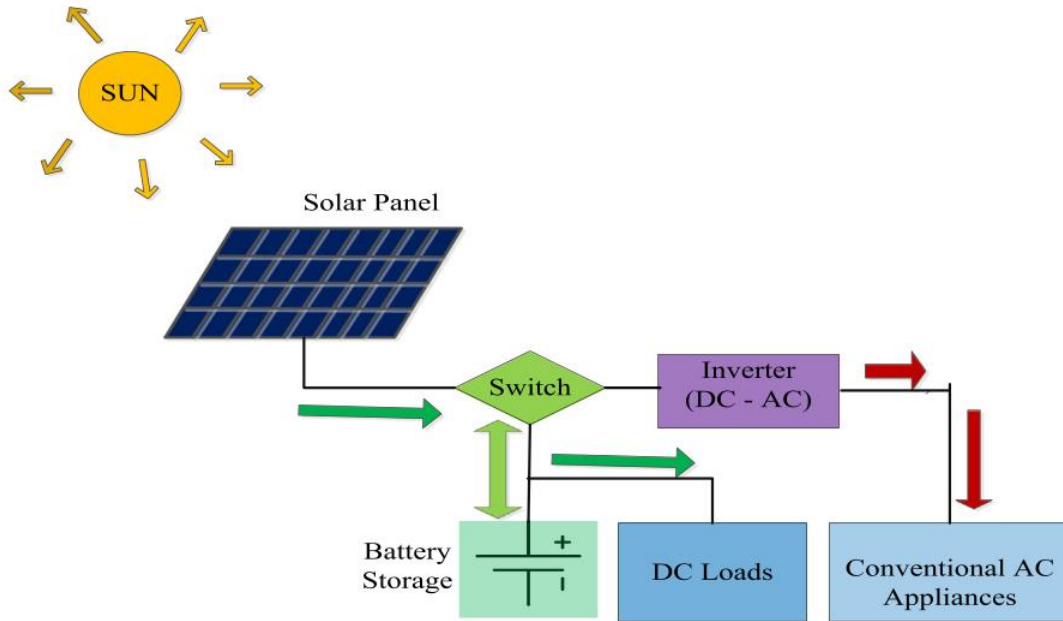


Figure I-1 Schematic diagram of a standalone PV system [13].

I.4.2 Solar thermo-electrical cooling

Peltier cooling systems can run on the power that solar PV devices produce in solar electric cooling. By exploiting the thermoelectric effect, which allows the conversion of heat into electricity and vice versa, it is possible to create a temperature gradient that results in cooling at one end and heating at the other. Peltier cooling devices are compact and reliable, but their efficiency is currently lower than that of vapor compression systems [14].

A thermoelectric refrigerator, illustrated in Figure I-2, features a generator comprising a limited number of thermocouples, which generate low thermoelectric power but are capable of producing a high current. This design provides the benefit of operating with a low-level heat source, making it suitable for converting solar energy into electricity. Furthermore, the combination of both components is compatible with using semiconductor-based thermoelectric materials such as Bi₂Te₃ [15].

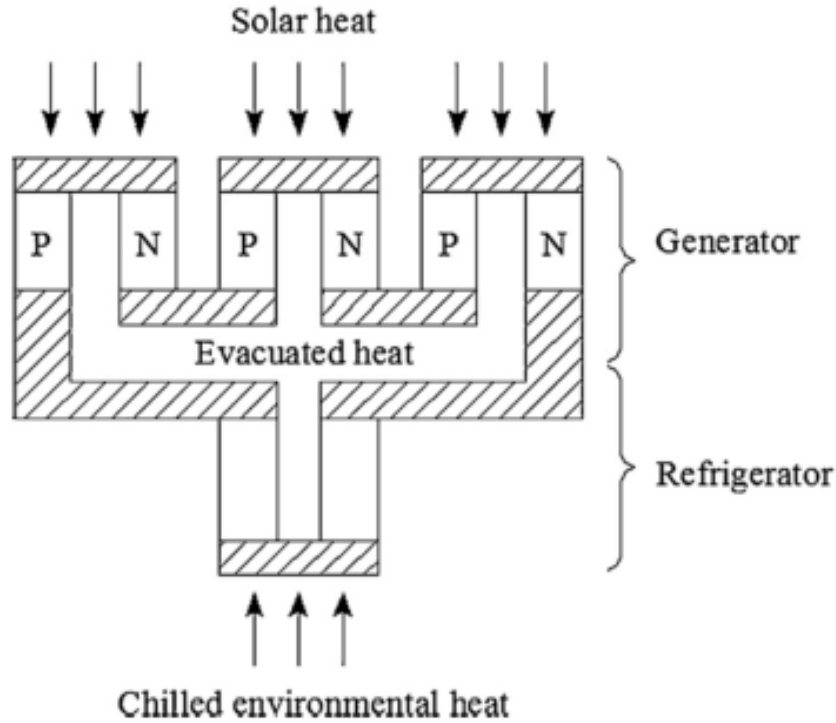


Figure I-2 Schematic of solar thermo-electrical cooling system [14].

I.4.3 Solar thermo-mechanical cooling

Solar thermal-mechanical cooling systems are gaining renewed attention for their versatile applications and potential to be utilized in a wide range of industries. These systems can be used for cooling purposes by utilizing suitable working fluids, and they can also generate electricity by connecting the main engine to an electric generator when cooling is not required. They are highly efficient and exhibit high performance in off-design conditions, allowing them to effectively use a wide temperature range of solar collectors. The thermo-mechanical solar cooling system operates in two steps: thermal energy is first converted into mechanical energy, which is then used to deliver the cooling effect. One example of such a system is the steam ejector system, which is linked to a parabolic solar collector. The steam generated by the collector flows through the ejector, causing the evaporator pressure to drop, resulting in heat absorption from the cold water and water vaporization in the evaporator. This system can operate at low pressure and low temperature for air-conditioning applications, and it can utilize low-temperature solar heat by lowering the operating pressure below atmospheric pressure. Overall, solar thermal-mechanical cooling

systems are a promising technology that can be used in various industries to reduce energy consumption, decrease carbon emissions, and promote sustainable development [16].

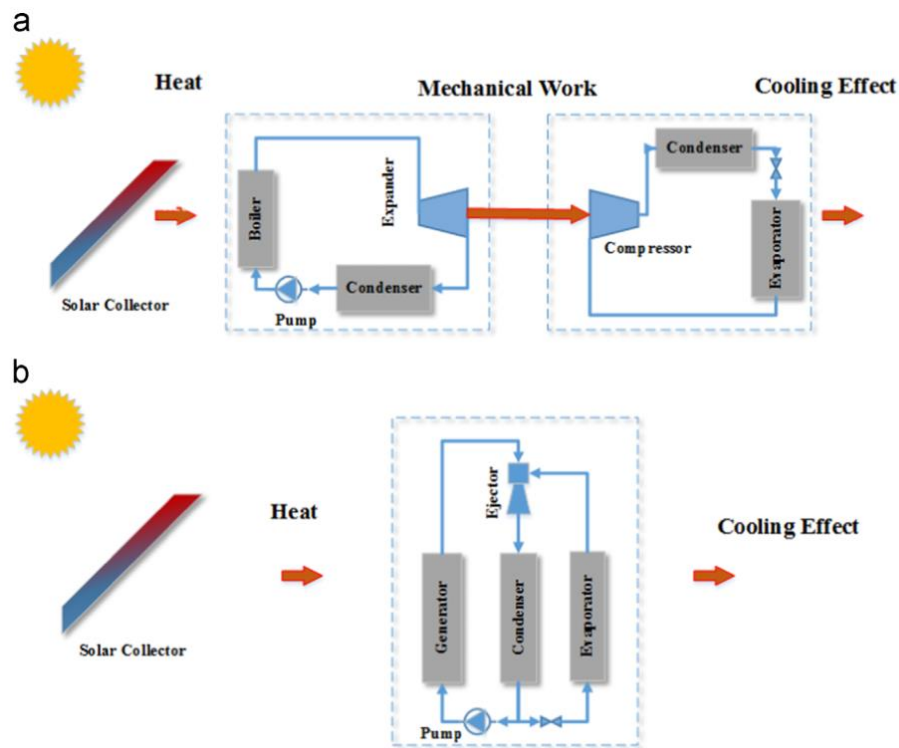


Figure I-3 Examining Thermo-Mechanical Cooling System Schematic Diagrams: A Comparison of Solar Rankine Cooling (a) and Solar Ejector Cooling (b) [16].

I.4.4 Solar cooling techniques using thermal energy

Solar thermal cooling systems are becoming increasingly popular due to their direct conversion of sunlight into heat and their potential to reduce energy consumption. These systems can absorb more than 95% of incident solar energy and consist of a solar collection array, a thermal storage tank, a thermal air conditioner, and a heat exchanger. Sorption technology is used to achieve the cooling effect through chemical or physical changes between the sorbent and the refrigerant. There are two main types of sorption technology: open and closed sorption systems, with closed sorption technology including absorption and adsorption refrigeration. As technology advances, solar thermal cooling systems can become more efficient, cost-effective, and accessible, contributing to a cleaner and more sustainable future [13].

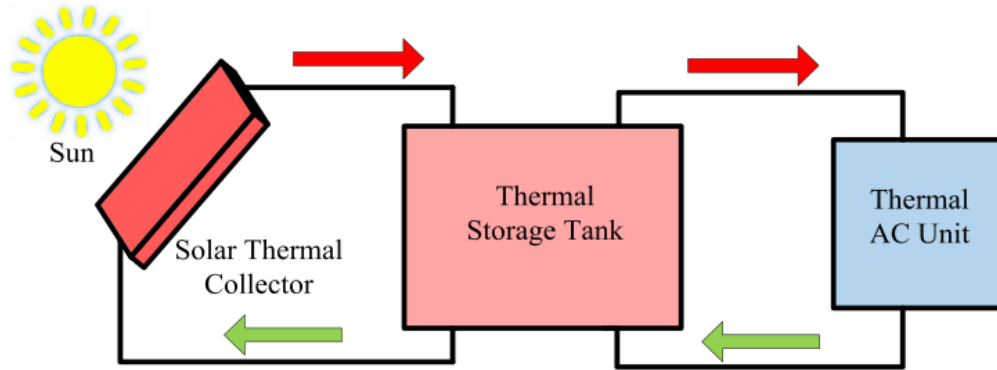


Figure I-4 The essential components of a solar thermal cooling system [13].

I.5 Sorption cooling systems

Thermal cooling techniques utilize sorption technology, which can be categorized as either open sorption systems or closed sorption systems. Desiccant cycles are an example of open sorption system [17].

Technologies based on absorption and adsorption are examples of closed systems:

- Absorption process between liquid-gas.
- Adsorption process between solid-gas.

The absorption phenomenon refers to the mixing of a gas with a liquid where the two fluids have a strong affinity for each other. This results in the transfer of material from one phase to the next, with the second phase allowing the material to interpenetrate and form a solution [14, 18, 19].

The basic process of any adsorption cycle involves the separation of a substance from one phase, which is then accumulated or concentrated on the surface of another phase. The attachment of fluid particles to the surface of a solid, known as adsorption, can occur through Van der Waals or electrostatic forces or through covalent bonding. Physisorption, which utilizes Van der Waals forces, is commonly used in commercial adsorption cooling cycles. During the adsorption process, the temperature of the solid adsorbent increases while the temperature of the liquid adsorbate decreases, making the process exothermic. An ideal adsorption process includes four stages: isosteric heating, desorption and condensation, isosteric cooling, and adsorption and evaporation [20].

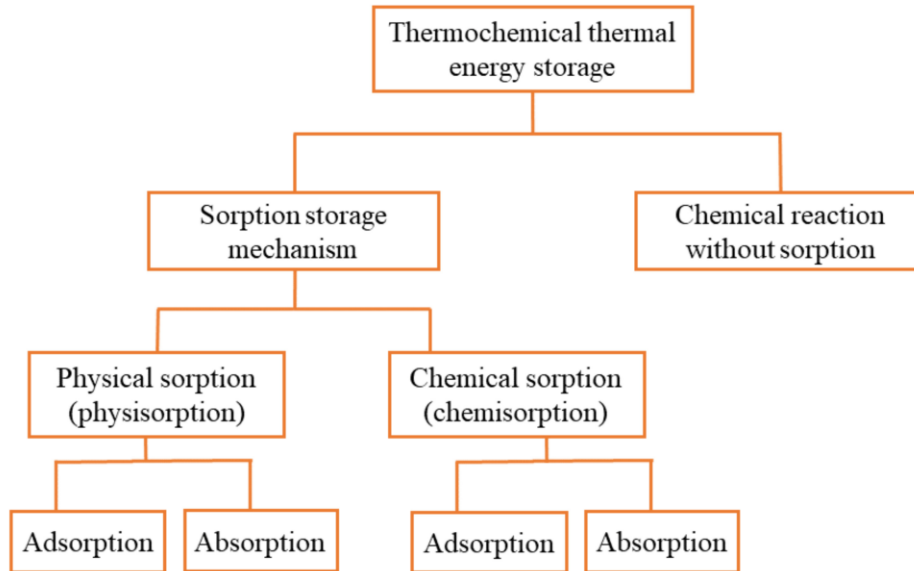


Figure I-5 Various thermochemical heat storage systems' mechanics [19].

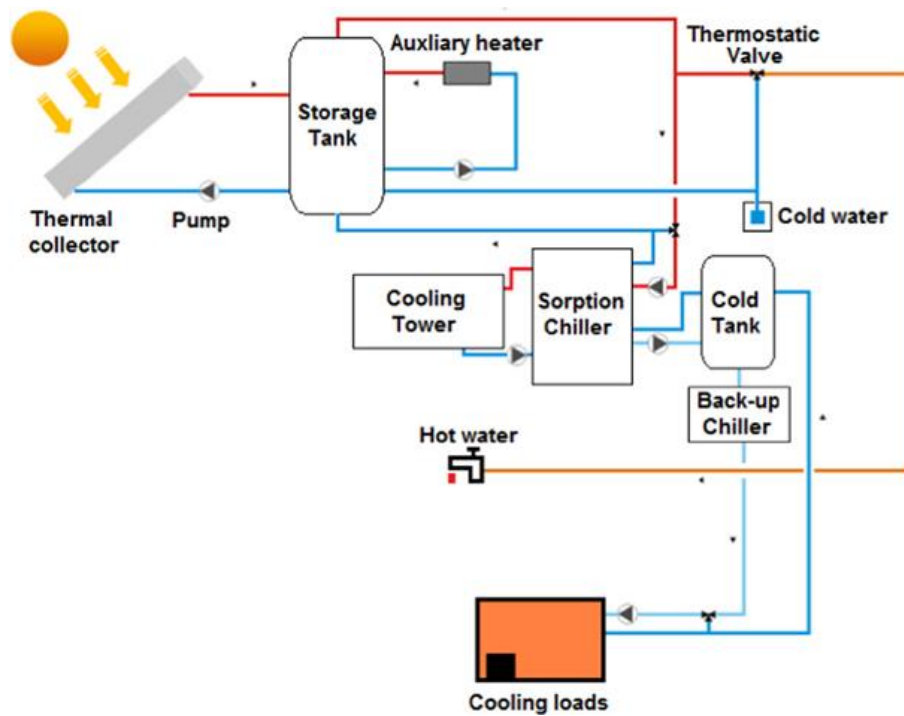


Figure I-6 Sorption refrigeration plant [21].

I.5.1 Desiccant Cooling Systems

In a solid desiccant cooling system, the desiccant wheel is the heart of the system, which is made up of a large number of thin corrugated sheets impregnated with the desiccant material. The desiccant wheel rotates slowly between two air ducts, one is used to dehumidify the process air, and the other is used to regenerate the desiccant wheel. During the dehumidification process, the air is dried by passing through the desiccant wheel, which adsorbs the moisture from the air. The dried process air is then passed through the sensible heat exchanger and cooling coil to reach the desired temperature and humidity level. The desiccant wheel's regeneration process involves heating the desiccant material to a high temperature, which drives out the moisture from the desiccant and releases it into the atmosphere. The regeneration heat source can be either an electrical heater or a solar/waste heat collector.

In addition to the rotary desiccant cooling system, there are also fixed-bed and fluidized-bed desiccant cooling systems. In the fixed-bed system, the desiccant is stationary, and the process air is passed through it, while in the fluidized-bed system, the desiccant is fluidized with air, and the adsorption and regeneration take place in a continuous process. The choice of desiccant cooling system depends on various factors, such as the required cooling capacity, the climatic conditions, the availability of energy sources, and the capital and operating costs [22].

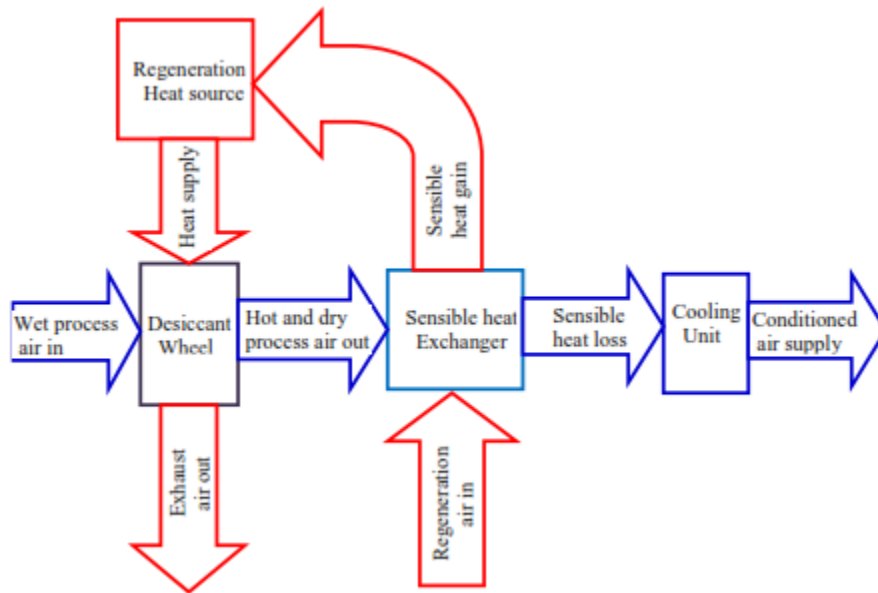


Figure I-7 Principle of solid desiccant cooling [22].

I.5.1.1 Operating principle

Desiccation exploits a double exchange of cold and humidity between the air flows entering (process air) and leaving (regeneration air) a building. This air circulation is generally ensured by an air handling unit (figure I-8). Figure I-9 air evolution processes are depicted in the diagram of moist air where [22-24] :

Phase 1-2: Outside air or forced air (also called process air) is drawn in through a filter, then passed through the "desiccant wheel" or "desiccation wheel". This rotary exchanger contains a solid sorption product. The latter absorbs water vapor from the outside air by adsorption. The outside air is thus dehumidified and in return sees its temperature increase.

Phase 2-3: The outdoor air is then cooled by heat exchange with the indoor exhaust air or the exhaust air. This exchange takes place through a rotating heat exchanger (non-hygroscopic).

Phase 6-7: To increase the heat exchange and therefore the cooling of the forced air, the extracted air is first cooled by humidifying it until saturation. This reduces the temperature as much as possible and increases the cooling capacity of the exchanger.

Phase 7-8: By passing through the heat exchanger, the extracted air is therefore heated.

Phase 8-9: In order to operate continuously, the desiccant wheel must be regenerated, i.e. it must dehumidify the adsorbent material. To do this, the portion of the wheel containing the humidity must cross the flow of extracted air which will have been previously heated to reach a temperature sufficient to vaporize the water molecules retained in the pores of the wheel.

Phase 9-10: Hot air circulates through the desiccant wheel, recharging it and allowing it to continue dehumidifying indefinitely. Finally, using a fan, the exhaust air is heated and humidified to a greater level than the outside air.

Phase 3-5: The forced air can still be sprinkled with water through a humidifier. The water will absorb the remaining calories in the air before it is propelled into the building to be cooled by a

CHAPTER I: Solar refrigeration technology

fan. This alternative makes it possible to cool the forced air but not to dehumidify. To do this, it is then necessary to replace this humidifier with a cold battery.

Phase 4-5: This system is said to be reversible because it can also be used for cooling and heating. In winter, this corresponds to a normal operating mode of heating by a centralized air system, using the sorption wheel as a heat recuperates, while supplementing the contributions of solar heat. The presence of a heating coil thus allows the regulation of the heating temperature in winter [24].

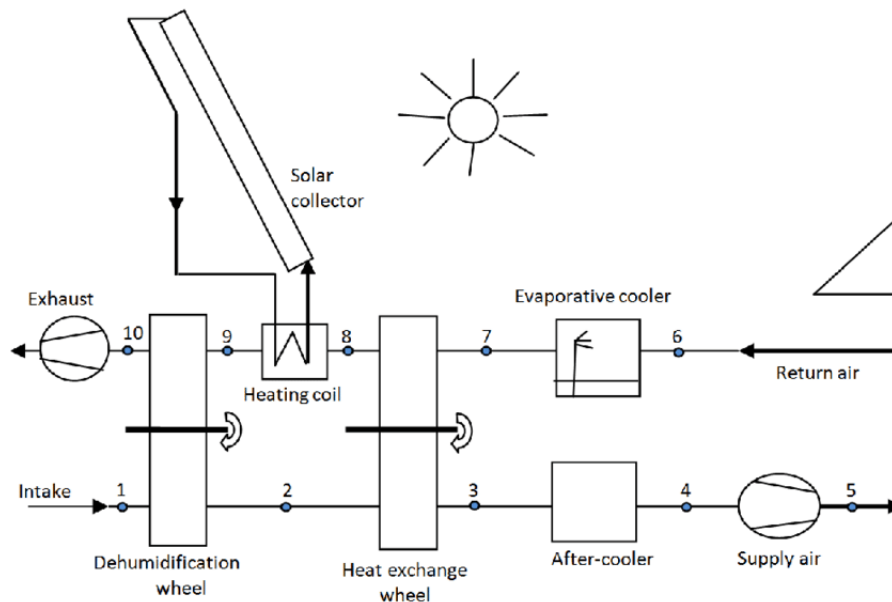


Figure I-8 Schematic of solid desiccant cooling with SC [24].

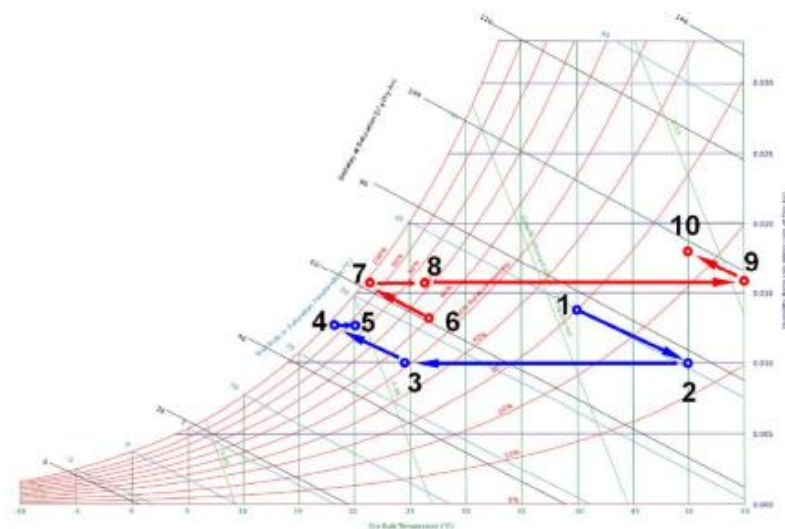


Figure I-9 The evolution of air in the diagram of moist air [23].

I.5.2 Absorption process between liquid-gas.

Adsorption is a surface phenomenon that involves overcoming the attractive forces between the adsorbate and the adsorbent, which requires a significant amount of activation energy. Absorption, on the other hand, involves the diffusion of the absorbate into the bulk of the absorbent, which typically requires less activation energy than adsorption [25, 26]. The water/lithium-bromide absorption refrigeration system is still used today in large-scale industrial and commercial applications, particularly in areas with limited electrical power supplies. In this system, water is the refrigerant, and lithium bromide is the absorbent. The process involves the absorption of water vapor by the lithium bromide, which is then separated by heat and pressure to release the water vapor as a refrigerant. The remaining lithium bromide solution is then recycled back to the absorber to continue the cycle. This process requires a source of heat, such as steam or hot water, to drive the absorption and separation of the two fluids. Absorption refrigeration systems have been used in a variety of applications, including air conditioning, refrigeration, and industrial process cooling [27]. Compared to other thermally operated technologies, absorption systems have a higher COP (coefficient of performance), making them their main advantage.

I.5.2.1 Operating principle

The absorption refrigeration system comprises four key components, namely the generator, pump, absorber, and evaporator. Together, these components facilitate the compression of the refrigerant vapor. The refrigerant vapor is drawn into the evaporator where it gains additional thermal energy, separating it from the solution. The refrigerant is then condensed in the condenser before being expanded by the evaporator to achieve cooling [28, 29]. A schematic of a basic closed cycle of absorption refrigeration is shown in Figure I.10.

Solar thermal absorption refrigeration technology involves using a chiller to absorb heat from a tank connected to a solar collector. There are three categories of absorption systems based on their solution regeneration and thermal operation cycles: single-effect, half-effect, and double-effect solar absorption cycles. Compared to a double-effect chiller, single-effect and half-effect chillers require lower temperatures [30]. The use of DAR (diffusion absorption refrigeration) and

hybrid systems can provide even better performance compared to traditional absorption refrigeration systems.

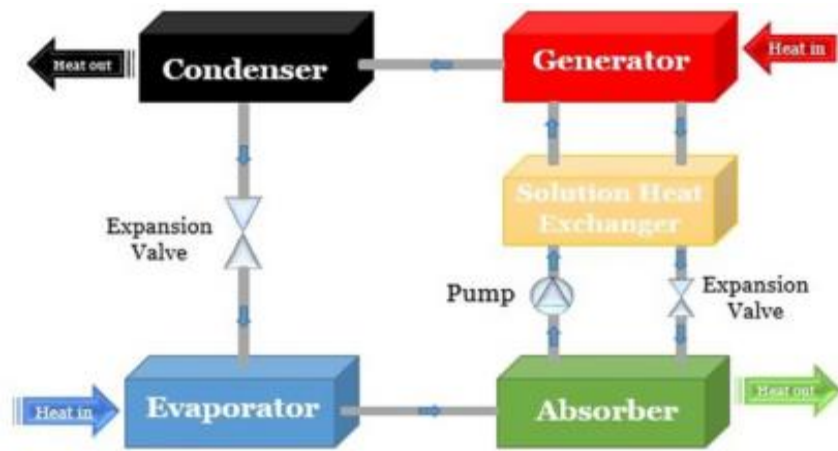


Figure I-10 General schematic of absorption system [16].

I.5.3 The adsorption phenomena

Adsorption is a ubiquitous process that occurs when one substance, known as the adsorbate, adheres to the surface of another material, known as the adsorbent. This process is typically divided into two categories: physical adsorption and chemical adsorption. When weak intermolecular forces like van der Waals forces hold the adsorbate molecules to the adsorbent surface, physical adsorption takes place. This process is non-selective and can lead to the formation of multiple layers of adsorbate molecules on the surface of the adsorbent. In contrast, chemical adsorption involves the formation of chemical bonds between the adsorbate and adsorbent molecules. Physical adsorption can be compared to the condensation process of a refrigerant within the adsorbent material, and the heat released during adsorption is similar to the heat released during the condensation process of the refrigerant. Applying heat or lowering the pressure can release the molecules that have been physically adsorbent from the adsorbent surface without them decomposing during the desorption process. Physical adsorption has a wide range of applications, including refrigeration, gas separation and storage, catalysis, and air purification. Although physical adsorption is a relatively simple and cost-effective process, it has limitations and is not suitable for all applications [31].

The most widely used adsorbents in energy adsorption refrigeration systems solar or residual heat are activated carbon, silica gel, and zeolite, while the most generally used adsorbents in energy adsorption refrigeration systems solar or residual heat are water, methanol (ethanol), or ammonia.

I.5.3.1 Operating principle Closed cycles with physical adsorption

Solar adsorption cooling systems utilize solar energy as their primary energy source and operate solely on thermal energy, eliminating the need for mechanical or electrical input. The refrigeration process takes place in a closed system consisting of an adsorbent bed in the solar collector, a condenser, a receiver tank with a two-way valve, and an evaporator (as shown in Figure I.11). The basic adsorption cycle consists of four steps, which are illustrated in the Clapeyron diagram, featuring two isobaric and two isosteric lines (as shown in Figure I.12).

During the daytime, the adsorbent material can be heated using solar energy to drive the desorption process, while during the night-time, the adsorbent can be cooled by radiating heat to the surroundings to drive the adsorption process.

A typical daytime adsorption cooling cycle consists of the following steps:

Adsorption: The adsorbent material is exposed to a gas or vapor, and the adsorbate molecules are attracted and held onto the surface of the adsorbent.

Pre-cooling: The adsorbent material is cooled to a lower temperature to increase its adsorption capacity. This can be achieved by passing a cooling fluid, such as water, over the surface of the adsorbent material.

Adsorption stabilization: The adsorbent material is kept at a constant temperature and pressure while the adsorbate continues to be adsorbed onto the surface of the material.

Cooling: The adsorbent material is used to cool a fluid or space by passing a cooling fluid or air over the surface of the adsorbent material. As the fluid or air passes over the adsorbent, the adsorbed gas or vapor is released, causing the fluid or air to cool down.

Desorption: The adsorbent material is then exposed to a higher temperature, typically using solar energy, to release the adsorbed gas or vapor from the surface of the adsorbent.

Regeneration: The desorbed gas or vapor is removed from the adsorption chamber, and the adsorbent material is regenerated by removing any remaining adsorbed gas or vapor using a vacuum or purging with an inert gas.

During the night-time period, the adsorption cooling device can still operate by utilizing the radiative cooling effect. The radiative cooling effect is a natural phenomenon where an object loses heat to its surroundings by emitting infrared radiation. By using an adsorbent material that has a high emissivity, the material can effectively radiate heat to the surroundings, causing them to cool down.

In a typical night-time adsorption cooling cycle, the following steps can be included:

Pre-cooling: The adsorbent material is cooled to a lower temperature to increase its adsorption capacity. This can be achieved by radiating heat from the adsorbent to the surroundings.

Adsorption stabilization: The adsorbent material is kept at a constant temperature and pressure while the adsorbate continues to be adsorbed onto the surface of the material.

Cooling: The adsorbent material is used to cool a fluid or space by passing a cooling fluid or air over the surface of the adsorbent material. As the fluid or air passes over the adsorbent, the adsorbed gas or vapor is released, causing the fluid or air to cool down.

Desorption: The adsorbent material is then exposed to a higher temperature to release the adsorbed gas or vapor from the surface of the adsorbent. This can be achieved by using a heating fluid, such as hot water or steam.

Regeneration: The desorbed gas or vapor is removed from the adsorption chamber, and the adsorbent material is regenerated by removing any remaining adsorbed gas or vapor using a vacuum or purging with an inert gas [2, 32].

The solar adsorption refrigeration cycle operates in two stages, with stages 1-3 occurring during the daytime and stages 3-1 occurring during the night-time. Depending on the driving heat temperature, which ranges from 60-95 °C, the adsorption cycle can achieve a COP of 0.3-0.7 [33].

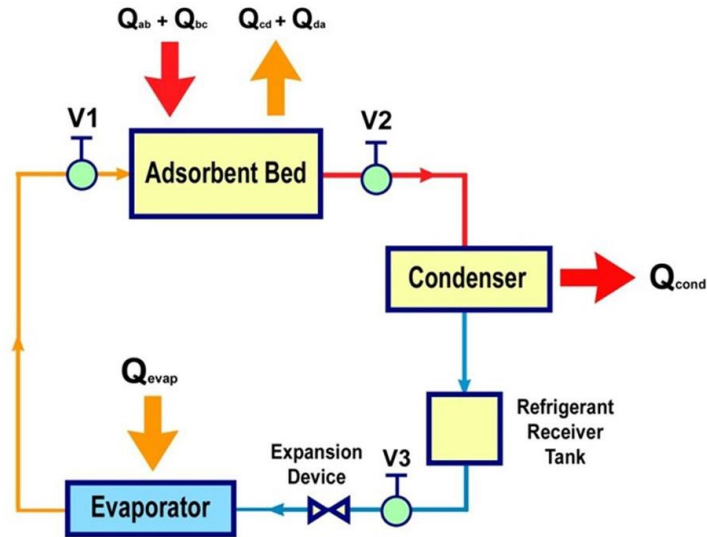


Figure I-11 Diagram of a Solar-Powered Adsorption Cooling System [32].

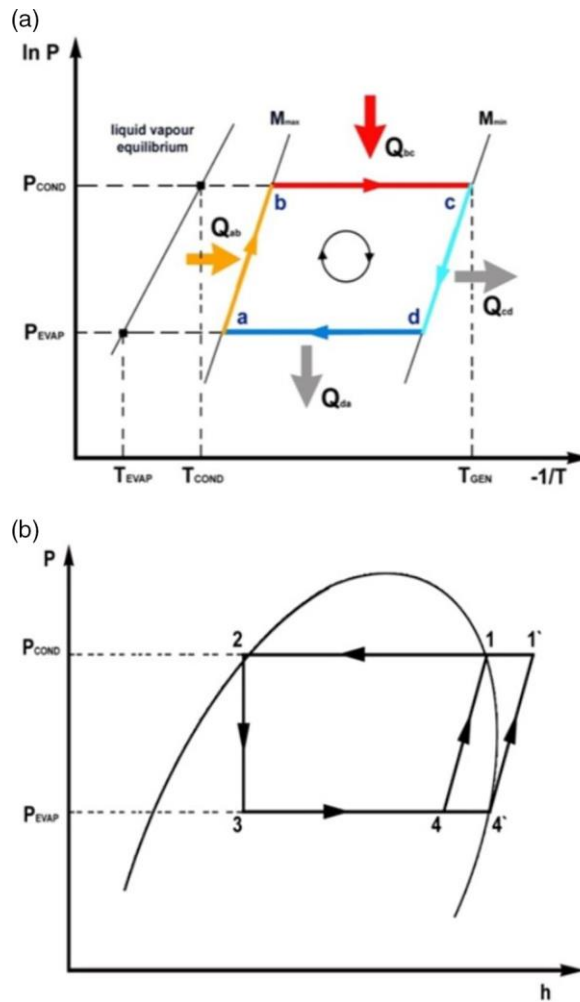


Figure I-12 Basic adsorption cycle [32].

I.5.3.2 Physical adsorption

Highly porous physical adsorbents like silica gel, activated carbon (AC), and zeolite can selectively trap and store refrigerants due to their high surface-to-volume ratios. When these adsorbents become saturated, they can be easily regenerated by heating.

An adsorption refrigeration system using silica-gel/H₂O and activated carbon (AC) with methanol or NH₃ as the refrigerant operates by cooling the adsorbent material to a low temperature, allowing the refrigerant to adsorb onto its surface, releasing heat in the process. Upon heating, the refrigerant desorbs from the adsorbent, evaporates, and cools in the evaporator in the presence of ambient air or water, producing a cooling effect. The refrigerant vapor then adsorbs onto the adsorbent material, and the cycle continues [34, 35]. The COP of an adsorption refrigeration system can range from 0.1 to 0.5, depending on the specific conditions of the system, and is typically lower than conventional vapor compression refrigeration systems. However, adsorption refrigeration systems have several advantages, including their ability to utilize low-grade thermal energy sources, low environmental impact, and the ability to operate without moving parts or harmful refrigerants, making them well-suited for specific applications. Regular maintenance and cleaning of the adsorbent material are necessary to maintain the system's performance and prevent fouling or degradation of the adsorbent [36]. Current solar adsorption technology can produce 4 -7 kg/m² of SC per day, with a cooling coefficient of 0.10 to 0.15 [37].

I.5.3.3 Chemical adsorption

Chemical adsorption is a process that involves the binding of a gas or vapor molecule to the surface of a solid or liquid substance through strong chemical bonds. Unlike physical adsorption, which involves weaker forces of attraction such as Van der Waals forces or hydrogen bonding, chemical adsorption forms a more stable and irreversible bond between the adsorbent and the adsorbate. This makes it a more energy-intensive process to reverse, requiring higher temperatures or other chemical reactions to release the adsorbed molecules.

Erhard et al. [38] In Germany, a demonstration adsorption refrigeration device was constructed using the strontium chloride/NH₃ pair. However, the cycle only achieved a global COP of 0.08, and the evaporation temperature reached -5°C during the cycle.

Maggio et al. [39]. Propose a mathematical model was created to assess the efficiency of a solar adsorption fridge that utilized a composite material composed of LiCl in the pores of silica gel as the adsorbent and methanol as the refrigerant. The fridge obtained a maximum solar COP of 0.33, and was capable of producing up to 20 kg of ice per m² of collector each day.

Metal hydride refrigeration systems use hydrogen as a refrigerant and are being considered for integration into hydrogen-fueled systems. However, like other adsorption technologies, metal hydride refrigeration faces research challenges related to improving specific cooling capacity and heat transfer in the beds. Single-stage systems can achieve a driving temperature as low as 80°C, depending on the hydride and the heat rejection temperature, with COPs around 0.5 [40].

I.6 Comparison adsorption versus absorption

Adsorption is the process by which ions or molecules of gases, liquids, or dissolved solids attach to a solid surface. During this exothermic process, molecules of a liquid or gas (called the adsorbate) collect on a solid surface (called the adsorbent). Porous materials, known as adsorbents, are capable of absorbing many times their volume in gases or liquids. It is important to note that the terms "adsorption" and "absorption" have different meanings, even though they are sometimes used interchangeably. Adsorption refers to the sticking of gas or liquid molecules to the surface of a solid, while absorption refers to the entry of gas or liquid molecules into the solid [41].

Table I-1 Comparison Between Various Solid Adsorbent Pairs

Adsorbent	Refrigerant	Adsorption Heat (kJ/kg)	Density of Refrigerant (kg/m³)	Considerations
Activated alumina	H ₂ O	3000	1000	Water is applicable except for very low operating pressure
Zeolite	H ₂ O	3300 – 4200	1000	Natural zeolite has lower values than synthetic zeolite
	NH ₃	4000 – 6000	681	
	CH ₃ OH	2300 – 2600	791	
Silica gel	CH ₃ OH	1000 – 1500	791	Suitable for temperature less than 200°C
Silica gel	H ₂ O	2800	1000	Used mostly for descent cooling
Calcium chloride	CH ₃ OH	1800 – 2000	791	Used for cooling
Metal hydrides	Hydrogen	2300 – 2600	1000	Used for air conditioning
Complex compounds	Salts and NH ₃ or H ₂ O	2000 – 2700	681	Used for refrigeration

Table I-2 Comparisons of the COP and SCP values of different studies.

Working pair	COP	SCP (kJ/kg)	Reference
Zeolite 13X–water	0.38	92.5	Zhang (2000) [42]
Activated carbon/methanol	0.4	150	Wang et al. (2001) [43]
Activated carbon/methanol	0.12–0.14	230.4	Li et al. (2002) [44]
Activated carbon/methanol	0.125	117.3	Wang et al. (2006) [45]
Activated carbon/methanol	0.211	83.72	Hassan et al. (2011) [46]
Activated carbon/methanol	0.48	114	Tso et al. (2014) [47]
Zeolite 13X/CaCl ₂ –water	0.16	106	Tso et al. (2015) [48]
Zeolite 13X/CaCl ₂ –water	0.3	401	Chan et al. (2018) [49]
Zeolite 13X/CaCl ₂ –water	0.24	208.2	Zhu et al. (2018) [50]
Activated carbon/methanol	0.49–0.67	113.7–114.8	Saravanan et al. (2022)
Zeolite/water	0.36–0.45	216–217.4	[32]

I.7 Conclusion

In this chapter, A state of the art review of the different technologies available to convert solar energy into a cooling effect is demonstrated. The study draws up the main means of production of solar cold, in this case electric solar air conditioning (photovoltaic), open cycle solar cooling by desiccation and closed cycle solar cooling by sorption.

For open sorption refrigeration systems, it has been shown that in hot and humid climates, or in ambient air with high humidity, a special and more complex design of the desiccant cooling process is required. This is because reducing the high humidity to a sufficiently low level allows the direct use of the desiccant cooler.

for closed systems, it has been shown that sorption refrigeration machines, especially absorption machines, are commercially available for high power applications. However, the market for small power absorption units (5-10 kW) is currently developing. Indeed, the bibliographic study shows that adsorption refrigeration machines have a relatively low solar COP.

When compared to absorption machines, adsorption machines are relatively big, requiring a significant quantity of material and huge exchangers. However, the generation temperature level

CHAPTER I: Solar refrigeration technology

is lower than that required by liquid sorbents. Adsorption machines generally require very few moving parts, reducing the need for maintenance. This is very important especially in a context of lack of maintenance, qualified technicians or parts not manufactured locally. This reinforces the choice to study the feasibility of adsorption solar installations in the Biskra region. Thus, the next chapter is dedicated to the state of the art of solar cold production technology by the adsorption phenomenon.

II. CHAPTER II: Literature search on technical solutions used for solar adsorption system adaptation.

II.1 INTRODUCTION

This chapter presents literature research on technical solutions used for solar adsorption system adaptation and the most common failure problems of this solar system. The objective is to give an overview of the techniques used in the field of cold production through the phenomenon of adsorption. For this, it seems appropriate to us to present the work carried out in the field of cold production by adsorption, which uses solar energy as a heat source in the Biskra region.

The effectiveness of such systems, as well as possible issues with design, installation, and operation, are, incidentally, highlighted by one case. This particular illustration was selected to illustrate the significance of system optimization. The acceptability and knowledge of new technologies are particularly low when they are introduced to the market. Due to incorrect application of technological fundamentals, there is a reduction in the ecological and financial consequences. Thus, the relationship between the function of the adsorption machine and ambient air temperature changes when the temperature reaches 35 °C in the summer season in the Biskra region.

II.2 Adsorption refrigerator « Intermittent cycle »

Adsorption cooling systems, as discussed in the preceding chapter, can operate at low temperatures (typically below 90 °C) [51-53], and combining adsorption cooling with solar collectors has grown in popularity in recent years.

The exploitation of solar energy is done by adsorption collectors in the case of intermittent cycles or by solar water heaters in the case of continuous cooling systems such as chillers. To this end, and to present a clear bibliographic synthesis of applied research activities and projects, it is appropriate to classify them into two different categories: adsorption refrigerators and two different categories: adsorption refrigerators with a single adsorber and adsorption chillers with two adsorbers (chiller).

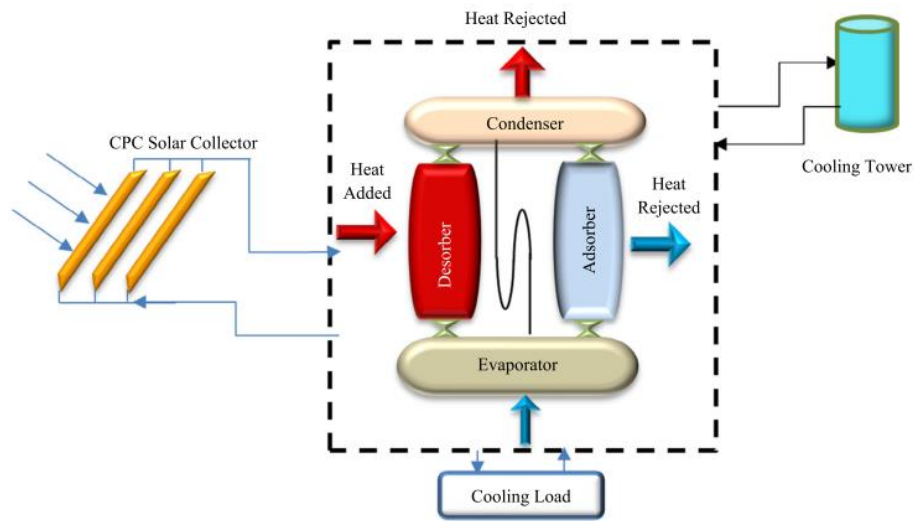


Figure II-1 A diagram illustrating the adsorption cooling process utilizing CPC solar collectors [54].

II.2.1 Adsorption chiller with single adsorber (Chiller)

In previous works, the control for a one-bed adsorption chiller with a separate condenser (C) and evaporator (E) is generated and tested. Figures II-2 and II-3 provide an overview of the components, the heat flow rates, and the temperatures that occur throughout a cycle with one bed of adsorption. In addition to this, the separate phase periods for adsorption τ_{ads} and desorption τ_{des} are noted.

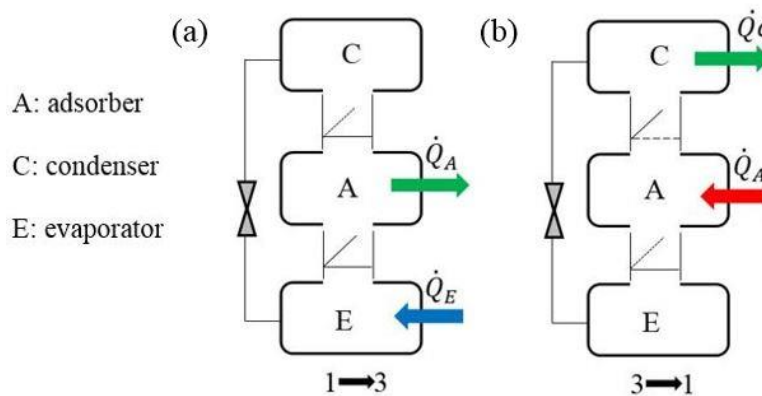


Figure II-2 Phases, heat fluxes, and a one-bed adsorption chiller setup. Adsorption and isosteric cooling (a), desorption and isosteric heating (b) [9].

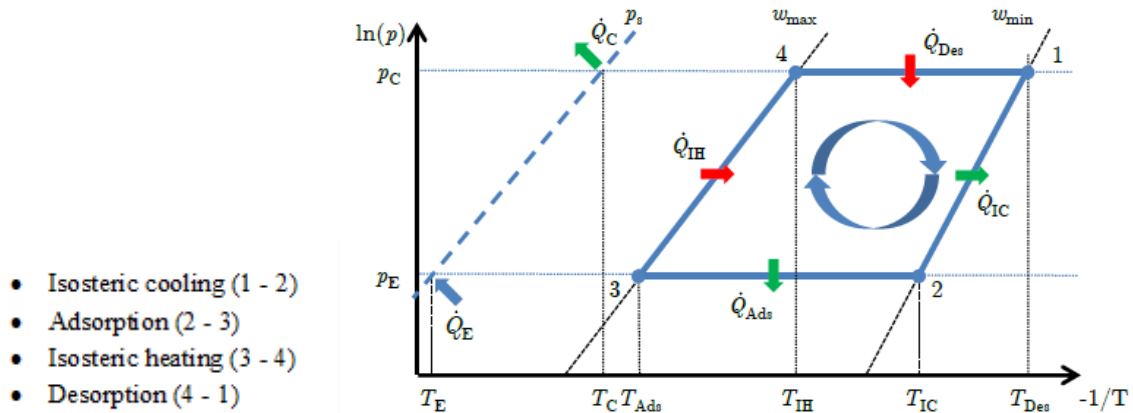


Figure II-3 The different phases of adsorption chiller with single chiller [55].

Isosteric Cooling and adsorption 1-3: The processes of isosteric cooling and adsorption can be divided into three states. In state 1, the adsorbent is at its minimum loading, w_{min} , and its maximum temperature, $T_{Des} = T_{high}$. All valves are closed at this point to prevent adsorption or desorption. Next, in state 2, the adsorbent is cooled isothermally until the pressure in the adsorber pad ($T_{ad_{ad}} = w_{min}$) equals the pressure in the evaporator p_E (T_{low}). A valve between the evaporator and adsorber can be used to achieve this. If the pressure in the evaporator is higher than that of the adsorber, the valve opens, and adsorption begins. During this phase, heat Q_E is transferred to the evaporator, while Q_{Ads} is needed to cool the adsorber to remove the released enthalpy of adsorption h_{ads} . The ideal adsorption phase ends when the adsorbent reaches its maximum loading, w_{max} , and its minimum temperature, $T_{Ads} = T_{mid}$, which is state 3. The duration of this phase is referred to as the adsorption phase time t_{ads} , which determines the temperature and loading reached in an actual cycle.

Isosteric heating and desorption 3-1: During the heating phase, the loading remains constant while the pressure gradually increases until the adsorber pressure pad ($T_{ad} = w_{max}$) equals the condenser pressure p_C (T_{mid}) in state 4. This is achieved in an adsorption chiller by using a valve between the adsorber and the condenser. Desorption begins as soon as the valve opens, with the adsorbate flowing from the adsorber to the condenser. While Q_{Des} cools the condenser, Q_C provides heat to the adsorber. In the ideal cycle, the desorption phase ends when the adsorbent

CHAPTER II: Literature search on technical solutions used for solar adsorption system adaptation.

reaches its maximum temperature ($T_{Des} = T_{high}$) and minimum loading (w_{min}), which is state 1. The duration of the desorption phase, called "des, determines the temperature and loading achieved in a real cycle.

II.2.2 Adsorption chiller with double adsorber (Chiller)

SorTech AG is a German company that manufactures adsorption chillers. The company's most popular model is the SorTech ACS, which is a small, compact chiller that can be used for a variety of applications, including home and office air conditioning, and industrial process cooling. The SorTech ACS is powered by heat, which can be provided by solar energy, biomass, or waste heat. The chiller is also very energy efficient, and can save up to 50% on energy costs compared to traditional air conditioners [56].

Here are some of the benefits of using an adsorption chiller:

- Energy efficient: Adsorption chillers are very energy efficient, and can save up to 50% on energy costs compared to traditional air conditioners.
- Eco-friendly: Adsorption chillers are powered by heat, which can be provided by renewable energy sources such as solar energy, biomass, or waste heat. This makes them a more sustainable option than traditional air conditioners, which use electricity.
- Quiet: Adsorption chillers are very quiet, and operate at a much lower noise level than traditional air conditioners.
- Compact: Adsorption chillers are small and compact, making them ideal for use in homes, offices, and small businesses.



Figure II-4 Adsorption chiller ACS 08 / ACS 15 [57].

In addition to their expertise in silica gel technology, SorTech has also gained significant knowledge in zeolith coating technology as shown in figure II-5, which enables them to coat three-dimensional structures made of various alloys. The special aspect of this technology is that it allows for the direct crystallization of Zeolith onto aluminum-based surfaces, resulting in highly energy-dense and space-efficient heat exchangers for SorTech's advanced sorption chillers and heat pumps.

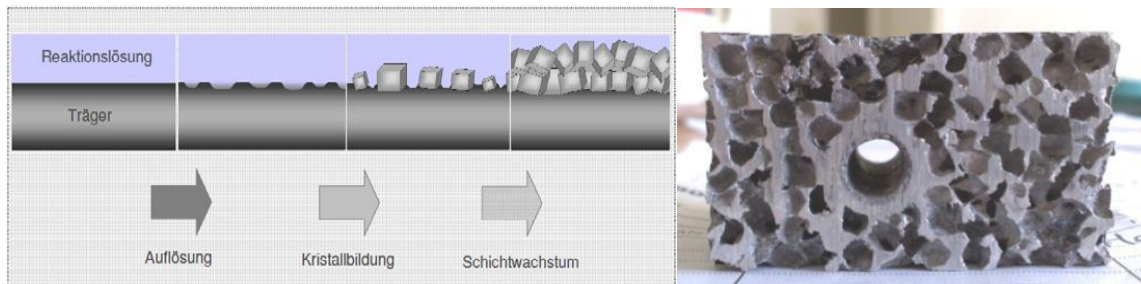


Figure II-5 Crystallization process (left); alloy sponge suitable for Zeolite coating (right).

Traditional air conditioners use electricity to compress a refrigerant, which causes it to evaporate and cool the surrounding air. Thermal-driven chillers use thermal energy to compress the refrigerant, which can come from a variety of sources. Adsorption chillers are a type of thermal-

CHAPTER II: Literature search on technical solutions used for solar adsorption system adaptation.

driven chiller that uses a solid adsorbent to absorb the refrigerant. This process releases heat, which is then dissipated into the surrounding environment. The refrigerant is then released from the adsorbent and condensed into a liquid, which absorbs heat from the surrounding air.

SorTech's adsorption chiller uses silica gel as an adsorbent. Silica gel is a porous glass with a high affinity for water, so it can absorb large amounts of water vapor. When the silica gel absorbs water vapor, it releases heat. This heat is then dissipated into the surrounding environment.

Adsorption chillers have a number of advantages over conventional air conditioners, including being more energy-efficient, more environmentally friendly, and able to run on a variety of renewable energy sources.

Step 1: Desorption – Drying of the adsorbent

Desorption is the process of heating the adsorbent, which causes the refrigerant to be released from the adsorbent and vaporize. This step releases heat, which is dissipated into the surrounding environment.

Step 2: Adsorption

After the water vapor has been adsorbed on the surface of the adsorbent, a reverse reaction occurs, causing the liquid condensate to evaporate after a cooling period. This time, the lower evaporator control valve opens, allowing the dry adsorbent to draw in the water vapor. The water then evaporates in the evaporator, creating a cooling effect that can be used for air conditioning. Adsorption releases heat, which must be dissipated.

Step 3: Return of condensate

The circuit is then closed after returning the liquid condensate to the evaporator. Two adsorbers operate together to provide a continuous flow of cold, with one adsorber desorbing while the other simultaneously creates cold by adsorbing.

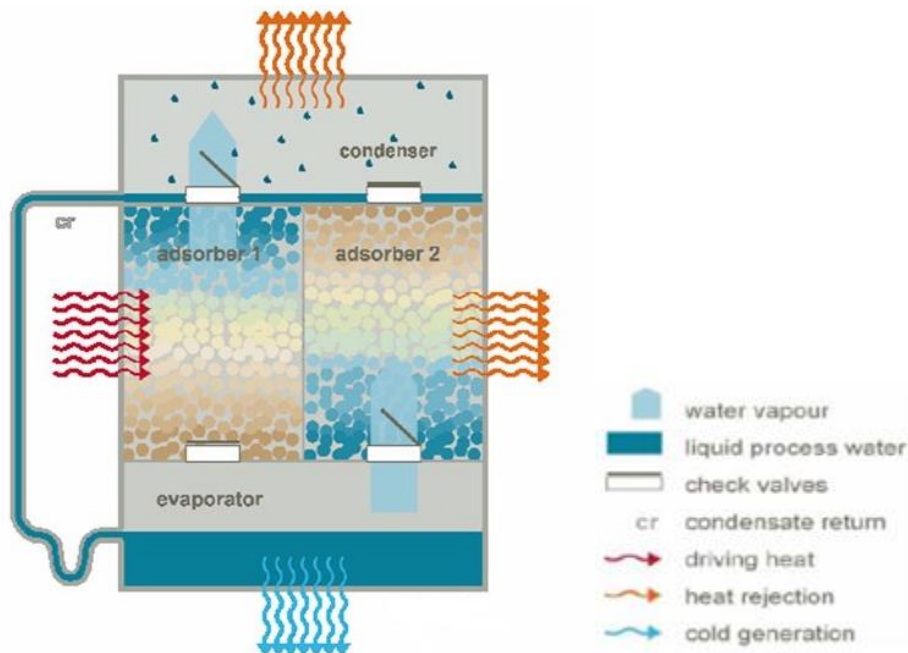


Figure II-6 Working process of the adsorption chiller [57].

II.3 Construction principles

II.3.1 Coating of the adsorber heat exchangers with silica gel

The use of silica gel pellets in adsorption chillers has been limited due to the low heat and mass transfer rates in a solid bed of pellets. However, SorTech AG has developed a technique to improve the power density of adsorption chillers by applying silica gel directly onto the surface of the adsorber heat exchanger. This process involves pasting the heat exchanger surface with silica gel pellets using an epoxy resin, that does not block the pellets' entrance pores. The technique is versatile and can be used with all types of granulation. The pellets themselves are typically small and circular, with diameters ranging from 1 to 3 mm. Improving heat and mass transfer in this way significantly enhances the efficiency of the adsorption chiller [57].



Figure II-7 Photo of a silica gel coated tube and fin adsorbed heat exchanger [57].

II.3.2 Compact self-supporting construction

A significant challenge in developing adsorption chillers is the construction of a vacuum vessel to contain the adsorber heat exchangers, evaporator, and condenser. Designing vacuum vessels using typical design rules leads to bulky and heavy constructions to ensure stability against atmospheric pressure. A design was developed where the heat exchangers and the internal structure of the machine serve as a support for the vacuum-tight envelope. This innovative design enables the use of thin stainless-steel metal sheets as vacuum containment, resulting in a lighter and simpler construction, as shown in the above figure II-6. This approach leads to substantial material and volume savings and represents a significant breakthrough in the construction of cost-effective adsorption chillers.

II.4 Effect of operating temperatures

Sah et al. [52] conducted a study to investigate the impact of various operating conditions on the performance of an adsorption chiller, as shown in Figures II-8 and II-9. Figure II-8 demonstrates that the cooling capacity of the chiller increases from 3.99 kW to 6.68 kW when the hot water inlet temperature rises from 60°C to 120°C, while the cooling water temperature is maintained at 25°C. This increase in cooling capacity is attributed to the higher driving

CHAPTER II: Literature search on technical solutions used for solar adsorption system adaptation.

temperature, which results in more refrigerant being desorbed and evaporated, leading to a higher cooling output. The COP of the chiller shows no significant change when the hot water inlet temperature is increased from 60°C to 70°C, but a sharp decrease is observed at higher temperatures due to increased irreversible losses.

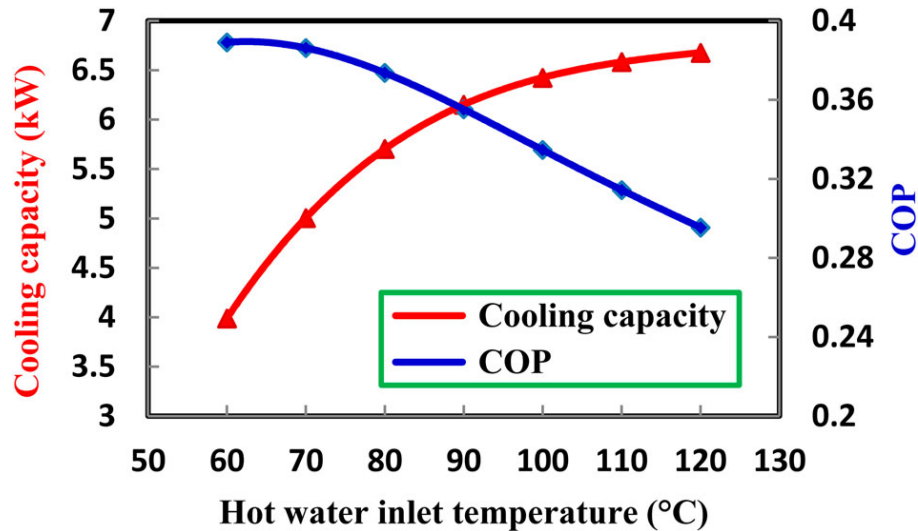


Figure II-8 Impact of Inlet Water Temperature on Cooling Capacity and Coefficient of Performance (COP) [52].

Figure II-9 illustrates that the cooling capacity and the COP of the chiller increase when the cooling water inlet temperature decreases from 32°C to 20°C. This is because a lower adsorption temperature allows for a larger amount of refrigerant to be adsorbed and desorbed during each cycle, leading to a higher cooling output and a higher COP. Specifically, the cooling capacity increases from 4.55 kW to 6.71 kW, while the COP rises from 0.33 to 0.37 as the cooling water inlet temperature drops from 32°C to 20°C.

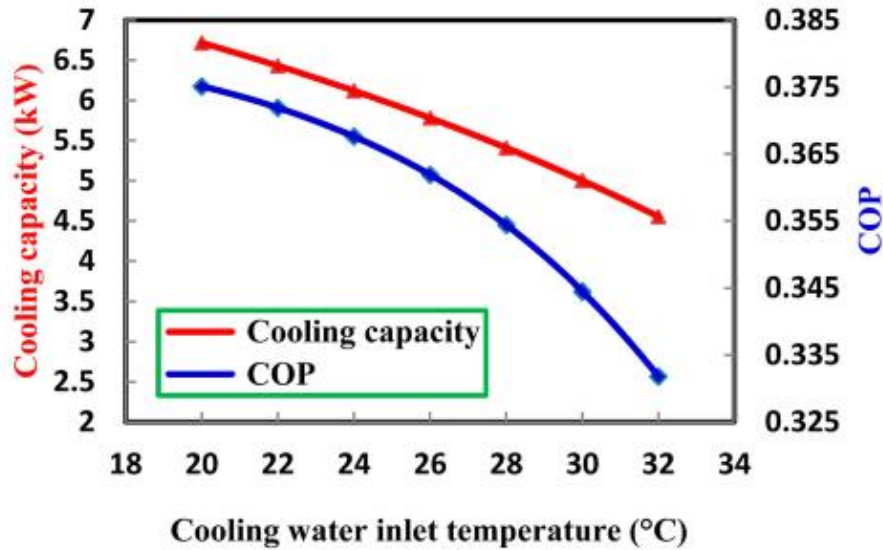


Figure II-9 Influence of the inlet temperature of cooling water on cooling capacity and performance coefficient [52].

II.5 The effect of high air temperature on the adsorption refrigeration system's operation

The cooling water is one of the principal fluids in the adsorption system and it is shown in table II-1, which shows the basic limits for operation in the best conditions since the cooling tower is responsible for lowering the cooling water temperature as a function of the head between the water inside the tower and the air outside.

Figure II-8 shows the variation of the ambient air temperature according to each month. We also note the highest temperatures recorded in summer, since they exceed 35 °C. The latter directly affects the operation of the adsorption refrigeration system. Thus, through the curve shown in Figure 8, it can be seen that the temperature of the ambient air in the Biskra region is much higher than the temperature of the cold water at the outlet, and this constitutes a major obstacle to the process of convection inside the cooling tower, resulting in a mandatory and unambiguous increase in the surface of the exchanger or the use of methods involving Cooling with water that is less than or equal to 30 °C is more efficient.

CHAPTER II: Literature search on technical solutions used for solar adsorption system adaptation.

Table II-1 The different working conditions of the adsorption cooling machine.

	Inlet	outlet
Hot water	85 °C	80 °C
Cooling water	30 °C	35 °C
Cold water	20 °C	25 °C

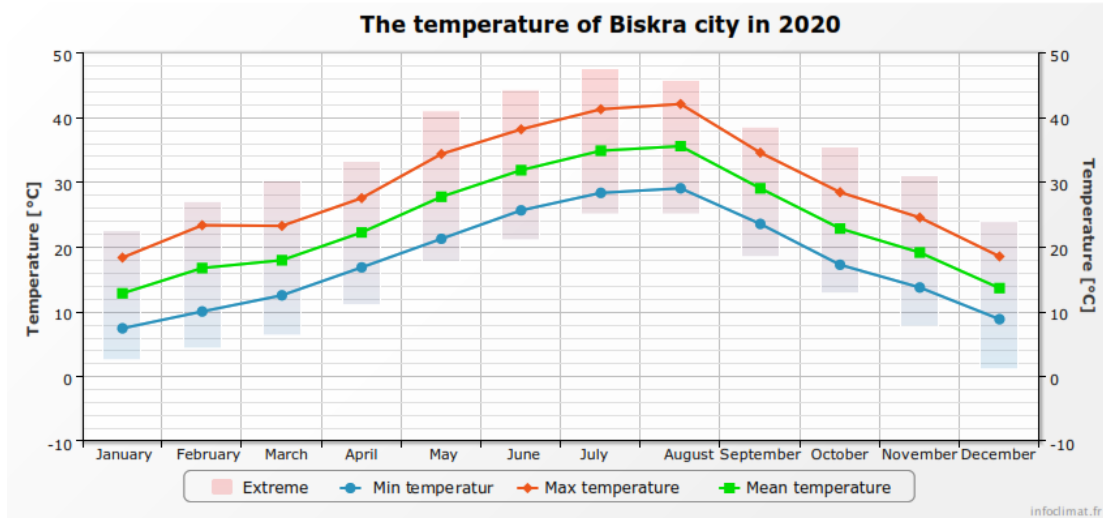


Figure II-10 The ambient air temperature of Biskra city in 2020 [58].

II.6 The technical solution proposed for the malfunctioning of a solar adsorption cooling system

A rich literature review is mentioned by Rouag et al. [59], The proposed solution in this study is based on harnessing a renewable energy source known as geothermal energy, which involves exchanging thermal energy with the Earth's subsurface. This energy is typically used for various applications, including heating and cooling systems, as well as generating electricity [60].

There is no defined categorization of geothermal energy in the literature, to the best of the writers' knowledge. Some researchers divided geothermal energy into four categories based on temperature fields: high (>180°C), average (>100°C), low (>30°C), and extremely low (10–30°C) [61, 62]. Geothermal fields are classified into two main types: deep systems (>400 m depth) and shallow systems (<400 m depth). While deep systems require specific geological conditions and

CHAPTER II: Literature search on technical solutions used for solar adsorption system adaptation.

high geothermal gradients, shallow systems can be developed in areas with normal geological settings and moderate geothermal gradients [63, 64].

According to a review of current research, authors generally connect the heating systems of heat pumps to water geothermal systems to enhance their performance [65, 66]. This combination has been studied for improving the performance of heat pump cooling systems.

In addition, the connection of the air geothermal systems with heat pumps remains relatively untapped. Among the most current technical methods for enhancing the performance of both conventional and solar cooling systems are:

Rouag et al. (2016) [67]. A technical solution is proposed to adapt a solar adsorption cooling system. This technique is defined by replacing the dry cooling tower with an earth-water heat exchanger (EWHE). EWHE is only connected to the chiller during ambient temperature peaks to prevent malfunctioning of the cooling system. The authors designed a typical EWHE for the Bikra region and found it to be an effective geothermal solution. However, they also noted that continued operation of the EWHE could cause soil saturation and diminish its performance over time. Accordingly, the authors recommend further study to account for the operating time of the EWHE.

Ounis et al. [68]. In order to enhance the efficiency of conventional vapor compression refrigeration systems, researchers have proposed a novel approach that involves using the condensed water from the evaporator to cool the condenser. This is achieved through the use of a specially designed accessory known as a humidified grid. By improving the operating conditions of the condenser, this approach can significantly reduce power consumption. Moreover, it has the potential to address the issue of system malfunction caused by high ambient temperatures exceeding the system's normal operating range.

Rouag et al. [69]. (2020) are proposed to study the coupling an earth-air heat exchanger (EAHE) with finned tube heat exchangers (such as the condenser or dry cooling tower) in order to reduce the inlet air temperature. This novel solution involves using an air mixer to connect the EAHE to the finned tube heat exchanger, resulting in what the authors call a Geothermal Air-Cooler (GAC). The objective of this approach is to improve the operating limits of the air-cooler and increase its efficiency.

CHAPTER II: Literature search on technical solutions used for solar adsorption system adaptation.

Soni et al. [70].” applied a similar approach to enhance the energy efficiency of a traditional air-conditioner by integrating it with an EAHE system, which was tested in three different configurations. The researchers found that supplying the entire fresh air from the EAHE to cool the condenser coil resulted in a considerable reduction in power consumption in the hybrid system compared to a conventional air-conditioner”.

The economic viability of the hybrid arrangements was assessed, revealing potential energy savings and favorable payback periods. According to the analysis, the proposed system could achieve an 11% reduction in energy consumption, with a return on investment of 3 years. For a similar system, Benhamza et al. (2017) [71], the integration of an EAHE with a conventional air conditioning system was found to improve the Energy Efficiency Ratio (EER) and COP by 19% and 20%, respectively.

Zapałowicz et al. (2018) [72]. proposed a novel air-conditioning system that integrates a conventional air-conditioner, earth-air heat exchanger (EAHE), and photovoltaic (PV) installation. The system works by using the EAHE to cool the building wall, which reduces heat gain into the interior and subsequently reduces the required cooling capacity of the air conditioner. This results in a lower demand for electric power supplied to the compressor, which improves the energy efficiency of the system. A simulation study was conducted to evaluate the performance of the proposed system. The results showed that the system can achieve a significant improvement in energy efficiency compared to a conventional air-conditioning system. The system is also more efficient in warm climates with high solar irradiance. The proposed system has the potential to be a more sustainable and cost-effective solution for air-conditioning in buildings. The system can help to reduce energy consumption and greenhouse gas emissions, while also providing a comfortable indoor environment.

Habibi et al. (2019) [73]. used a mathematical model to simulate the performance of the different heat pump systems over a 30-year period. The model took into account the variations in building loads, ambient air temperature, soil temperature, and COP of the system. The results of the study showed that the vertical ground water heat exchanger (VGWHE) system had the highest performance, followed by the horizontal ground water heat exchanger (HGWHE) system and the earth-air heat exchanger (EAHE) system. The VGWHE system also had the highest energy

CHAPTER II: Literature search on technical solutions used for solar adsorption system adaptation.

efficiency, followed by the HGWHE system and the EAHE system. The study concluded that connecting heat pumps with shallow geothermal heat exchangers can improve their performance. The results of the study are important for the design and optimization of ground source heat pump (GSHP) systems.

II.7 Innovative solutions to improve adsorption machine function in Biskra city

Rouag et al. (2014) [69] Have proposed a technical solution to address the problem of malfunctioning air-cooling heat exchangers, such as air condensers and dry cooling towers, during extreme temperatures in hot regions. The proposed solution involves using an air mixer to connect a finned tube heat exchanger to an Earth-Air Heat Exchanger (EAHE), resulting in the creation of a Geothermal Air Cooler (GAC). The GAC system is designed to improve the efficiency of air heat exchangers used in air conditioning systems. A schematic of the GAC system is shown in Figure II-11, where a condenser or dry cooling tower is connected to the GAC.

The proposed GAC system offers several advantages over traditional cooling solutions. Firstly, it does not have any negative impact on the environment. Secondly, it requires minimal additional electrical power, which is consumed mainly by geothermal exhaust fans. Finally, it replaces the water used in cooling towers with air, thus reducing electrical consumption by using an exhaust fan instead of a pump. In addition to improving the performance of conventional and solar cooling systems, GAC can also replace industrial air coolers. EAHE can also be utilized to build air coolers in hot temperatures and heaters in lower temperatures.

CHAPTER II: Literature search on technical solutions used for solar adsorption system adaptation.

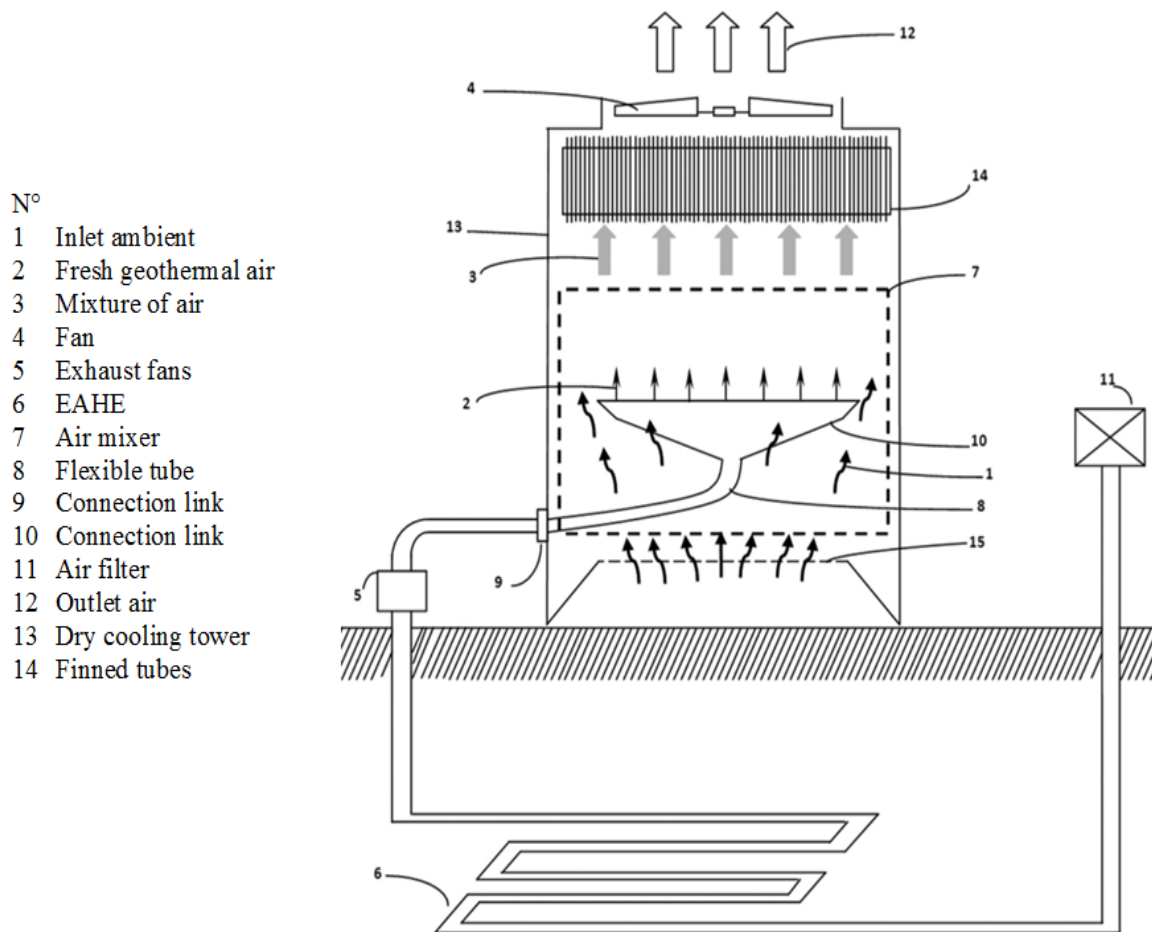


Figure II-11 Scheme of the air condenser (or DCT) coupled to GAC composed by the air mixer and the EAHE [69].

Ounis et al. [68], proposed an invention relating to the general field of air-cooled heat exchangers. It aims to improve the operation of cooling, air conditioning, and refrigeration conditioning installations and makes it possible to remedy the problems of malfunctioning refrigeration installations in the event of ambient temperatures exceeding the temperature limits of their operation. The principle is to couple an air cooler or an air condenser with a humidified grid (6) supplied by a source of water and/or by the condensates coming from the air heat exchangers, in particular, but not exclusively, evaporators (1). The device is also equipped with a water collector (8), to recover the water and/or condensates to be then reused to humidify the grid (6). The latter makes it possible to lower the temperature of the ambient air (9), sucked in by the fan (5). At the outlet of the grid (6), the cooled air (10) passes through the finned coil (4) and thus

CHAPTER II: Literature search on technical solutions used for solar adsorption system adaptation.

improves the efficiency of the latter. In the case of the extreme climatic conditions mentioned above, such as, for example, during heat waves, the air-cooled (10) by the grille (6) makes it possible to avoid the malfunctioning of the system.

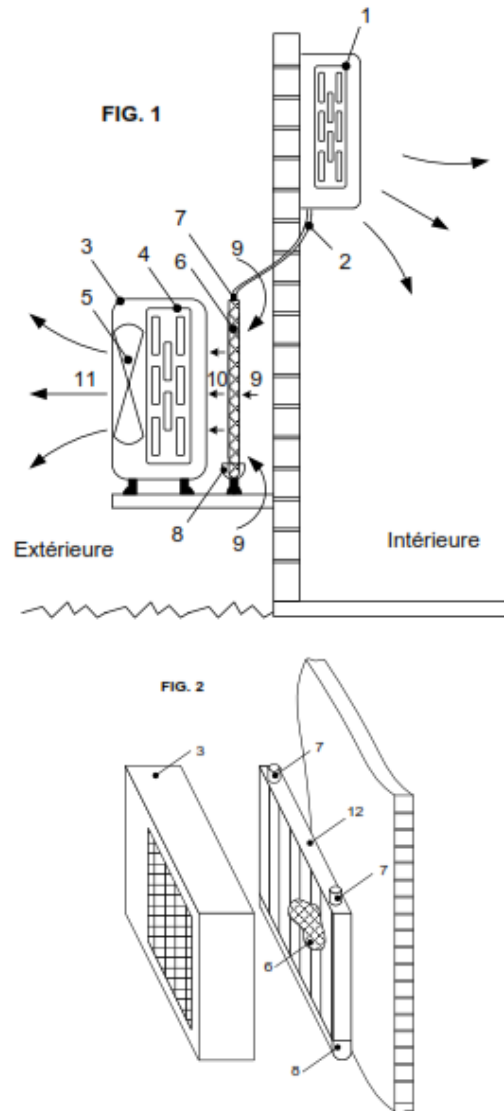


Figure II-12 Scheme of humidified grid accessory for increasing the efficiency of air exchangers and condensers [68].

Melhegue et al. [74] proposed an ‘Adsorption chiller / geothermal air cooler’ coupling device with new elements ensuring the cooling of the adsorber. As shown in Figure II-13, the device allows the coupling of an adsorption refrigeration machine to a geothermal air cooler. The example in Figure II-13 shows the adsorption refrigeration machine, which comprises: an adsorber

CHAPTER II: Literature search on technical solutions used for solar adsorption system adaptation.

1, an air condenser 2, generally in the form of a finned coil heat exchanger; an evaporator 3 installed in a refrigeration enclosure 11, and a set of valves 8, 9, and 10 connecting, respectively, components 1 to 2; 2 to 3; and 3 to 1 of the refrigeration machine. The geothermal air cooler, shallow as the example in Figure 1, comprises an air-soil exchanger 4, an air filter 12, a fan 7 sucking in the geothermal air, an air distribution valve 6, and an air diffuser 5, pushing the geothermal air towards the inlet of the condenser 2.

The "refrigerating machine/aero-cooler" coupling device of the present invention is composed of the following new elements: i) A connector 13 connecting the geothermal air-ground exchanger 4 and the adsorber 1 via the distribution valve air 6; ii) An air diffuser/mixer 14 delivering geothermal air to the inlet of the adsorber 1's air channel 15; and iii) Two manual and/or automatic mechanisms for the air inlet and outlet 16 and 17 of the channel 15. Thus, the coupling device of the present invention works intermittently with the "air-soil geothermal exchanger system/condenser" by making it possible to improve the coupling mentioned in particular by cooling the adsorber 1 in a manner: a) conventional by natural or forced convection using ambient air; b) using geothermal air according to the invention; and c) by mixing ambient air and geothermal air according to the invention.

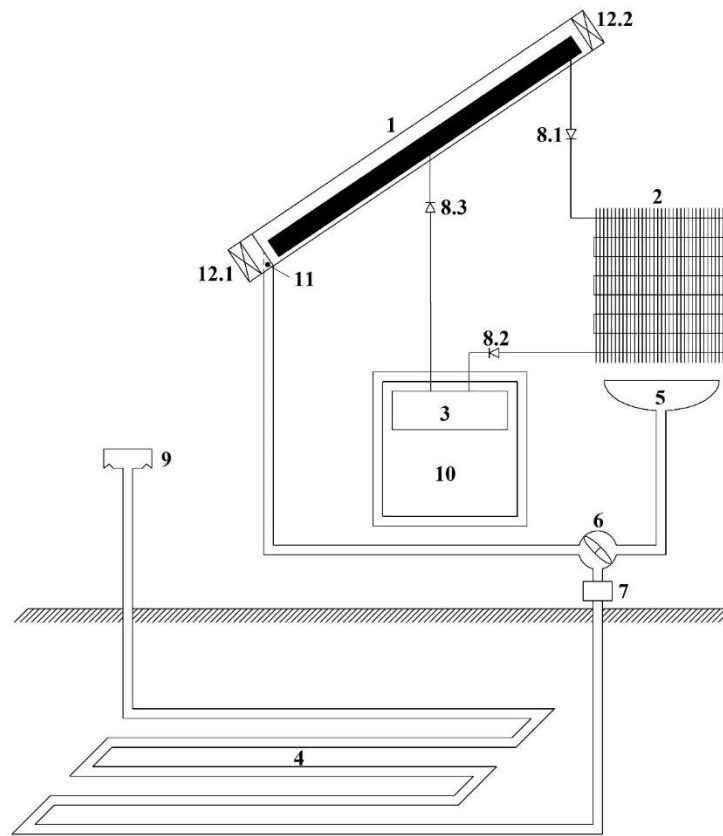


Figure II-13 Scheme of the ‘Adsorption chiller/geothermal air cooler’ coupling device with new elements ensuring the cooling of the adsorber [74].

Kheireddine and Benchabane [75]. In 2023, a proposed invention relates to the general field of heat exchangers using air and water, more particularly to the two fields of air-cooled wet heat exchangers and ground/ (water or air) geothermal heat exchangers. The present invention relates to the combination of a cooling tower with a ground/ (water or air) geothermal system and two direct water evaporation systems, namely: a water spray system and a cooling system by direct evaporation by pad.

The invention aims at improving the operation of air-cooling towers known in the prior art. More particularly, the present invention is a technological solution, easy to realize, to remedy the problem of malfunctioning of refrigeration systems when the ambient temperature exceeds the operating limits of these systems. The invention allows the extension of the operating time of these

CHAPTER II: Literature search on technical solutions used for solar adsorption system adaptation.

systems by adding new elements to the cooling tower, especially for dry and hot climates. The new elements of the present invention ensure in particular the cooling of: i) the ambient air by direct evaporation of water through a pad, ii) the humid air by direct contact with the sprayed cooling water, iii) the cooling water by two sub-systems, namely: a ground/(water or air) geothermal system and a system for the return of condensate recovered from the evaporator of the refrigerating machine.

The present invention will be better understood by studying a particular embodiment taken by way of example, which is not limiting, and illustrated by the two annexed drawings in which:

Figure II-14a represents, according to the invention, a cooling tower with new elements for cooling: i) the ambient air by direct evaporation of water through a pad, ii) the humid air by direct contact with the sprayed cooling water, iii) the cooling water by a ground/(water or air) geothermal system and/or by condensate recovered from the evaporator of the refrigerating machine.

Figure II-14b represents, according to the invention, a cross-section of: i) the cooling water basin 15, and ii) the water/ (water or air) exchanger 9 coupled to a geothermal ground/(water or air) exchanger.

As shown in figures II-14a and II-14b, the device of the present invention allows the improvement of the efficiency of air heat exchangers by new elements based on direct water evaporation and geothermal energy. The cooling tower of figure II-14a is equipped with a delivery or extraction fan 2 which ensures the cooling of the finned coil 3. The latter elements are the basic parts of dry cooling towers. According to the present invention, the ambient air 6, which is generally dry, is first cooled by direct evaporation of water through the porous medium (pad) 5. The cooled air becomes humid and passes, by a second direct water evaporation system, through a set of spray nozzles 4 of fresh water 14 before passing through the finned battery 3. The cooling water 14 is cooled by a third ground/ (water or air) heat exchanger system 11.

The device of the present invention is composed of the new elements described in the following: The tank 15, mounted on a support 13 and containing the cooling water 14, is cooled by the water/(water or air) heat exchanger 9, which is itself coupled with the above-mentioned geothermal heat exchanger 11. This coupling can be ensured, for example, in a closed loop with,

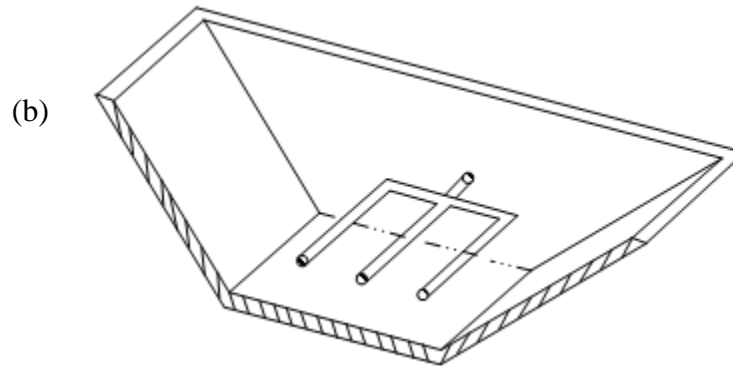


Figure II-14 Scheme of: a) cooling tower with a ground/ (water or air) geothermal system and two direct water evaporation systems, b) cooling water basin.

II.8 Conclusion

Through this chapter, it has been shown that many techniques for the design, construction and installation and maintenance of adsorption chillers have been developed. Activated carbon/methanol and silica gel/water couples, which could be produced locally, are widely used because they are inexpensive and allow low temperatures to be easily reached with low regeneration temperatures (around 80°C).

According to the above-mentioned bibliographic study, the performance of a solar adsorption machine is highly dependent on climatic conditions. It should be noticed that practically all of the above-mentioned experiments were conducted in cold climates or during moderate seasons such as spring. The average ambient temperature in arid regions, such as the region of Biskra (Algeria), can exceed 34°C in summer and even approach 35°C in July-August [58]. These external conditions undoubtedly have a considerable impact on the air heat exchangers, which are the condenser in the refrigerator and the cooling tower in the chiller. The second part of this thesis has been devoted to developing, investigating, and evaluating innovative options for improving the operation of these exchangers and adapting refrigeration equipment to hot climates.

III. CHAPTER III: Hybrid cooling tower coupled with a geothermal heat exchanger

III.1 Introduction

The present chapter describes the development of a simple calculation methodology to design an evaporative cooling tower (ECT) coupled with horizontal ground-water heat exchanger (GWHE). The ECT-GWHE system is proposed as a technical solution to enhance the thermal performance of the ECT by taking the case study of an adsorption device driven mainly by solar energy in the dry and hot climate of Biskra (Algeria), where the GWHE system only works in hot temperatures for a short time (less than 7 hours). Three operation modes of the ECT-GWHE system are investigated, namely: dry, wet counter-current, and wet co-current modes. The heat and mass transfer phenomena within the ECT and the GWHE are thermally analysed and modelled mathematically. The method of Runge-Kutta 4th order is applied to solve the system of four differential equations, for the counter-current and co-current flow arrangements, describing the evaporative cooling process in the wet cooling tower. A Matlab code was developed according to the presented calculation methodology allowing the thermal design of the ECT-GWHE system. The developed methodology was validated, and a good agreement was found with numerical simulations and experimental results obtained from the literature. It was concluded that the coupling of ECT with GWHE is an effective solution in hot and arid regions. Besides, ECT with a sprayed-water system in counter-current mode is the best method for high heat and mass transfer rates.

The main objective of this study is the development and the validation of a simple calculation methodology to design an evaporative cooling tower (ECT) coupled to a ground-water heat exchanger (GWHE). The new ECT-GWHE system is proposed as a technical solution to improve the ECT's thermal performance. Hot air temperatures in the semi-arid region of Biskra (Algeria) are considered as a case study. The three operation modes of the ECT-GWHE are studied, namely: dry, wet counter-current, and wet co-current modes. To the authors' best knowledge, the present study is the first investigation on the ECT-GWHE system in a dry and hot climate.

III.2 System Descriptions

Figure III-1 shows the studied system formed by an ECT coupled with a GWHE. The ECT can work in cross-flow arrangement of ambient air and process fluid. When the ECT works in the wet mode, the air and the spray water can flow according to two configurations: co-current mode (Fig. III-1a) and counter-current mode (Fig III-1b). In this study, the use of a close ECT-GWHE system pattern was investigated for hot climatic conditions in the city of Biskra (Algeria), where the peak temperature exceeds 48 °C in summer season [76].

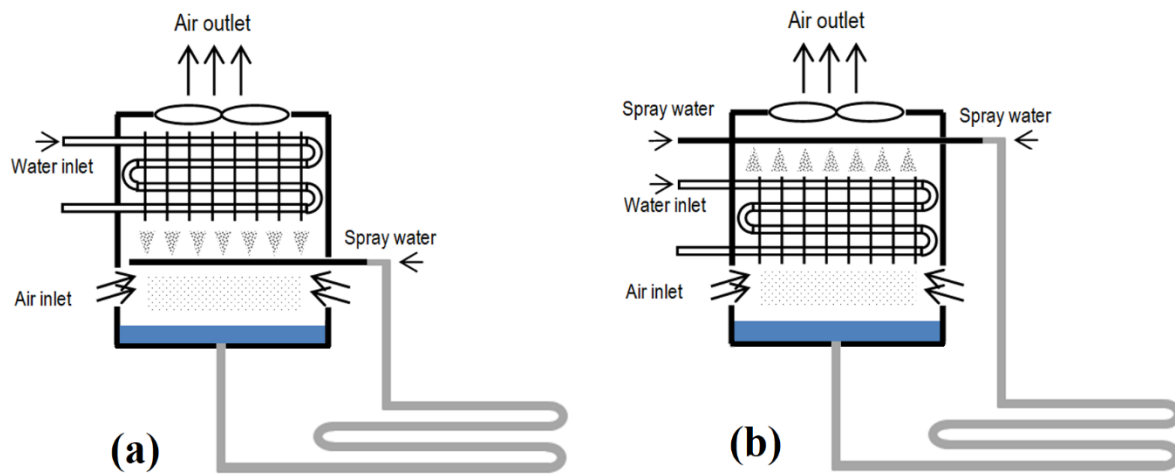


Figure III-1 Evaporative cooling tower (ECT) coupled with a ground-water heat exchanger (GWHE) called ECT-GWHE system: (A) in co-current and (B) in counter-current modes.

III.2.1 Evaporative Cooling Tower

The ECT-GWHE system can work in three different configurations depending on the operating modes of the ECT. Figure III-2 shows the three operating modes of the ECT: (A) Dry mode: In this case the ECT operates without a spray water system; (B) Wet counter-current mode: In this case, the sprayed water and the airflow are in opposite directions. Process fluid and air flow operate in cross-direction; and (C) Wet co-current mode. Most evaporative air coolers include the wet parallel-flow heat exchangers [77]. The airflow is going in the cross-direction of the process fluid. Moreover, the water is injected parallel to the airflow [78].

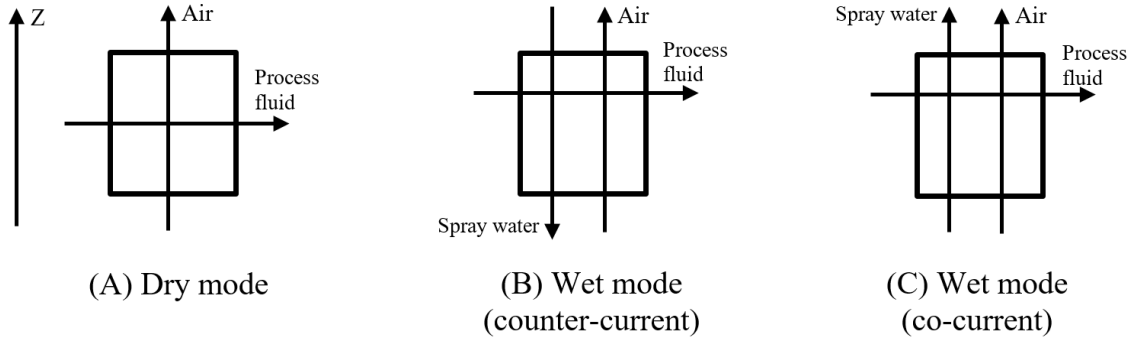


Figure III-2 Fluids directions in the three operating modes of the ECT: (A) Dry mode, (B) Wet counter-current mode and (C) Wet co-current mode.

The studied ECT has the same geometric properties of DCT of the Sortech ACS08 machine [79]. The ECT is a heat exchanger of a finned tube ordered in several rows. The tubes are placed in staggered rows in a goal for ensuring multiple passages per row. Each row contains the same number of tubes. Ambient air at 2.27 m/s is cross-flowing with a process fluid at 0.5 m/s inside the tubes. Table III-1 shows the geometric and thermophysical proprieties of the heat exchanger of the present ECT.

Table III-1 Geometric and thermophysical parameters of the finned tube heat exchanger of present ECT.

Tubes material	Copper
Fins material	Aluminum
Heat transfer area A , m ²	271.43
Tube inner and outer diameters, mm	9-11
Tubes volumes, l	36.67
Length of the finned tubes, mm	2000
Width of the finned tubes, mm	1009
Finned thickness, mm	0.4
Distance between the fins, mm	2.40
Number of fins	305
Longitudinal tube pitch, mm	20
Transversal tube pith, mm	35
Water temperature (spray), °C	24
Water mass flow rate (spray), \dot{m}_w , kg/s	0.187
Air temperature, T_a , °C	48
Mass flow rate of the air, \dot{m}_a , kg/s	4.3
Maximum air velocity, V_a m/s	3.5
Water temperature (serpentine), T_f , °C	41

Water mass flow rate (serpentine), \dot{m}_f , kg/s	0.9308
Number of rows, N	10

III.2.2 Horizontal Ground Water Heat Exchanger

The GWHE is a simple type of horizontal heat exchanger made by PVC tubes such as a plate serpentine shape at a 3m depth inside the ground. It is a secondary system that is connected to the ECT and is used to extract geothermal energy for the purpose of cooling the spray water.

ECT is coupled with a GWHE to decrease the spray water temperature of the outlet of the tower, to guarantee the water temperature to be approximately near the soil temperature. The geothermal characteristics of the ground-water heat exchanger are shown in Table III-2.

Table III-2 The geothermal characteristics of GWHE.

Tube length, m	100
D_i and D_o , m	0.036 - 0.04
λ_t , W/m·K	0.46
\dot{m}_w , kg/s	0.187
λ_s , W/m·K	1.5
T_s , °C	24
T_w , °C	24 – 35

III.3 Calculation Methodology

In this section, the calculation methodologies of (i) the dry cooling mode, (ii) wet cooling mode by spray water and (iii) ground water heat exchanger are explained in detail. The Runge-Kutta method is employed to solve the differential equation systems to calculate the temperature distribution in the tubes of the ECT.

III.3.1 Governing equations of the ECT heat and mass transfer

III.3.1.1 Dry cooling mode

The heat transfer exchange rate can be estimated as:

$$\phi = \dot{m}_f C_{p_f} (T_{f, in} - T_{f, o}) \quad (III-1)$$

The total exchange area of the finned tube heat exchanger is calculated by the Eq.(III-2) [80]:

$$A = \frac{\phi}{U \Delta T_{LM}} \quad (III-2)$$

The following relation describes the equation used for the finned tube heat exchanger:

$$\Delta T_{LM} = \frac{(T_{a, in} - T_{f, o}) - (T_{a, o} - T_{f, in})}{\ln \left(\frac{T_{a, in} - T_{f, o}}{T_{a, o} - T_{f, in}} \right)} \quad (III-3)$$

Eq.(III-4) is used to calculate the heat exchanger's overall heat transfer coefficient [81]:

$$U = \left(\left(h_i^{-1} + \mathfrak{R}_i \right) \frac{S_e}{S_i} + \frac{S_e}{2\pi \lambda_t} \ln \left(\frac{D_e}{D_i} \right) + \frac{1}{\eta_G h_e} + \mathfrak{R}_e \right)^{-1} \quad (III-4)$$

The external heat transfer coefficient of the air side is calculated by the correlation from Wang et al. [82]:

$$h_a = j \rho_a C_{p_a} V_a Pr_a^{-2/3} \quad (III-5)$$

To estimate the heat transfer coefficient for a plate fin profile and staggered tube configuration, the following equation is used to calculate the Colburn factor [83] :

$$j = 0.086 Re_D^{J_3} N^{J_4} \left(\frac{S_a}{D_e} \right)^{J_5} \left(\frac{S_a}{D_h} \right)^{J_6} \left(\frac{S_a}{P_t} \right)^{-0.93} \quad (III-6)$$

Where;

$$Re_D = V_a D_e \rho_a / \mu_a \quad (III-7)$$

$$\left\{ \begin{array}{l} j_3 = -0.361 - \frac{0.042N}{\ln(\text{Re}_D)} + 0.158 \ln \left(N \left(\frac{S_a}{D_c} \right)^{0.41} \right) \\ j_4 = -1.224 - 0.076 \frac{(P_t/D_h)^{1.42}}{\ln(\text{Re}_D)} \\ j_5 = -0.083 + 0.076 \frac{N}{\ln(\text{Re}_D)} \\ j_6 = -5.735 + 1.21 \ln(\text{Re}_D/N) \end{array} \right. \quad \text{(III-8)}$$

Where h_i , is calculated by Eq.(III-9) [84]:

$$h_i = Nu \lambda_w / D_i \quad \text{(III-9)}$$

Nu for the water inside the pipe is predicted as follows [85]:

$$\left\{ \begin{array}{l} \text{For } 0.6 < Pr < 1.5 \rightarrow Nu = 0.0214 (Re^{0.8} - 100) Pr_f^{0.4} (1 + (D_i / L_t)^{2/3}) \\ \text{For } 1.5 < Pr < 500 \rightarrow Nu = 0.012 (Re^{0.87} - 280) Pr_f^{0.4} (1 + (D_i / L_t)^{2/3}) \end{array} \right. \quad \text{(III-10)}$$

Number of fins is calculated per meter of length as follows [83] :

$$N_{fin-m} = 1/(S_a + e) \quad \text{(III-11)}$$

III.3.1.2 Wet counter-current mode

Heat and mass transfer proprieties of the ECT can be determined by mass and energy balance with the following assumptions [86-90]:

- In the range of temperatures taken into consideration, dry air temperature, serpentine water temperature, and specific heat capacity are taken constant.
- Spray water is coupled with a geothermal heat exchanger to ensure a constant temperature.
- Under steady-state situations, the mass and heat transfer processes move in a direction perpendicular to the walls of the tower.
- The specific enthalpy is zero, at 0°C, for the dry air, water and serpentine water.
- Heat transmitted by radiation is not included since the process happens at very low temperature differences.

CHAPTER III: Hybrid cooling tower coupled with a geothermal heat exchanger

- The air at the contact is at the same temperature as the water, and its humidity is at equilibrium.
- The interface of the falling water film has low thermal resistance.

The sensible and latent heat exchange between the air flow and falling water layer causes the change in temperature of the dry air along the wet tube's surface. The energy balance of (i) the serpentine water and (ii) the descending water layer results in the ordinary differential equations (ODEs) given in Eq.(III-12) [91, 92] with the boundary conditions in Eq.(III-13):

$$\left\{ \begin{array}{l} \frac{dT_a}{dA} = \left(\frac{h_c}{\dot{m}_a} + C_{p_{v, sat}} \frac{dw}{dA} \right) \frac{(T_w - T_a)}{C_{p_m}} \\ \frac{dT_w}{dA} = - \frac{1}{\dot{m}_w C_{p_w}} \left[h_c (T_w - T_a) + \dot{m}_a \frac{dw}{dA} (C_{p_{v, sat}} T_a + C_{p_w} T_w + H_v) + U (T_w - T_f) \right] \\ \frac{dT_f}{dA} = \frac{U (T_w - T_f)}{\dot{m}_f C_{p_f}} \\ \frac{dw}{dA} = \frac{h_m}{\dot{m}_a} (w_{sat}(T_w) - w_a) \end{array} \right. \quad \text{(III-12)}$$

With the boundary condition.

$$\left\{ \begin{array}{l} T_a(z=0) = T_{a, in} \\ T_w(z=L) = T_{w, in} \\ T_f(z=L) = T_{f, in} \\ w(z=0) = w_{in} \end{array} \right. \quad \text{(III-13)}$$

The specific heat capacity of humid air C_{p_m} is defined by Eq. (III-14):

$$C_{p_m} = C_{p_a} + w C_{p_{v, sat}} \quad \text{(III-14)}$$

The water mass, evaporated per unit of the water-vapor interface of the heat exchange area, is referred by the term dw/dA in Eq. (III-12). The saturated air humidity ratio is estimated by Eq. (III-15):

$$w_{sat}(T_w) = 0.622 \frac{P_{sat}(T_w)}{P_a - P_{sat}(T_w)} \quad (\text{III-15})$$

The saturation pressure $P_{sat}(T_w)$ of humid air is defined as:

$$P_{sat}(T_w) = \exp \left(23.3265 - \frac{3802.7}{T_w + 273.18} - \left(\frac{472.68}{T_w + 273.18} \right)^2 \right) \quad (\text{III-16})$$

Wet-bulb temperature of humid air can be determined from the following formulas [93] :

$$T_{wb} = 2.265 (1.97 + 4.3T_a + 10000w_{sat})^{0.5} - 14.85 \quad (\text{III-17})$$

Using the description of air humidity ratio, the following formula is used to evaluate the rate of change of cooling water mass \dot{m}_w per unit of heat exchange area:

$$\frac{d\dot{m}_w}{dA} = \dot{m}_a \frac{dw}{dA} \quad (\text{III-18})$$

III.3.1.3 Wet co-current mode

Finally, the parallel-flow configuration based on ODEs constituted as follows [89]. Assumptions are the same as above and only the direction of flow is different.

$$\left\{ \begin{array}{l} \frac{dT_a}{dA} = \left(\frac{h_c}{\dot{m}_a} + Cp_{v,sat} \frac{dw}{dA} \right) \frac{(T_w - T_a)}{Cp_m} \\ \frac{dT_w}{dA} = \frac{1}{\dot{m}_w Cp_w} \left[h_c (T_w - T_a) + \dot{m}_a \frac{dw}{dA} (Cp_{v,sat} T_a + Cp_w T_w + Hv) + U (T_w - T_f) \right] \\ \frac{dT_f}{dA} = \frac{U (T_w - T_f)}{\dot{m}_f Cp_f} \\ \frac{dw}{dA} = \frac{h_m}{\dot{m}_a} (w_{sat}(T_w) - w_a) \end{array} \right. \quad (\text{III-19})$$

with the boundary conditions:

$$\begin{cases} T_{a(z=0)} = T_{a,in} \\ T_w(z=L) = T_w,in \\ T_f(z=L) = T_f,in \\ W(z=0) = W_{in} \end{cases} \quad (\text{III-20})$$

III.3.2 Coefficient of heat transfer in the ECT

III.3.2.1 Smooth tube case

The following equation, Eq.(III-21), describes h_c between the air stream and falling water film with $L_e=1$ [94].

$$h_c = h_m C p_m \quad (\text{III-21})$$

where h_m is the coefficient of mass transfer determined by the following relation:

$$h_m = 6 \times 10^{-8} Re_a^{0.9} Re_w^{0.15} D_0^{-1.6} \quad (\text{III-22})$$

Here, Re_w is the Reynold number of the sprayed water stream.

The following equation determines the total heat transfer coefficient, U , estimated between the water film, the tube walls and the serpentine water [87, 95]:

$$U = \left(\frac{r_o}{r_i} \frac{1}{h_f} + \frac{r_o}{k} \ln \left(\frac{r_o}{r_i} \right) + \frac{1}{h_c} \right)^{-1} \quad (\text{III-23})$$

where the Dittus-Boelter relation provides the value of h_f , the convection heat transfer coefficient of serpentine water [96]:

$$h_f = \left(\frac{0.023 Re_f^{0.8} Pr_f^{0.3} \lambda}{D_i} \right) \quad (\text{III-24})$$

III.3.2.2 Finned tube case

A technique for analysing the properties of heat and mass transmission has previously been presented for finned tube heat exchangers under humidifying conditions. The overall heat transfer coefficient U , in this case, is changed concerning the geometrical dimensions of both fins and tubes [78, 97].

$$U = \left(\left(h_i^{-1} + \mathfrak{R}_i \right) \frac{S_e}{S_i} + \frac{S_e}{2\pi\lambda_t} \text{Ln} \left(\frac{D_e}{D_i} \right) + \frac{1}{\eta h_a} + \mathfrak{R}_e \right)^{-1} \quad (\text{III-25})$$

The coefficient of heat transfer of the air, h_a , is affected by the air velocity between the fins. The Colburn factor j is used to calculate h_a for an array of staggered tubes and a herringbone-wavy fin profile [98].

$$j = 0.394 \text{Re}_D^{-0.357} \left(\frac{Ph_t}{Ph_l} \right)^{-0.272} \left(\frac{S_{fin}}{D} \right)^{-0.205} \left(\frac{X_{fin}}{P_d} \right)^{-0.558} \left(\frac{P_d}{S_{fin}} \right)^{-0.133} \quad (\text{III-26})$$

$$h_a = \lambda j \text{Re}_d \text{Pr}^{0.33} / D \quad (\text{III-27})$$

The equation below can be used to determine the surface of the wavy fins [98].

$$A_f = \left[1 + \left(\frac{P_d}{X_f} \right)^2 \right] A'_f \quad (\text{III-28})$$

III.3.3 Heat transfer modelling of the GWHE

The following assumptions were used to modelling the GWHE system based on steady-state analysis:

- The horizontal GHE's maximum operating time is limited to a few hours, even during the hottest parts of the day.
- The soil is uniform around the heat exchanger and with a constant conductivity.
- The water flow is steady through the heat exchanger length.
- The thermophysical characteristics of water are estimated using correlations obtained from the literature.

CHAPTER III: Hybrid cooling tower coupled with a geothermal heat exchanger

- The soil's characteristics are isotropic and that the soil and pipe are in perfect contact.

The resolution of the heat transfer equation serves as the foundation for the calculation model, as shown in Figure III-3 [99-101]:

$$m C_p (T(x) - T(x + dx)) = \frac{T(x) - T_s}{R_{th}} dx \quad (\text{III-29})$$

Here, R_{th} is the overall thermal resistance of the water soil heat exchanger between the pipe water and surrounding soil, as measured by the relation (III-30) [100-102]:

$$R_{th} = R_w + R_t + R_s \quad (\text{III-30})$$

$$R_w = \frac{1}{h_i P_i} \quad (\text{III-31})$$

Where

$$h_i = Nu \lambda_w / d_i \quad (\text{III-32})$$

According to Equation (III-33), the following relations are considered:

Where $2300 < Re < 10^5$ and $1.5 < Pr < 500$.

$$Nu = 0.012 (Re^{0.87} - 280) Pr^{0.4} \left(1 + (d_i / L)^{0.66} \right) \quad (\text{III-33})$$

The thermal resistance of the tube, R_t , and the thermal resistance of the soil annulus, R_s , are given by Eqs. (III-34) and (III-35), respectively [99-101].

$$R_t = \frac{\ln(r_e / r_i)}{2 \pi \lambda_t L} \quad (\text{III-34})$$

$$R_s = \frac{\ln(r_s / r_e)}{2 \pi \lambda_s L} \quad (\text{III-35})$$

CHAPTER III: Hybrid cooling tower coupled with a geothermal heat exchanger

The suitable thickness of the soil annulus has been investigated in several works in the literature [101, 103-105]. The result of all these studies is that the soil's thickness varies with how long the heat exchanger is working. The GWHE operation is limited to a few hours at most and r_s is considered equal to $2r_i$ (fig. III-3).

After dividing Eq. (29) with dx , the equation can be rewritten as follows [99-101]:

$$-m C_p \frac{dT}{dx} = \frac{T(x) - T_s}{R_{th}} \quad (\text{III-36})$$

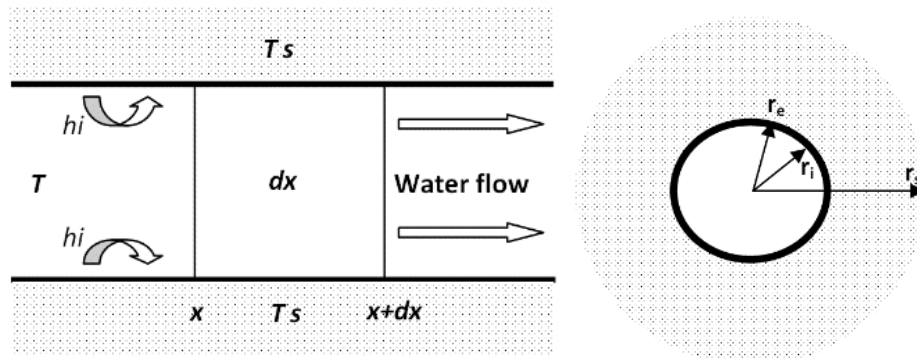


Figure III-3 The thermal balance of a horizontal geothermal heat exchanger (Ground/Water), GWHE.

Then

$$T(x) = C_1^{st} \exp\left(\frac{-x}{\dot{m} C_p R_{th}}\right) + C_2^{st} \quad (\text{III-37})$$

By considering boundary conditions, we find the constants A and B:

$$\text{For } x \rightarrow \infty, T(x) = T_s \rightarrow C_2^{st} = T_s$$

$$\text{For } x \rightarrow 0, T(x) = T_0 \rightarrow C_1^{st} = T_0 - T_s$$

$$T(x) = (T_0 - T_s) \exp\left(\frac{-x}{\dot{m} C_p R_{th}}\right) + T_s \quad (\text{III-38})$$

Also, $T(x)$ can be written as:

$$T(x) = (T_0 - T_s) \exp\left(\frac{-x}{\rho C_p S V R_{th}}\right) + T_s \quad (\text{III-39})$$

Eq. (III-40) represents the pressure drop across the full tube length. This is based on the total of the tube's pressure loss [106].

$$\Delta P_t = \Delta P_{lin} + \Delta P_{sing} + \Delta P_{i-o} \quad (\text{III-40})$$

To determine the linear pressure losses, Eq. (III-41) is used:

$$\Delta P_{lin} = \Lambda \rho_w L \frac{v_w^2}{2d} \quad (41)$$

Laminar or turbulent flow characteristics affect how the loss ratio of load Λ is calculated in Eq.(III-42) [106]:

For $2100 < Re < 10^5$, the Blasius formula is used:

$$\Lambda = 0.3164 Re^{-0.25} \quad (\text{III-42})$$

The following formulas are used to estimate singular and inlet-outlet pressure losses [106]:

$$\Delta P_{sing} = \xi \rho_w \frac{v_w^2}{2} \quad (\text{III-43})$$

$$\Delta P_{i-o} = \frac{3}{4} \rho_w v_w^2 \quad (\text{III-44})$$

III.3.4 Solving procedure

The governing equations, Eqs. (III-12) and (III-19), with Eqs. (III-13) and (III-20) as boundary conditions are used to estimate the heat and mass transfer in the ECT. These equations are solved numerically in the literature [87, 107] by using Runge Kutta 4th order integration method. The analytical method is used to predict the distribution of the temperature in the tube rows of the ECT. In this study, the Runge-Kutta is also employed to solve the ODE systems for the counter-current and co-current flow arrangements as shown in Figure III-4.

CHAPTER III: Hybrid cooling tower coupled with a geothermal heat exchanger

Here ε is the convergence criterion of the calculation, and it becomes as follows:

$$\varepsilon_1 = \frac{\Delta W}{W}, \varepsilon_2 = \frac{\Delta T_a}{T_a}, \varepsilon_3 = \frac{\Delta T_w}{T_w}, \varepsilon_4 = \frac{\Delta T_f}{T_f} \quad (\text{III-45})$$

For $i=1,4$ then $\varepsilon = \min(\varepsilon_i)$

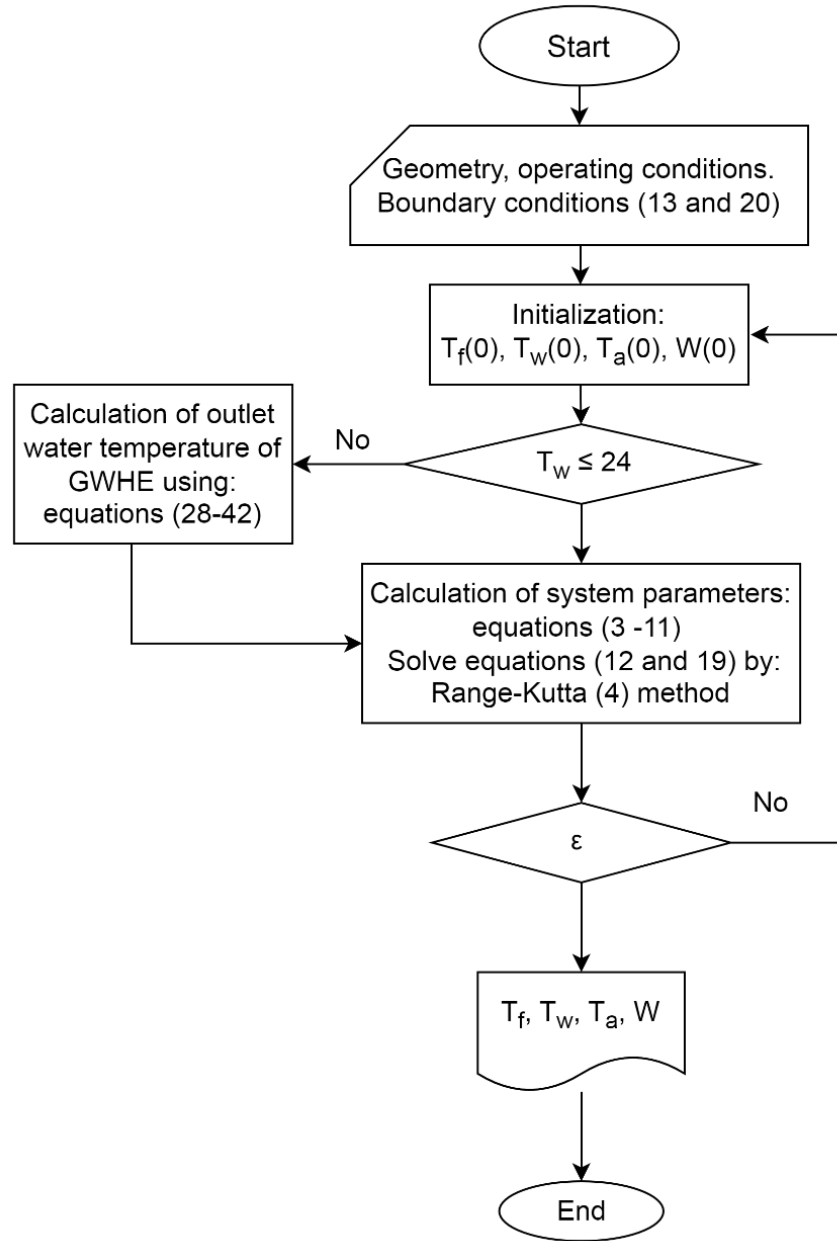


Figure III-4 Flowchart diagram describing the solving procedure of the ECT-GWHE system.

III.4 Verification and validation of the calculation methodology

III.4.1 Smooth tube case

For WCT in the case of the tube without fins under the configuration counter-current mode, the spray water crosses the heat exchanger from the top to the bottom while the air and the process fluid flow in opposite directions as shown in Figure III-2B.

In Table III-4, a comparison is made between the calculation results of Papaefthimiou et al. [87] and the present numerical results for process fluid T_f . This comparison is made for the same essential inlet conditions as given in Table III-3.

Table III-3 Geometry and thermophysical characteristics of the heat exchanger used by Papaefthimiou et al. [87].

Tubes material, -	Copper	$T_{w-spray}$, °C	20
A, m ²	27	$\dot{m}_{w-spray}$, kg/s	1.85
D_{i-o} , m	0.015-0.0191	\dot{m}_a , kg/s	2.07
Lt, m	0.913	T_{pfi} , °C	35
N,	16	\dot{m}_{pf} , kg/s	2.67
N_{t_rows} ,	31	$D_{t-pitch}$, mm	1.5

Table III-4 Comparison between calculation results of Papaefthimiou et al. [87] and present numerical results for process fluid T_f .

Wetted tube surface (m ²)	Counter-current mode		Difference error % (Counter-current)
	T_f (°C), Papaefthimiou et al	T_f (°C) present work	
0	15.60	15.6	0
1.8	15.32	15.34	0.10
3.6	15.11	15.15	0.17
5.4	14.96	14.99	0.20
7.2	14.83	14.86	0.19
9.05	14.72	14.75	0.14
10.8	14.63	14.64	0.06
12.6	14.54	14.54	0.04

14.4	14.46	14.44	0.17
16.3	14.38	14.33	0.33
18.0	14.29	14.22	0.50
19.9	14.20	14.10	0.68
21.7	14.09	13.97	0.88
23.5	13.98	13.83	0.19
25.3	13.85	13.68	1.30
27.0	13.72	13.51	1.53

III.4.2 Finned tube case

The air and the spray water flow similarly as detailed in subsection III-4.1. The authors point out that $z = 10$ and $z = 0$ indicate respectively the bottom and the top rows, which represents the boundary conditions in Eqs. (III-13) and (III-20).

The numerical results were validated with the experimental study conducted by Wiksten and Assad [108] for the same geometrical and thermophysical parameters (Table III-5). The experimental setup consists of a heat exchanger with finned-tube placed beneath a spray water system. The validation results with the measurements of Wiksten and Assad [108] are illustrated in Table III-6, where the highest relative error was found to be 6.71%.

Table III-5 Geometrical and thermos-physical parameters of the finned-tube heat exchanger of Wiksten and Assad [108]

Tubes material, -	Copper	$T_{w-spray}$, °C	17.3
Material of fins, -	Aluminum	T_a , °C	24
A, m ²	270.6	$\dot{m}_{w-spray}$, kg/s	0.6714
D_{i-o} , mm	10-12	\dot{m}_a , kg/s	0.902
Vt, liter	37	T_{pfi} , °C	25.2
Ph_l , mm	29.4	\dot{m}_{pf} , kg/s	0.375
Ph_{tr} , mm	34	$D_{t-pitch}$, mm	1.5

Table III-6 Comparison between predicted and experimental values of Wiksten and Assad [108] for wavy finned-tube heat exchanger temperatures.

Row-level	T _f (°C) (exp)	T _f (°C) (calc)	Relative Error %	T _a (°C) (exp)	T _a (°C) (calc)	Relative Error %	T _w (°C) (exp)	T _w (°C) (calc)	Relative Error %
0	25.20	25.20	0	17	16.51	2.8	17.9	17.79	0.60
1	22.47	22.89	1.84	16.60	16.17	2.55	17.13	16.93	1.10
2	20.44	21.03	2.90	16.4	16.00	2.41	16.64	16.24	2.35
3	19.07	19.54	2.47	16.25	16.01	1.465	16.29	15.68	3.69
4	18.01	18.34	1.813	16.29	16.22	0.42	15.97	15.24	4.56
5	17.30	17.37	0.38	16.48	16.66	1.13	15.82	14.89	5.84
6	16.72	16.60	0.67	16.98	17.40	2.49	15.56	14.65	5.79
7	16.33	16.01	1.90	17.77	18.49	4.07	15.62	14.57	6.71
8	16.09	15.61	2.98	19.17	19.99	4.30	15.66	14.75	5.77
9	16.05	15.46	3.68	21.24	21.9	3.14	16.25	15.53	4.38
10	16.40	15.79	3.77	24	24	0	17.8	17.8	0

III.5 Results and discussion

The results of the design of an ECT coupled to GWHE are presented in this section in detail based on the above calculation methodology. The GWHE operates only for short periods and do not exceed 7 hours of continuous operation.

III.5.1 Water temperature discussion

When there is a high ambient temperature, the ECT employs the addition of water spray to the air flow. This transported the energy into the air by improving the heat transfer through convection and evaporation process. Eq. (III-18) can be used to estimate the optimal spray water flow rate, which is approximately 0.187 kg/s as shown in Table III-1.

In addition, when the temperatures of ambient air and inlet process are high, the optimal inlet spray water temperature is estimated to be approximately equal to the air wet bulb temperature at the inlet [87]. With air temperatures as high as 48°C and relative humidity as low as 9%, the initial wet bulb temperature range is around 22.5°C. As a result of the predetermined estimation, the effective spray water temperature was determined according to the soil temperature range from 22°C to 24°C.

CHAPTER III: Hybrid cooling tower coupled with a geothermal heat exchanger

Figure III-5 represents the effect of the temperature of the spray water on the ECT temperature after four tests as shown in Table III-7 with a spray water mass flow rate of 0.187 kg/s. Since this spray water was injected directly into the ECT, it did not pass into the GWHE before. As a result, the spray water temperature is an important parameter because when the spray water temperature increases, the ECT's performance decreases.

The temperature of the spray water plays a crucial role in determining the specific humidity of the air. As the temperature of the sprayed water increases, the evaporation rate of the water also increases. This results in a higher evaporation mass flow rate, which means more water molecules are transitioning from a liquid state to a gaseous state in a given period of time.

When the water evaporates, it increases the amount of moisture in the air, leading to an increase in the specific humidity of the air. The amount of water vapor in a given volume of air is measured by the specific humidity, which is usually given as a ratio of the mass of water vapor to the total mass of air.

As the temperature of the sprayed water continues to increase, the rate of evaporation will also increase, leading to a further increase in the specific humidity of the air. This highlights the importance of controlling the temperature of the spray water in applications where the specific humidity of the air needs to be accurately controlled or measured, such as in industrial processes or meteorological studies.

Table III-7 The inlet flow temperatures of ECT.

Test	Ta °C	Tf °C	Tw °C
1	48	41	18
2	48	41	24
3	48	41	30
4	48	41	38

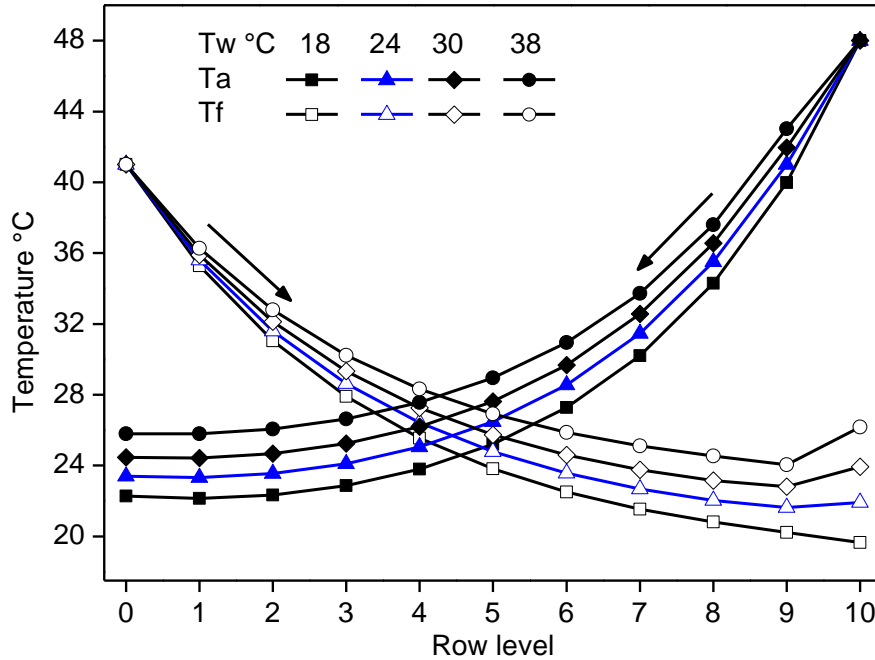


Figure III-5 Effect of the temperature of the spray water on the process fluid temperature for different spray water temperatures, $\dot{m}_w = 0.187$ kg/s.

III.5.2 Thermal design of the GWHE

Experimental evidence has shown that elevating spray water temperature results in an increase in water consumption. Thus, a part of the spray water is evaporated and the rest returns to the water tank. When the sprayed water temperature is hot, the rate of evaporation increases, leading to a higher evaporation mass flow rate. This means that more water is transitioning from a liquid state to a gaseous state in a given period of time, and the amount of residual water in the tank decreases [109]. The effect of pre-cooling the spray water system on the specific humidity of the air is related to the temperature of the spray water. As mentioned, the temperature of the spray water is decisive for determining the rate of evaporation of the water, and consequently the specific humidity of the air. By pre-cooling the spray water, the temperature is reduced, leading to a lower evaporation mass flow rate and a corresponding decrease in the specific humidity of the air. Besides, several factors can affect the maximum achievable heat flow rate, such as the geometry of the heat exchanger, the thermal properties of the soil and the operating conditions. Designing and installing a ground heat exchanger system should take into account the specific conditions and requirements of each location to ensure optimal performance and efficiency. Generally, the

maximum thermal cooling power produced by one meter of the ground heat exchanger is around the value of 100 W/m [99, 110]. Thereby, the optimal length of the geothermal heat exchanger, which will ensure a constant spray water temperature, is estimated based on a critical water temperature value of 35 °C and mass flow rate of 0.187 kg/s. Figure 7 shows the variation in water temperature along the axis of the geothermal heat exchanger tube and the effect of inlet water temperatures. These results correspond to an outlet temperature of 24°C; equal to the ground temperature when the GWHE operates for a short period of 7 hours or less to avoid soil saturation [99, 110]. The results obtained from Figure III-6 indicated that the length of the exchanger tube must be less than 100m. Melhegueg et al. [111], for the same reason, represent the operation of GHE for a short period of continuous operation (less than 70 hours) where the soil loading dominates the soil recovery.

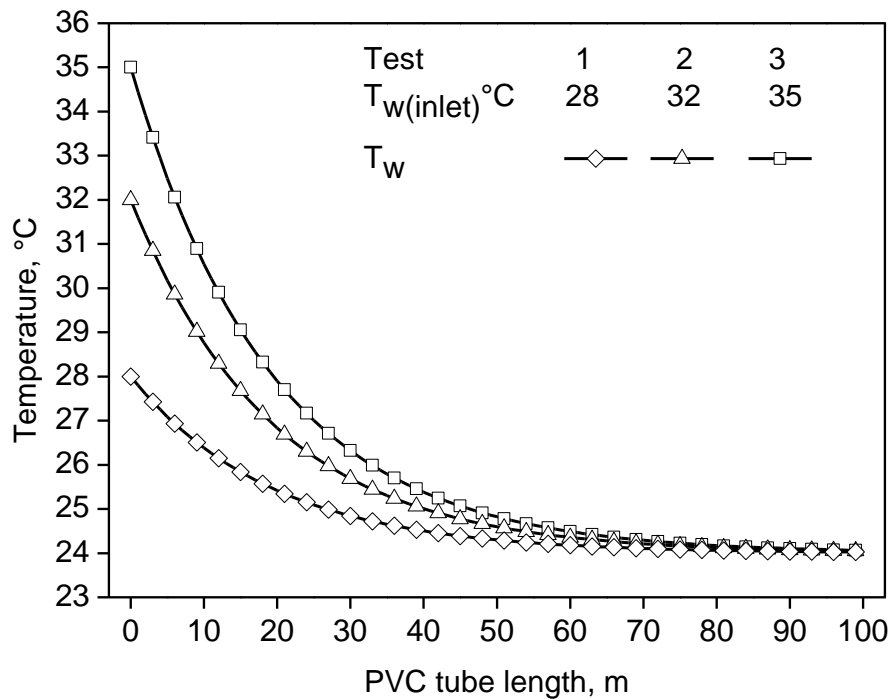


Figure III-6 Water temperature variation in the ground heat exchanger with different water inlet temperatures for a mass flow rate of $\dot{m}_w = 0.187$ kg/s.

III.5.3 ECT-GWHE system operation

Figure III-7 presents the temperature changes in the dry mode (A). Immediately, we note an increase in the temperature of the process fluid. On the other hand, the air temperature drops from

48°C to 46°C, which means poor functioning of the cooling tower system. This directly results in a malfunction in the adsorption cooling system.

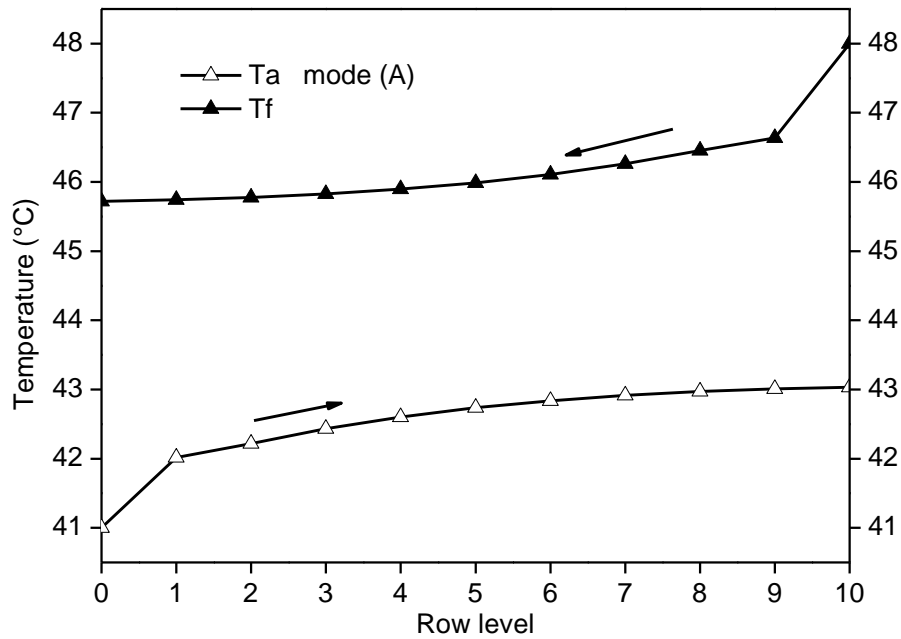


Figure III-7 ECT-GWHE temperature variations in dry mode (A), without spray water circulation.

The ODEs, Eqs. (III-12) and (III-19) and associated boundary conditions are numerically solved by the Runge-Kutta 4th order method [112] to predict the thermal analysis under the effect of the spray water system.

Figures III-8 and III-9 show the variation in the process fluid temperature T_f , air temperature T_a , and spray water temperature T_w . The process fluid and air temperature are reduced and reached to the operating limits of the adsorption cooling system (<32 °C). However, the inlet spray water temperature differs slightly from the value at the outlet because the exit water is circulated through the water tank at the bottom of the tower before entering the GWHE. If the spray water temperature exceeds 25 °C, it is entered directly into the geothermal heat exchanger and then used in the spray system again.

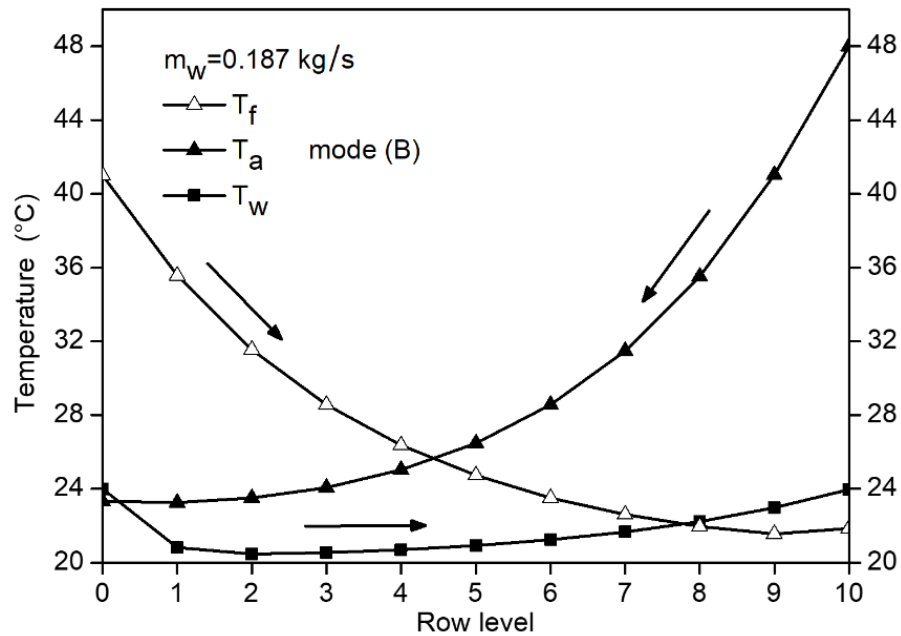


Figure III-8 ECT-GWHE temperature variations in counter-current mode (B), $\dot{m}_w = 0.187 \text{ kg/s}$, $T_w = 24 \text{ }^\circ\text{C}$.

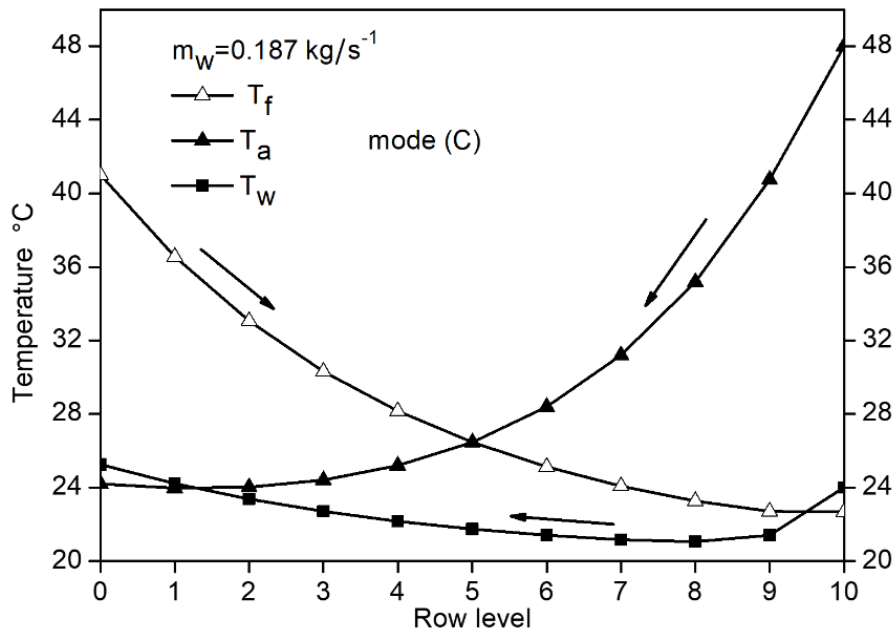


Figure III-9 ECT-GWHE temperature variations in co-current mode (C), $\dot{m}_w = 0.187 \text{ kg/s}$, $T_w = 24 \text{ }^\circ\text{C}$.

III.6 Conclusion

This study presents a technical solution to enhance thermal performance of the ECT by taking the case study of an adsorption cooling machine driven in solar energy in the dry and hot climate of Biskra (Algeria). The objective is to develop a simple calculation methodology to design ECT-GWHE system. Three operation modes of the ECT-GWHE system are investigated, namely: dry mode, wet counter-current mode, and wet co-current mode. The impact of critical ambient air conditions of Biskra city ($T_a = 48$ °C and HR = 9%) on the thermal properties of ECT-GWHE system is examined.

A model was developed to analyse the impact of the surrounding air conditions on the thermal performance. The developed calculation methodology was validated, and a good agreement with experimental and numerical results from the literature were found. Results showed that a GWHE of 70 m of length is sufficient to decrease sprayed water temperature from 35 °C to 24°C. In this case, the proposed ECT-GWHE system can easily decrease the process fluid temperature under the operating limits of the solar adsorption cooling device. When the air temperature reaches 48 °C, the counter-current mode in the ECT gives better performances in the critical ambient air conditions. Consequently, it has been proven that coupling of the two systems (evaporative cooling tower and ground water heat exchanger) is an effective solution to improve the thermal performance of adsorption cooling systems in hot arid and semi-arid regions such as the Biskra region.

IV. CHAPTER IV: Thermal analysis of the performance of a hybrid cooling tower coupled with a geothermal exchanger

IV.1 Introduction

In the present chapter a new combination system is established to improve the performance of the direct evaporative cooler (DEC). Ground-Water Heat Exchanger (GWHE) is coupled to the DEC of a hybrid cooling tower. A mathematical model has been developed and validated to depict the heat and mass transfer that occurs in the DEC between the air and water, as well as between the ground and water in the geothermal heat exchanger. The key variables taken into consideration are the ambient air temperature and the mass flow rate and the temperature of water. The effect of the inlet hot air velocity and temperature, and water mass flow rate, on the evaporated water is investigated. The findings indicate that the mathematical model of a DEC coupled to GWHE predicts optimal characteristics, leading to a reduction in the air temperature from 48°C to 32°C at the heat exchanger inlet of the cooling tower. Results indicate that the coupling proposed in this study is deemed an innovative technical solution to address the dysfunction problem of cooling towers and solar adsorption cooling systems in hot and dry climates.

The present chapter proposes a new application for the shallow ground heat exchanger. The GWHE is used in hot and dry climates as a pre-cooler of the water supplied to the DEC. The objective of this coupling (the GWHE with a DEC) is to better cool the air of the CT of the adsorption system driven by solar energy. In this regard, the thermal analysis of the CT is studied in three cases according to the nature of the cooling air: i) dry CT, ii) CT with air humidified by a DEC iii) CT with air humidified by a DEC coupled to a GWHE ensuring a constant water temperature for the DEC.

IV.2 System description

Figure IV-1 shows the new DEC proposed in this study which consists of three principal elements: i) DCT in its basic shape, ii) Pad cooling (direct evaporative cooler), in the present work

CHAPTER IV: Thermal analysis of the performance of a hybrid cooling tower coupled with a geothermal exchanger

the GLASdek 7090 type is proposed for the pad, iii) The third element is the GWHE, which is the new element proposed in this study.

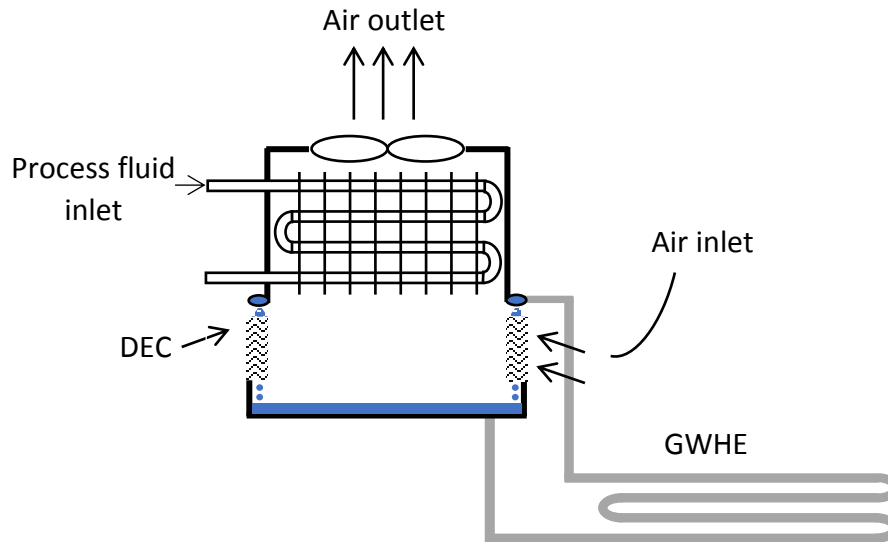


Figure IV-1 Schematic description of the new DEC tower.

IV.2.1 Dry cooling tower (DCT)

A dry cooling tower of the ACS 08 adsorption machine is considered an example for this study [113]. According to Kheireddine et al. [79], the maximum operating air temperature of the dry cooling tower can't exceed 35°C. For that, the FTHE of this cooling tower is responsible for cooling the process fluid in the ACS 08 by ambient air in forced convection to be less than 35°C.

Table IV-1 shows the most important geometric and thermophysical parameters of the FTHE of the present DEC.

CHAPTER IV: Thermal analysis of the performance of a hybrid cooling tower coupled with a geothermal exchanger

Table IV-1 Geometric and thermo-physical parameters of the FTHE of present DEC.

Tubes material, -	Copper	$T_{w-spray}$, °C	24
Fins material, -	Aluminium	T_a , °C	48
A, m ²	271.43	$\dot{m}_{w-spray}$, kg/s	1.12
S_{fin} , mm	2.40	L, mm	2000
D_{i-o} , m	0.009-0.010	\dot{m}_a , kg/s	4.3
L_{tot} , m	576	T_{pfi} , °C	41
N,	10	\dot{m}_{pf} , kg/s	0.9308
N_{t_rows} ,	29	P_t , mm	35

IV.2.2 Direct evaporative cooler (DEC)

DEC is a type of air conditioning system that cools air through the process of evaporation. It operates by passing hot, dry air over a wet surface, where water evaporates and cools the air. DEC's are a cost-effective and energy-efficient cooling solution, particularly in hot, dry climates. In this case, air humidification decreases the temperature of the air entering the FTHE [114, 115].

In the present study, the GLASdek 7090 is used as a pad evaporative cooler in the DEC by using the geometric characteristics as shown in Table IV-2.

Table IV-2 Geometric characteristics of the DEC.

Geometric	(GLASdek 7090)
Width, B, m	0.3048
The height, H, m	1.2192
The thickness, D, m	0.138
The number of pores per unit area, N, m ² /m ³	440
Wave angle, α	45
Wave angle, β	45
Wave height, h, mm	7

CHAPTER IV: Thermal analysis of the performance of a hybrid cooling tower coupled with a geothermal exchanger

IV.2.3 Ground water heat exchanger (GWHE)

A GWHE is coupled to the DEC for the pre-cooling of water prior to its injection into the system. This helps stabilize the water temperature and provides improved performance. The GWHE is constructed using a cylindrical PVC tubes such as a plate serpentine shape at a 3m depth inside the ground, with a diameter of 0.06 meters and a length of 110 meters, and it is directly connected to the DEC system. This design provides a cost-effective and environmentally friendly solution for temperature regulation in DEC. The characteristics of the GWHE are shown in Table IV-3.

Table IV-3 Characteristics of the designed WGHE.

Type of exchanger	GWHE
Tube length, m	110
Outside / inside diameter, m	0.06/0.056
Mass flow rate of water, kg / s	0.081 - 0.243
Soil Thermal Conductivity, W. m ⁻¹ . K ⁻¹	1.5
PVC thermal Conductivity tube, W. m ⁻¹ . K ⁻¹	0.46
Soil temperature, °C	24
Water temperature in the inlet, °C	32

IV.3 Mathematical model

In the current configuration, three parts of calculations are adopted:

(i) The DCT calculation side: The parametric calculation used for the FTHE is the Logarithmic Mean Temperature Difference, LMTD, method developed by the authors in a previous work. This method estimates the difference in temperature between the process fluid at the inlet and the outlet of the heat exchanger [79].

The rate of heat transfer exchanged can be expressed as,

$$\phi_f = \dot{m}_f C p_f (T_{f, in} - T_{f, o}) \quad (IV-1)$$

CHAPTER IV: Thermal analysis of the performance of a hybrid cooling tower coupled with a geothermal exchanger

The total exchange surface of the FTHE can be calculated by Eq.(IV-2) [80] :

$$A = \frac{\phi}{U \Delta T_{LM}} \quad (IV-2)$$

The following relation describes the LMTD method used for the FTHE:

$$\Delta T_{LM} = \frac{(T_{a,in} - T_{f,o}) - (T_{a,o} - T_{f,in})}{\ln \frac{(T_{a,in} - T_{f,o})}{(T_{a,o} - T_{f,in})}} \quad (IV-3)$$

A technique for analyzing the properties of heat and mass transmission has previously been presented for FTHEs under humidifying conditions. The overall heat transfer coefficient U , in this case, changed concerning the geometrical dimensions of both fins and tubes [78, 97]. Eq.(IV-4) is employed to calculate the heat exchanger's overall heat transfer coefficient [81]:

$$U = \left[\left(\frac{1}{h_i} + \mathfrak{R}_i \right) \frac{S_e}{S_i} + \frac{S_e}{2\pi\lambda_t} \ln \frac{D_e}{D_i} + \frac{1}{\eta_G h_e} + \mathfrak{R}_e \right]^{-1} \quad (IV-4)$$

The external heat transfer coefficient of the air side can be calculated by using the following correlation from Wang et al. [82]:

$$h_a = j \rho_a C p_a V_a Pr_a^{-2/3} \quad (IV-5)$$

The Colburn factor in the following equation must be used to calculate the heat transfer for a plate fin profile and staggered tube configuration [83] :

$$j = 0.086 Re^{j^3} N^{j^4} (S_a/D_e)^{j^5} (S_a/D_h)^{j^6} (S_a/P_t)^{-0.93} \quad (IV-6)$$

where;

$$Re = V_a D_e \rho_a / \mu_a \quad (IV-7)$$

CHAPTER IV: Thermal analysis of the performance of a hybrid cooling tower coupled with a geothermal exchanger

$$\begin{cases} j_3 = -0.361 - 0.042N / \ln(Re) + 0.158 \ln \left[N (S_a / D_c)^{0.41} \right] \\ j_4 = -1.224 - 0.076 (P_t / D_h)^{1.42} / \ln(Re) \\ j_5 = -0.083 + 0.076N / \ln(Re) \\ j_6 = -5.735 + 1.21 \ln(Re/N) \end{cases} \quad (IV-8)$$

The internal heat transfer coefficient h_i is calculated as a function of Nusselt number [84]:

$$h_i = Nu \lambda_w / D_i \quad (IV-9)$$

Where the correlation (IV-10) of Nusselt number for water flowing inside the pipe [85].

$$\begin{cases} \text{For } 0.6 < Pr < 1.5 \rightarrow Nu = 0.0214 (Re^{0.8} - 100) Pr_f^{0.4} \left[1 + (D_i / L_t)^{2/3} \right] \\ \text{For } 1.5 < Pr < 500 \rightarrow Nu = 0.012 (Re^{0.87} - 280) Pr_f^{0.4} \left[1 + (D_i / L_t)^{2/3} \right] \end{cases} \quad (10)$$

Number of fins per meter of length is calculated as follows [83] :

$$N_{fin-m} = \frac{1}{(S_a + e)} \quad (IV-11)$$

The heat transfer coefficient of the air side h_a is affected by the air velocity between the fins. And the Colburn factor j is used to calculate the heat transfer for an array of staggered tubes and a herringbone-wavy fin profile [98].

$$j = 0.394 Re_D^{-0.357} \left(\frac{Ph_t}{Ph_l} \right)^{-0.272} \left(\frac{S_{fin}}{D} \right)^{-0.205} \left(\frac{X_{fin}}{P_d} \right)^{-0.558} \left(\frac{P_d}{S_{fin}} \right)^{-0.133} \quad (IV-12)$$

The heat transfer coefficient on the air side is obtained from [98].

$$h_a = \frac{\lambda_a j Re_D Pr^{0.33}}{D} \quad (IV-13)$$

The equation below can be used to determine the surface of the wavy fins [98].

CHAPTER IV: Thermal analysis of the performance of a hybrid cooling tower coupled with a geothermal exchanger

$$A_f = \left[1 + \left(\frac{P_d}{X_f} \right)^2 \right] A'_f \quad (IV-14)$$

(ii) The DEC calculation side: is a semi-analytical model developed by [93, 115]. It is based on energy conservation and heat and mass transfer analysis. This model predicts the heat and mass transfer in the DEC system by using the geometric parameters as shown in Table IV-2.

Inlet boundary conditions to DEC.

$$T_a = T_1, W_a = W_1, D = 0$$

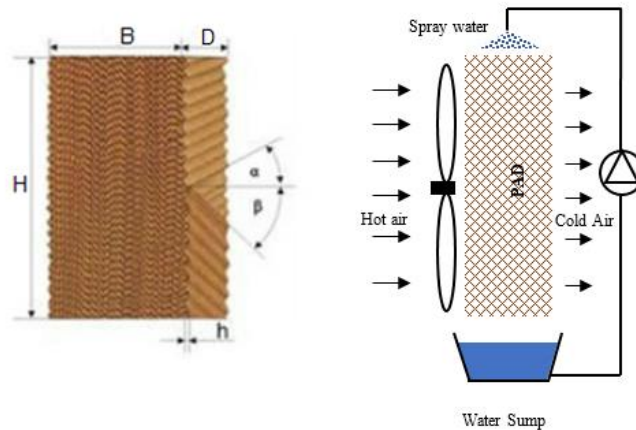
The following equations are used to calculate variations in humidity ratio and temperature of moist air in one direction, x:

$$T_a = T_{sat} + (T_1 - T_w) \exp \left(- \frac{h_c N B H D}{\dot{m}_a C_p} \right) \quad (IV-15)$$

$$W_a = W_{sat} - \frac{C_p}{L_v} (T_1 - T_{sat}) \exp \left(- \frac{h_c N B H D}{\dot{m}_a C_p} \right) \quad (IV-16)$$

Where $\Delta W = W_{sat} - W_a$

Evaporative cooling uses water evaporation to lower air temperature. Figure IV-2 shows a schematic diagram of the process, which involves a water supply, cooling pad, fan. As air passes through the wet pad, water evaporates, cooling the air. This process is energy-efficient and ideal for dry climates with low humidity levels.



CHAPTER IV: Thermal analysis of the performance of a hybrid cooling tower coupled with a geothermal exchanger

Figure IV-2 Schematic diagram of the evaporative cooling process.

(iii) **The GWHE calculation side:** is based on a mathematical model developed to estimate the water temperature variations inside the heat exchanger. The model is grounded on the resolution of the heat transfer equation [99, 100].

The water temperature inside GWHE can be written as:

$$T(x) = (T_0 - T_s) \exp\left(\frac{-x}{rCpSvR_{th}}\right) + T_s \quad (IV-17)$$

GWHE systems use thermal resistances to transfer heat between the earth and the fluid circulating in the heat exchanger. Table 4 lists the equations for the thermal resistances used in GWHE systems. These resistances impact the system's efficiency and performance, making them important to consider during design and installation.

Table IV-4 Equations of thermal resistances in GWHE's system.

Equations	Reference
$R_{th} = R_w + R_t + R_s$	
$R_w = \frac{1}{h_i P_i}, h_i = Nu \lambda_w / d_i$	[100, 102]
$R_t = \frac{\ln(r_e / r_i)}{2\pi\lambda_t L}$	
$R_s = \frac{\ln(r_s / r_e)}{2\pi\lambda_s L}$	
$Nu = 1.64 \left(\left(\frac{L}{D_h} \right) Re Pr \right)^{1/3}$	
	[116]

The transitory soil temperature that is around the pipe is influenced by the thickness of the soil annulus. For this reason, the soil thickness varies with the operation duration of the ground heat exchanger (short duration or long duration) [99, 100, 103, 117, 118]. This soil annulus was assumed to be equal to the radius of the pipe ($r_s = 2r_i$) in the current research since GWHE is

CHAPTER IV: Thermal analysis of the performance of a hybrid cooling tower coupled with a geothermal exchanger

only used for a short time period when the ambient air temperature is over 35 °C, as shown in Figure IV-3.

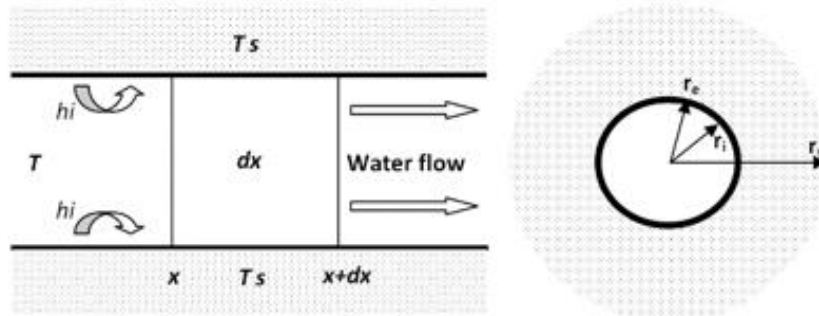


Figure IV-3 Thermal equilibrium of the primary pipe of a GWHE.

IV.4 Comparison and model validation

Table IV-2 shows the geometric characteristics of the porous material of the type (GLASdek 7090), the same characteristics used as data in the developed semi-analytical calculation code to produce a lower humid air temperature of 35°C.

Using heat and mass transfer equations, it is discovered that there is a good agreement between the outlet air temperatures after applying the total conservation equation between the water sprinkled on the top edges of the pad and the dry air through the pores. The comparison of the results is presented in Table IV-5.

Table IV-5 Results and comparison.

Inlet temperature	Outlet temperature			
Ta (dry bulb/ °C)	Ta (wet bulb/ °C) Present calculation	Ta (wet bulb/ °C) Comparison [115]	Ta (wet bulb/ °C) Experimental [115]	Ta (saturated °C)
27.21	22.8152	22.76	22.9	20.15
27.84	22.3745	22.32	22.66	19.06
28.54	23.5662	23.51	23.5	20.55
28.9	23.7644	23.71	23.81	20.65
29.32	22.6717	22.6	22.37	18.64
29.91	23.7971	23.74	23.78	20.09

CHAPTER IV: Thermal analysis of the performance of a hybrid cooling tower coupled with a geothermal exchanger

30.5	23.2541	23.18	22.77	18.86
30.83	23.9452	23.87	24.1	19.77
31.5	27.2608	27.22	27.6	24.69
31.86	25.8778	25.82	25.49	22.25
32.31	24.1802	24.1	23.94	19.25
32.86	23.8587	23.76	24.01	18.4
33.09	25.9935	25.92	25.49	21.69
33.73	27.1004	27.03	27.1	23.08
34.06	25.6127	25.52	25.73	20.49
34.46	27.4445	27.37	27.31	23.19
35.01	25.8904	25.8	25.9	20.36
35.81	28.2965	28.22	27.84	23.74
36.8	30.3572	30.29	30.4	26.45
37.06	28.5691	28.48	28.01	23.42

The continuous repetition of the water misting process on the pad produces a heat transfer between water and hot air, directly leading to a high-water temperature. Consequently, the amount of residual water has decreased. In other words, which involved an increase in water temperature as a cause of an increase in water consumption as experimentally proven in the literature [119, 120].

IV.5 Results and discussions

IV.5.1 Climatically conditions of this study

Since the objective is the adaptation of an adsorption cooler to hot and arid climates especially in Biskra city in the summer, it's necessary to choose the extreme climatic conditions in the year. From infoclimat website [76], it's found that the Biskra's hottest typical day in 2021 is July 1st. The hourly relative humidity and the hourly air ambient temperature of the chosen day is presented in Figure IV-4.

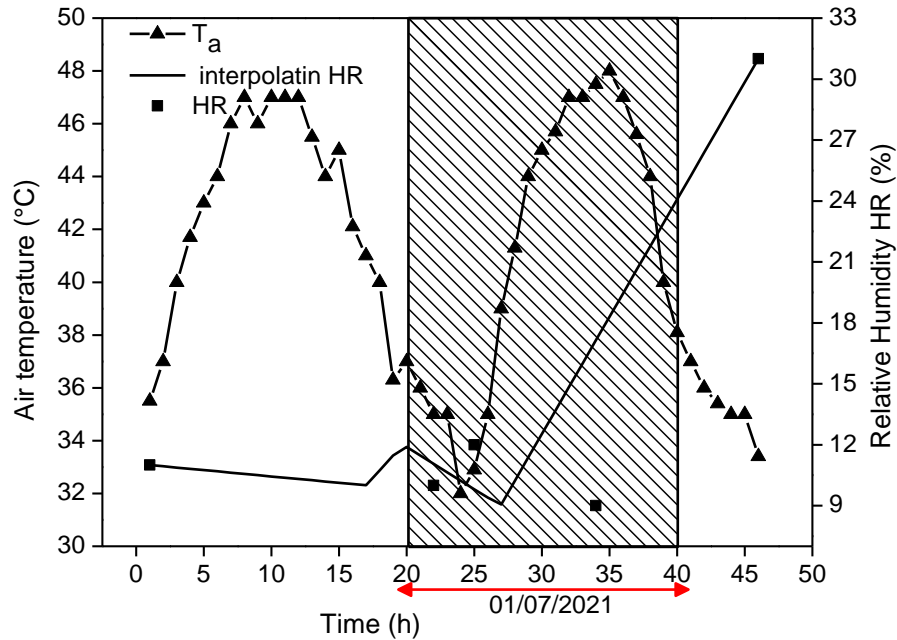


Figure IV-4 The temperature and relative humidity variations of the hottest day in Biskra city in 2021.

IV.5.2 GWHE thermal design

Table 3 shows the different parameters of the GWHE. Using Eq. (IV-3), the ground water heat exchanger dimensions required to cool the water for re-injection within the pad are calculated based on the temperature of the inlet water and the mass flow of the water.

This test was executed in the climatic conditions of Biskra region. By assumptions, we consider the temperature of the water leaving the pad is equal to the temperature of the air outlet, and the temperature of the water re-injected into the pad is equal to the soil temperature.

The temperature of the water leaving the pad has been estimated as the critical temperature of the system for three different water flow rates (0.081, 0.162, and 0.243 kg/s). It is worth mentioning that the temperature of the ground beyond 3 m remained relatively stable, fluctuating between 22 and 24 °C. Figure 5 indicates that as the water flow rate increases, the water outlet temperature also increases, peaking at 0.243 kg/s. The rise in water velocity results in a higher outlet water temperature, primarily due to the reduction in water residence time in the GWHE tubes. In case there is a requirement to augment the water flow within GWHE, using a satisfactory

CHAPTER IV: Thermal analysis of the performance of a hybrid cooling tower coupled with a geothermal exchanger

low flow rate and increasing the number of GWHEs would allow for the desired low temperature and higher water flow to be attained.

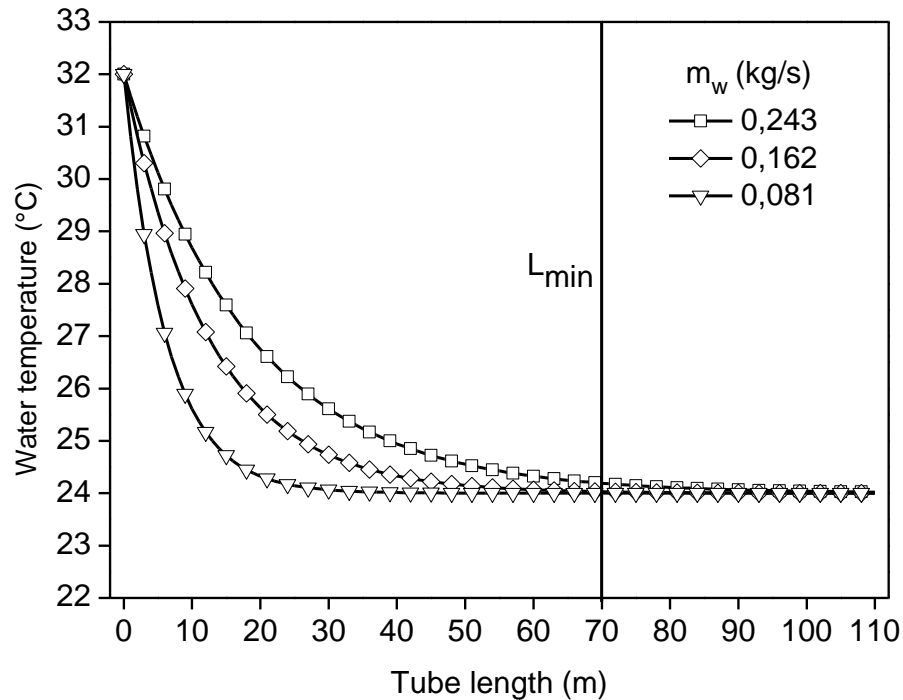


Figure IV-5 Variation of water temperature along the geothermal heat exchanger with different mass flow rates.

Figure IV-6a illustrates the impact of hot air temperature on the process fluid within the DCT. The dysfunction of the system was identified through the observation of an increase in process fluid temperature when the DEC and SWS were not activated.

CHAPTER IV: Thermal analysis of the performance of a hybrid cooling tower coupled with a geothermal exchanger

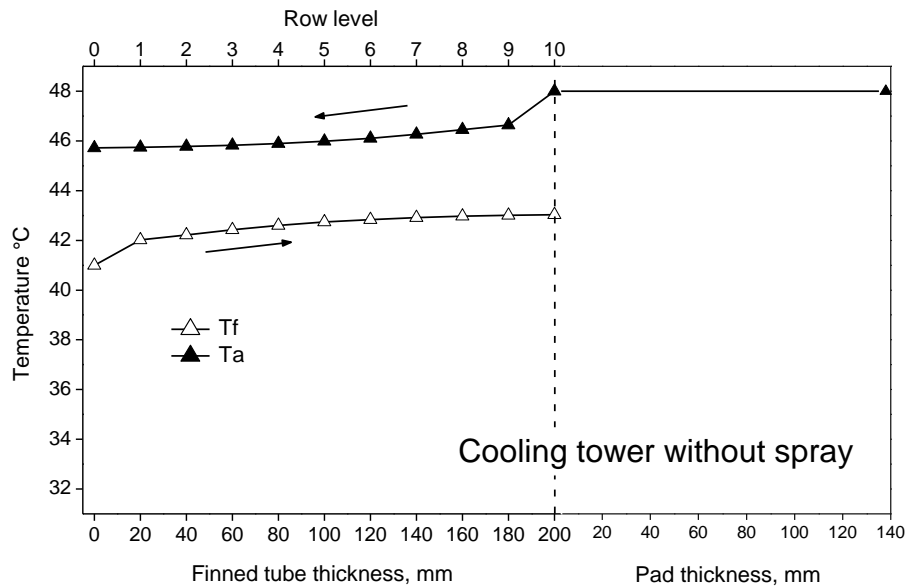


Figure IV-6 a) The effect of hot air temperature on process fluid within the DCT.

Figure IV-6b shows the calculated outlet air temperature from the DEC system compared with the ambient inlet temperature. As seen, the outlet air temperature is always lower than the inlet temperature, and the difference between the two increases with the increasing ambient temperature. This can be explained by the high ambient air temperature leading to more water evaporation and then high performance. From the results obtained from Figure IV-6b, it is clear that the proposed system (GWHE coupled to DEC system) can maintain the temperature of the air below the functioning limits of DCT in hot and dry climates.

CHAPTER IV: Thermal analysis of the performance of a hybrid cooling tower coupled with a geothermal exchanger

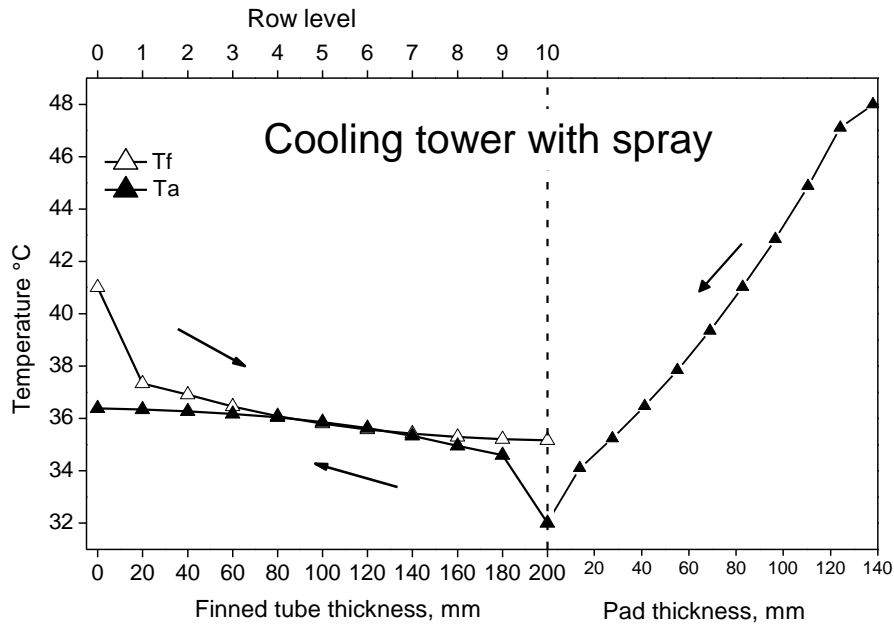


Figure 6b The variation of the process fluid and air temperature within DEC in wet mode.

Figure IV-7 represents the variation of the humidity ratio during 24 hours of the hot day in the city of Biskra. This variation is related to the ambient air temperature and the relative humidity at the pad inlet. Therefore, at the outlet, the humidity is increased after the water evaporates, and reached its maximum value at the minimum value of the relative humidity at the inlet. This can be explained that during lower relative humidity days, the air is relatively drier, meaning it has less moisture content. As the air enters the direct evaporative cooler, it has a greater capacity to absorb water vapor due to its lower moisture content. As a result, more water evaporates into the air, which leads to greater cooling of the air. This, in turn, leads to a greater reduction in the outlet air temperature, making it possible to reach minimum temperatures.

CHAPTER IV: Thermal analysis of the performance of a hybrid cooling tower coupled with a geothermal exchanger

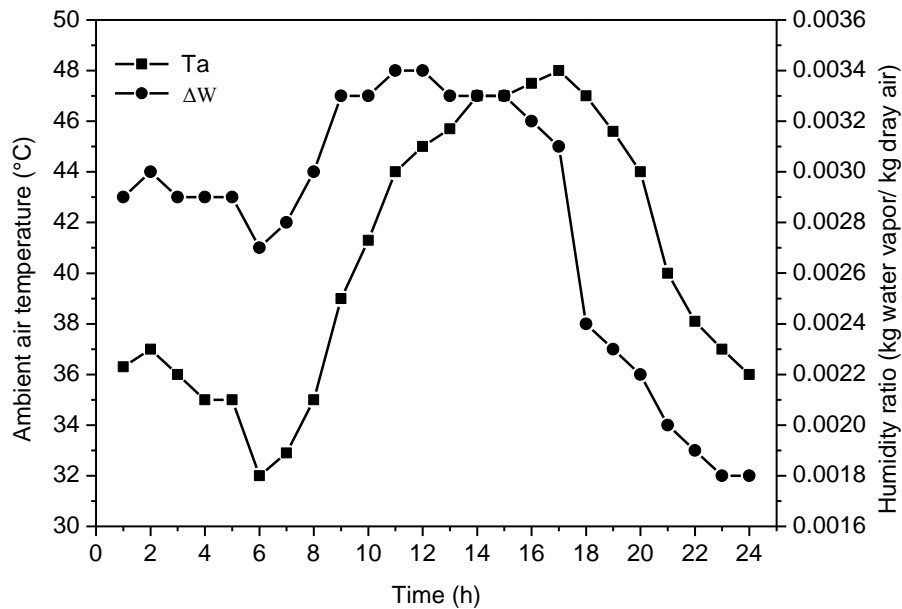


Figure IV-7 Variation of ambient air temperature and humidity ratio for 24 hours (July 1st 2021).

Figure IV-8 represents the effect of heat and mass transfer between water and dry air. In the present study, we created an optimal system by increasing the performance of DEC by choosing the perfect values of water temperature, air velocity, and pad thickness. Water temperature is directly related to soil temperature, it varied between 22°C and 24°C, which is roughly constant during the summer season. However, GWHE ensures a constant water temperature for the DEC. On the other side, the optimal water temperature is 2.5°C upper than the inlet wet bulb temperature, and air velocity is 2 m/s, as experimentally verified by Kabeel et al. [119].

The entraining wet bulb temperature in the present study varied between 14 °C as the minimum and 27 °C as the maximum, with the relative humidity varying between 9% and 31%, as shown in Figure IV-4.

At a high ambient air temperature of 48 °C, the maximum evaporated water mass flow rate is 10.8 kg/h, demonstrating that increasing ambient temperature causes progressive water consumption due to evaporation, as shown in Figure 8.

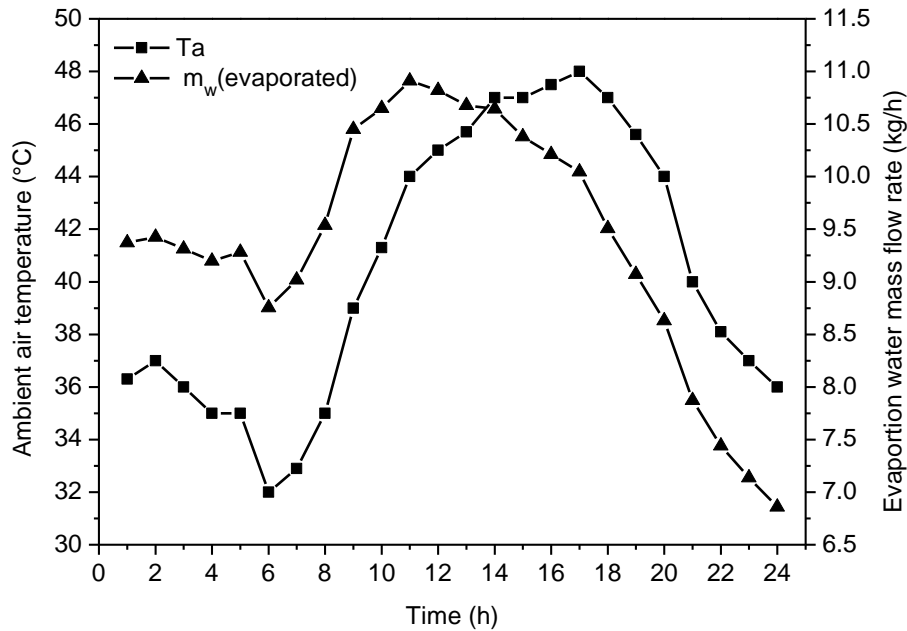


Figure IV-8 Evaporation water mass flow rate for 24 hours of the hot day (July 1st 2021) in Biskra city.

IV.6 Conclusion

The current study focused on the adaptation of adsorption cooling systems to hot and arid climates, especially in the region of Biskra (Algeria). A solar adsorption chiller with a DCT obtained from the literature are taken as an example of study. Besides, the thermal analysis of the heat and mass transfer in DEC is investigated. As a new application, the DEC was connected to a GWHE to lower the inlet air temperature to the DCT. The objective is to enhance the performance of the cooling tower and the whole solar adsorption cooling system in general.

The analysis shows that the speed of the air inlet and humidity are two factors influencing the DEC's cooling efficiency. For the amount of air needed, the front air speed of the direct evaporative cooler module should be about 2 m/s. At a high ambient air temperature of 48°C, the maximum evaporated water mass flow rate is 10.8 kg/h.

The GWHE is an important element to pre-cool the water used by DEC for cooling hot and dry air in the Saharan region. GWHE is ensuring the operational continuity of the hybrid cooling tower in critical conditions where air and water are hot. Finally, this type of coupling presented in

CHAPTER IV: Thermal analysis of the performance of a hybrid cooling tower coupled with a geothermal exchanger

this paper can be considered an innovative technical solution for the dysfunction problem of cooling towers and solar adsorption cooling systems in general in hot and dry climates.

v. CHAPTER V: New evaporative hybrid cooling tower coupled with a ground heat exchanger

V.1 Introduction

In this chapter presents the development of a simple calculation methodology to design a hybrid cooling tower (HCT) coupled with a horizontal ground-water heat exchanger (GWHE). The HCT-GWHE system is proposed as a technical solution to enhance the thermal performance of the HCT by taking the case study of an adsorption device driven mainly by solar energy in the dry and hot climate of Biskra (Algeria). Four operation levels of the HCT-GWHE system are investigated, namely: GWHE, direct evaporative cooler DEC, spray water system (SWS) and finned tube heat exchanger. The heat and mass transfer phenomena within the HCT and the GWHE are thermally analysed and modelled mathematically. The method of Runge-Kutta 4th order is applied to solve the system of four differential equations, describing the evaporative cooling process in the HCT. A Matlab code was developed according to the presented calculation methodology allowing the thermal design of the HCT-GWHE system. The developed methodology was validated, and a good agreement was found with numerical simulations and experimental results obtained from the literature. It was concluded that the coupling of HCT with GWHE is an effective solution in hot and arid regions. Besides, HCT with a sprayed-water system in counter-current mode is the best method for high heat and mass transfer rates.

The objective of this study is to investigate the potential of utilizing supersaturated humid air as a cooling method for HCT systems. The primary goal is to improve the stability and efficiency of HCT systems under unfavourable ambient air conditions, which can affect the overall performance of the system. The study will employ theoretical analysis to evaluate the feasibility and effectiveness of using supersaturated humid air as a cooling method for HCT systems. Additionally, the study aims to identify the advantages and limitations of this approach to provide insights into potential improvements for HCT systems. Ultimately, the objective is to contribute to the development of more sustainable and efficient cooling solutions for HCT systems.

V.2 V.2. System Descriptions

Figure 1 illustrates the system under investigation, which is comprised of an HCT and a GWHE. The HCT operates on the basis of cross-flow air and process fluid exchange. The HCT can operate in two modes: dry and wet. The wet mode is triggered by humid air created through direct contact between ambient air and spray water. This study examines the use of a compact HCT-GWHE system design in hot and arid climatic conditions in Biskra, Algeria, where summer temperatures regularly reach above 48°C [76].

The HCT-GWHE system is an innovative solution that integrates four separate systems into one cohesive unit. The HCT component comprises three systems: the DCT, SWS, and DEC. The HCT is then combined with the GWHE to create the complete HCT-GWHE system.

DCT that is coupled with a spray water system and reinforced by a Direct Evaporative Cooler (Pad) is a type of cooling tower that combines three cooling methods for maximum cooling efficiency. The spray water system helps to reduce the temperature of the process fluid, while the Direct Evaporative Cooler (Pad) provides additional cooling by evaporating water into the incoming air stream. This combination of cooling methods results in a more efficient cooling tower that is capable of providing improved thermal performance, reduced water consumption, and lower maintenance costs compared to traditional cooling towers.

The use of a GWHE in a Hybrid Cooling Tower (HCT) system can result in improved cooling efficiency and reduced energy consumption. By circulating water through a network of underground pipes and using the naturally cooler ground water as a heat sink, the GWHE can effectively lower the temperature of the water tank in the HCT. This, in turn, helps to reduce the temperature of the process fluid, leading to improved cooling performance.

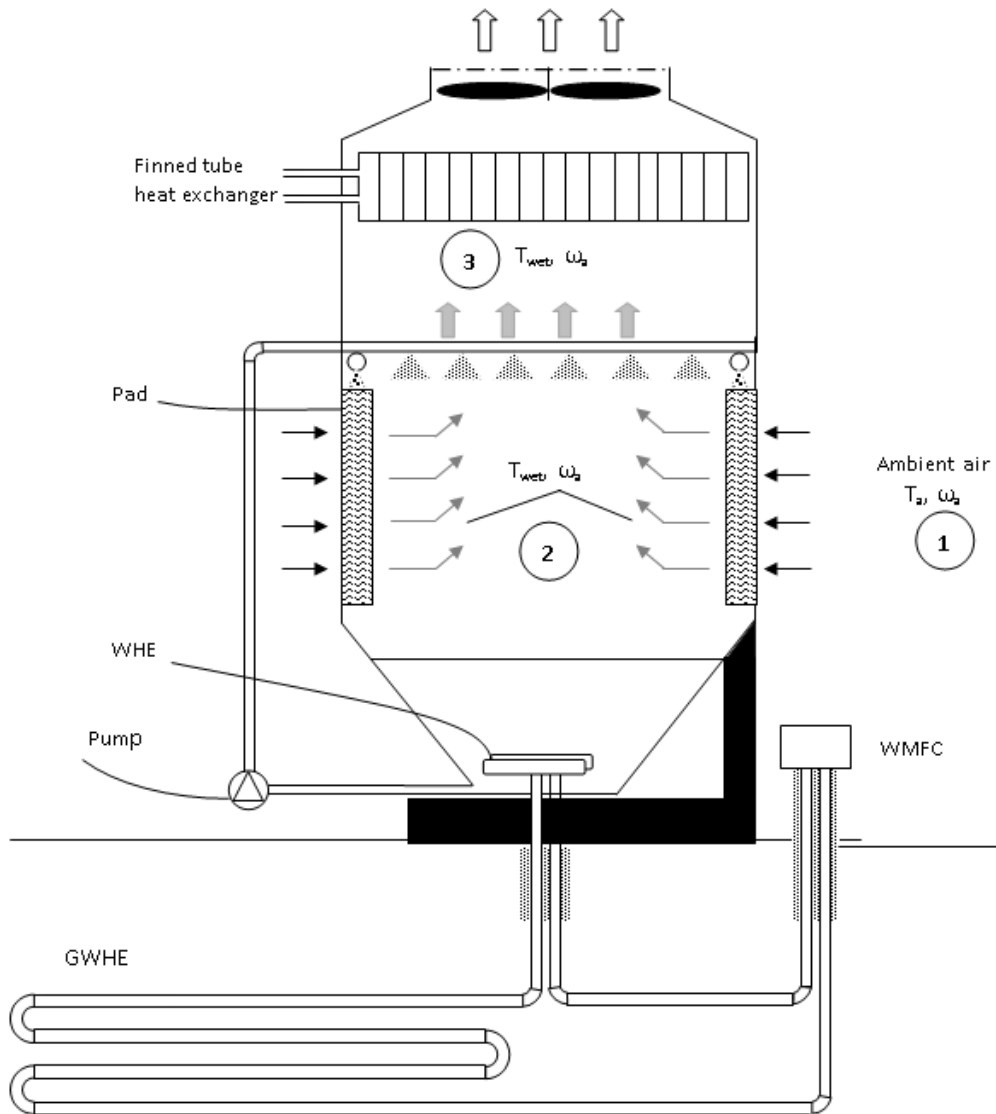


Figure V-1 Schematic diagram of HCT-GWHE

V.2.1 Dry Cooling Tower (DCT)

The studied DCT has the same geometric proprieties of DCT of the Sortech ACS08 machine [79]. The HCT is a finned tube heat exchanger with several rows, with the tubes placed in staggered rows to ensure multiple passages per row. Each row contains the same total number of tubes. The flow arrangement is a cross-flow, with ambient air acting as the external fluid and forcing forced convection to blow across tube banks at a maximum mass flow rate of 4.3 kg/s^{-1} . A mass flow rate of 0.9308 kg/s^{-1} is generated inside the tubes by the process fluid. The ambient air that is

CHAPTER V: New evaporative hybrid cooling tower coupled with a ground heat exchanger

circulated by fans and passes through a finned tube heat exchanger, where the flow is referred to as cross-flow, cools the process fluid that has to be cooled (ethylene glycol 34 vol, %).

Table V-1 shows the most geometric and thermophysical parameters of the finned tube heat exchanger of the present HCT.

Table V-1 Geometric and thermo-physical parameters of the finned tube heat exchanger of present HCT.

Tubes material, -	Copper	$T_{w-spray}$, °C	24
Fins material, -	Aluminium	T_a , °C	48
A, m ²	271.43	$\dot{m}_{w-spray}$, kg/s	1.12
S_{fin} , mm	2.40	L, mm	2000
D_{i-o} , m	0.009-0.010	\dot{m}_a , kg/s	4.3
L_{tot} , m	576	T_{pfi} , °C	41
N,	10	\dot{m}_{pf} , kg/s	0.9308
N_{t_rows} ,	29	P_{tr} , mm	35

V.2.2 The direct evaporative cooler (DEC)

DEC is a type of air conditioning system that cools air through the process of evaporation. It operates by drawing hot, dry air over a wet surface, where water evaporates and cools the air. DEC's are a cost-effective and energy-efficient cooling solution, particularly in hot, dry climates. In this case, air humidification lowers the air temperature before passing it to the finned tube heat exchanger [114, 115].

In the present study that use the GLASdek 7090 as a pad evaporative cooler in the DECT, by using the geometric characteristics as shown in table V-2.

CHAPTER V: New evaporative hybrid cooling tower coupled with a ground heat exchanger

Table V-2 Geometric characteristics of the DEC.

Geometric	(GLASdek 7090)
Width, B, m	2
The height, H, m	2*0.5
The thickness, D, m	0.138
The number of pores per unit area, N, m ² /m ³	440
Wave angle, α	45
Wave angle, β	45
Wave height, h, mm	7

V.3 Horizontal Ground Water Heat Exchanger (GWHE)

The GWHE is a simple kind of horizontal heat exchanger made by PVC tubes such as a plate serpentine shape at a depth of 3 meters inside the ground. It is a secondary system that is connected to the HCT and is used to extract geothermal energy for the purpose of cooling of spray water.

HCT is coupled with a Ground-Water Heat Exchanger (GWHE) to decrease the spray water temperature of the outlet of the tower, to guarantee water temperature approximately near the soil temperature. The geothermal characteristics of the ground-water heat exchanger are shown in Table V-3.

Table V-3 The geothermal characteristics of GWHE.

Tube length, m	100
D_i and D_o , m	0.057 - 0.06
λ_t , W/m·K	0.46
\dot{m}_w , kg/s	0.1
λ_s , W/m·K	1.5
T_s , °C	24
T_w , °C	24 – 28

V.4 Calculation Methodology

V.4.1 Governing equations of the HCT heat and mass transfer

a) Finned tube heat exchanger zone

The rate of heat transfer exchanged can be expressed as,

$$\phi_f = \dot{m}_f C_{p_f} (T_{f,in} - T_{f,o}) \quad (V-1)$$

The total exchange surface of the finned tube heat exchanger can be calculated by using the following Eq.(V-2) [80] :

$$A = \frac{\phi}{U \Delta T_{LM}} \quad (V-2)$$

The following relation describes the (LMTD) method used for the finned tube heat exchanger:

$$\Delta T_{LM} = \frac{(T_{a,in} - T_{f,o}) - (T_{a,o} - T_{f,in})}{\ln \left(\frac{T_{a,in} - T_{f,o}}{T_{a,o} - T_{f,in}} \right)} \quad (V-3)$$

A technique for analysing the properties of heat and mass transmission has previously been presented for finned tube heat exchangers under humidifying conditions. The overall heat transfer coefficient U , in this case, changed concerning the geometrical dimensions of both fins and tubes [78, 97]. Eq.(V-4) is used to calculate the heat exchanger's overall heat transfer coefficient [81]:

$$U = \left[\left(\frac{1}{h_i} + \mathfrak{R}_i \right) \frac{S_e}{S_i} + \frac{S_e}{2\pi\lambda_f} \ln \frac{D_e}{D_i} + \frac{1}{\eta_G h_e} + \mathfrak{R}_e \right]^{-1} \quad (V-4)$$

The external heat transfer coefficient of the air side can be calculated by using the following correlation from Wang et al. [82]:

$$h_a = j \rho_a C_{p_a} V_a Pr_a^{-2/3} \quad (V-5)$$

CHAPTER V: New evaporative hybrid cooling tower coupled with a ground heat exchanger

The Colburn factor in the following equation must be used to calculate the heat transfer for a plate fin profile and staggered tube configuration [83] :

$$j = 0.086 Re^{j^3} N^{j^4} (S_a/D_e)^{j^5} (S_a/D_h)^{j^6} (S_a/P_t)^{-0.93} \quad (\text{V-6})$$

where;

$$Re = V_a D_e \rho_a / \mu_a \quad (\text{V-7})$$

$$\begin{cases} j_3 = -0.361 - 0.042N / \ln(\text{Re}) + 0.158 \ln \left[N (S_a/D_c)^{0.41} \right] \\ j_4 = -1.224 - 0.076(P_t/D_h)^{1.42} / \ln(\text{Re}) \\ j_5 = -0.083 + 0.076N / \ln(\text{Re}) \\ j_6 = -5.735 + 1.21 \ln(\text{Re}/N) \end{cases} \quad (\text{V-8})$$

The internal heat transfer coefficient h_i is calculated as a function of Nusselt number [84]:

$$h_i = Nu \lambda_w / D_i \quad (\text{V-9})$$

Where the correlation (V-10) of Nusselt number for water flowing inside the pipe [85].

$$\begin{cases} \text{For } 0.6 < Pr < 1.5 \rightarrow Nu = 0.0214 \left(\text{Re}^{0.8} - 100 \right) \text{Pr}_f^{0.4} \left[1 + (D_i/L_t)^{2/3} \right] \\ \text{For } 1.5 < Pr < 500 \rightarrow Nu = 0.012 \left(\text{Re}^{0.87} - 280 \right) \text{Pr}_f^{0.4} \left[1 + (D_i/L_t)^{2/3} \right] \end{cases} \quad (\text{V-10})$$

Number of fins per meter of length is calculated as follows [83] :

$$N_{fin-m} = \frac{1}{(S_a + e)} \quad (\text{V-11})$$

The heat transfer coefficient of the air side h_a is affected by the air velocity between the fins. And the Colburn factor j is used to calculate the heat transfer for an array of staggered tubes and a herringbone-wavy fin profile [98].

CHAPTER V: New evaporative hybrid cooling tower coupled with a ground heat exchanger

$$j = 0.394 \text{Re}_D^{-0.357} \left(\frac{Ph_t}{Ph_l} \right)^{-0.272} \left(\frac{S_{fin}}{D} \right)^{-0.205} \left(\frac{X_{fin}}{P_d} \right)^{-0.558} \left(\frac{P_d}{S_{fin}} \right)^{-0.133} \quad (\text{V-12})$$

The heat transfer coefficient on the air side is obtained from [98].

$$h_a = \frac{\lambda_a j \text{Re}_D \text{Pr}^{0.33}}{D} \quad (\text{V-13})$$

The equation below can be used to determine the surface of the wavy fins [98].

$$A_f = \left[1 + \left(\frac{P_d}{X_f} \right)^2 \right] A'_f \quad (\text{V-14})$$

b) Spray water zone

When a stream of air comes into contact with a spray of water from a nozzle, heat and mass transfer occurs between the two fluids.

Heat transfer occurs because there is a temperature difference between the air and water. Heat is transferred from the warmer fluid to the cooler one. The rate of heat transfer depends on several factors, including the temperature difference between the two fluids, the surface area of contact between them, and the thermal conductivity of the fluids.

Mass transfer occurs because water droplets from the spray are carried by the air stream. As the air flows over the droplets, they evaporate, transferring mass from the liquid phase to the gas phase. The rate of mass transfer depends on several factors, including the relative humidity of the air, the temperature difference between the air and water, and the size and concentration of the droplets.

The tower is divided into numerous small regions along the vertical axis and the droplets and gas are considered to be flowing parallel to each other according to the methodology of one-dimensional model [121].

Several simplifying assumptions are made:

CHAPTER V: New evaporative hybrid cooling tower coupled with a ground heat exchanger

- The radial and angular velocities of the droplets and air are assumed to be zero.
- The droplets and air are uniformly distributed over the cross section of the spray
- Heat transfer by radiation is neglected.
- The effect of pressure change on physical properties along the height direction is neglected.
- The process is done under adiabatic condition.

$$\left\{ \begin{array}{l}
 \frac{dT_a}{dz} = \left(\frac{6h_{a,d}}{\lambda C p_a} \right) \frac{(T_a - T_w)}{U_d D_d} \\
 \frac{dT_w}{dz} = \frac{6[h_{a,d}(T_w - T_a) + \beta_d \gamma (\omega_{sat} - \omega)]}{\rho_w C p_w U_d D_d} - \frac{6\beta_d T_w (\omega_{sat} - \omega)}{\rho_w U_d D_d} \\
 \frac{dD_d}{dz} = \frac{-2\beta_d (\omega_{sat} - \omega)}{\rho_w U_d} \\
 \frac{d\omega}{dz} = \frac{6\beta_d (\omega_{sat} - \omega)}{\lambda \rho_w U_d D_d} \\
 \frac{dU_d}{dz} = \frac{g(\rho_w - \rho_a)}{\rho_w U_d} - \frac{0.75C_d \rho_a (U_d - U_a)^2}{D_d \rho_w U_d}
 \end{array} \right. \quad (V-15)$$

By using the boundary conditions as follows:

$$\left\{ \begin{array}{l}
 T_{a(z=H)} = T_{a,in} \\
 T_w(z=0) = T_{w,in} \\
 D_d(z=L) = D_{d,in} \\
 U_d(z=0) = U_{d,in} \\
 \omega_{(z=H)} = \omega_{in}
 \end{array} \right. \quad (V-16)$$

The specific heat capacity of moist air Cp_m , which is defined as:

$$Cp_m = Cp_a + \omega Cp_{v, sat} \quad (V-17)$$

Where the saturated air humidity ratio is calculated using the following relation:

$$\omega_{sat}(T_w) = 0.622 \frac{P_{sat}(T_w)}{P_a - P_{sat}(T_w)} \quad (V-18)$$

CHAPTER V: New evaporative hybrid cooling tower coupled with a ground heat exchanger

The saturation pressure $P_{sat}(T_w)$ of moist air at the water temperature is defined as;

$$P_{sat}(T_w) = \exp \left(23.3265 - \frac{3802.7}{T_w + 273.18} - \left(\frac{472.68}{T_w + 273.18} \right)^2 \right) \quad (\text{V-19})$$

Wet-bulb temperature of moist air can be determined from the following formulas [93] :

$$T_{wb} = 2.265(1.97 + 4.3T_a + 10000\omega_{sat})^{0.5} - 14.85 \quad (\text{V-20})$$

Using the description of air humidity ratio, the following formula is used to evaluate the rate of change of cooling water mass \dot{m}_w per unit of heat exchange area:

$$\frac{d\dot{m}_w}{dA} = \dot{m}_a \frac{d\omega}{dA} \quad (\text{V-21})$$

The energy and material transfer processes are typically similar in nature, therefore the mass transfer coefficient between droplets and air can be expressed as [122]:

$$\beta_d = \frac{\rho_a D_v \text{Nu}}{D_d} \quad (\text{V-22})$$

Where $h_{d,a}$ is defined as the heat transfer coefficient between the air and the droplets as follows:

$$h_{d,a} = \frac{\lambda_a \text{Nu}}{D_d} \quad (\text{V-23})$$

Where Nu is the Nusselt number, which can be obtained as Eq. (V-24) [123].

$$\text{Nu} = \begin{cases} 2 + 0.5 \text{Re}_d^{0.5}, & 10 < \text{Re}_d \leq 1.8 \times 10^3 \\ 2 + 0.3 \text{Re}_d^{0.5664}, & 1.8 \times 10^3 < \text{Re}_d \leq 1.5 \times 10^5 \end{cases} \quad (\text{V-24})$$

Where the drag coefficient of a droplet is given by the following correlation [124].

CHAPTER V: New evaporative hybrid cooling tower coupled with a ground heat exchanger

$$C_d = \begin{cases} \frac{24}{\text{Re}} \left(1 + \frac{1}{6} \text{Re}^{2/3} \right), & \text{Re} \leq 1000 \\ 0.44, & \text{Re} > 1000 \end{cases} \quad (\text{V-25})$$

V.4.2 Pad zone

The DEC calculation side; is a semi-analytical model developed by [93, 115]. It is based on energy conservation and heat and mass transfer analysis. This model predicts the heat and mass transfer between air and water in DEC system by using the geometric parameters as shown in table V-2.

Inlet boundary conditions to DEC.

$$T_a = T_1, \quad W_a = W_1 \quad \text{at } x = 0$$

The following equations are used to calculate variations in humidity ratio and temperature of moist air in one direction, x:

$$T_a = T_{\text{sat}} + (T_1 - T_w) \exp\left(-\frac{h_c N B H D}{\dot{m}_a C_p}\right) \quad (\text{V-26})$$

$$\omega_a = \omega_{\text{sat}} - \frac{C_{p_a}}{L_v} (T_1 - T_{\text{sat}}) \exp\left(-\frac{h_c N B H D}{\dot{m}_a C_{p_a}}\right) \quad (\text{V-27})$$

Where $\Delta\omega = \omega_{\text{sat}} - \omega_a$

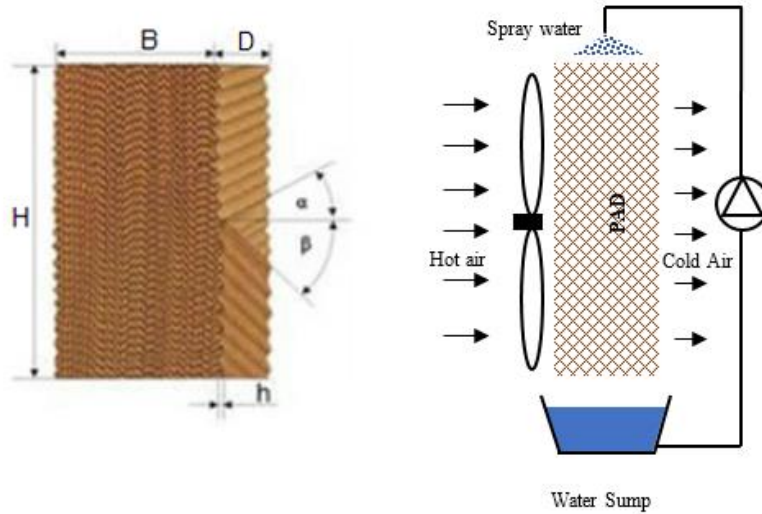


Figure V-2 Schematic diagram of evaporative cooling process.

V.4.3 Heat transfer modulization of the WHE

When modeling the system based on steady-state analysis, the following assumptions were used:

- The water tank surrounding the heat exchanger is assumed to have uniform temperature distribution.
- Constant water conductivity is assumed throughout the experiment.
- Water flow through the WHE pipes is assumed to be steady.
- The tank is considered to be adiabatic, meaning that no heat transfer occurs to the surroundings.
- Negligible water flow rate is assumed within the tank.

Under the given assumptions, the mathematical model for heat transfer between the hot water outside the pipe and the cold water inside the pipe can be expressed using the following equation:

The heat transfer rate using the following equation:

$$\phi = UA_{tot} \Delta T \quad (V-28)$$

Where the overall heat transfer coefficient can calculate by using the following equation:

$$U = \left[\frac{1}{h_i} + \frac{D_e}{2\lambda_w} \ln \frac{D_e}{D_i} + \frac{D_e}{D_i} \frac{1}{h_{nc}} \right]^{-1} \quad (V-29)$$

CHAPTER V: New evaporative hybrid cooling tower coupled with a ground heat exchanger

Where h_{nc} is the heat transfer due to natural convection outside the tube;

$$h_{nc} = \frac{\lambda_w Nu_{nc}}{D_t} \quad (V-30)$$

Where Nu_{nc} is the Squire-Eckert formulation, can be written as follows [125];

$$Nu_{nc} = \left\{ 0.60 + 0.387 \left[\frac{Ra_D}{\left[1 + (0.559 / Pr)^{9/16} \right]^{16/9}} \right]^{1/6} \right\}^2 \quad (V-31)$$

Ra_D is Rayleigh number

$$Ra_D = \frac{L^3 g \beta \Delta T}{\nu \alpha} \quad (V-32)$$

Where β is the coefficient of thermal expansion, can be calculated as the following equation [125];

$$\beta = \frac{1}{T_\infty} \quad (V-33)$$

V.4.4 Heat transfer modulization of the GWHE

When modeling the system based on steady-state analysis, the following assumptions were used:

- The horizontal GHE's maximum operating time is limited to a few hours, even during the hottest parts of the day.
- The soil is uniform around the heat exchanger.
- Soil conductivity is constant.
- The flow of water is steady through the length of geothermal pipes.
- Using correlation from the literature, the thermophysical characteristics of water are estimated.
- By assuming that the soil's characteristics are isotropic and that the soil and pipe are in perfect contact.

CHAPTER V: New evaporative hybrid cooling tower coupled with a ground heat exchanger

The resolution of the heat transfer equation serves as the foundation for the calculation model, as shown in figure 4 [99-101]:

$$\dot{m}_w C p_w [T_w(x) - T_w(x + dx)] = \frac{[T_w(x) - T_s]}{R_{th}} dx \quad (V-34)$$

Where R_{th} is the overall thermal resistance of the water soil heat exchanger between the pipe water and surrounding soil, as measured by the relation (V-35) [100-102]:

$$R_{th} = R_w + R_t + R_s \quad (V-35)$$

$$R_w = \frac{1}{h_i P_i} \quad (V-36)$$

Where

$$h_i = \frac{Nu \lambda_w}{d_i} \quad (V-37)$$

According to Equation (V-38), the Nusselt number for water flow within a pipe is a function of the Reynolds number Re [85].

Where $2300 < Re < 10^5$ and $1.5 < Pr < 500$.

$$Nu = 0.012 (Re^{0.87} - 280) Pr^{0.4} \left[1 + \left(\frac{d_i}{L_t} \right)^{0.66} \right] \quad (V-38)$$

R_t and R_s , are the thermal resistance of the tube and the soil annulus, respectively, given by the equations (V-39) and (V-40) [99-101].

$$R_t = \frac{\ln(r_e / r_i)}{2\pi\lambda_t L_t} \quad (V-39)$$

$$R_s = \frac{\ln(r_s / r_e)}{2\pi\lambda_s L_t} \quad (V-40)$$

CHAPTER V: New evaporative hybrid cooling tower coupled with a ground heat exchanger

The suitable thickness of the soil annulus has been investigated in several works in the literature. The result of all of these studies is that the soil's thickness varies with how long the heat exchanger is working [101, 103-105].

In this study, the GWHE operation is limited to a few hours at most. As indicated in Figure V-4, the thickness of the soil annulus was considered to be equal to the pipe's radius ($r_s = 2r_i$).

After dividing the equation (V-34) with dx , this equation can be written as follows [99-101]:

$$-\dot{m}_w C_{p_w} \frac{dT}{dx} = \frac{(T_w(x) - T_s)}{R_{th}} \quad (V-41)$$

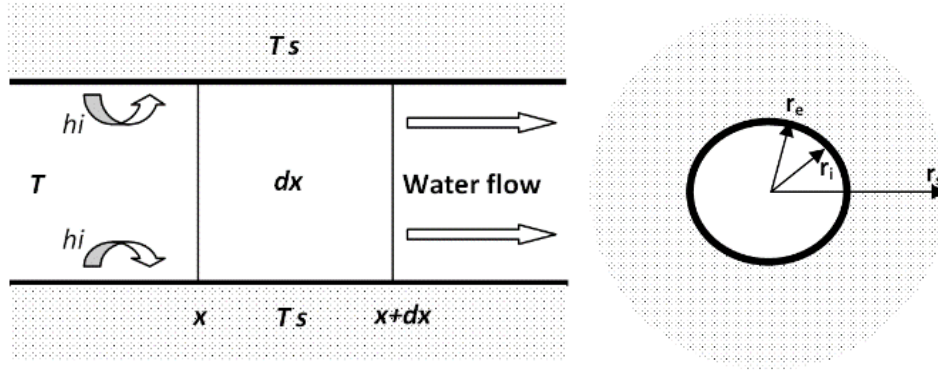


Figure V-3 The thermal balance of a horizontal geothermal heat exchanger (Ground/Water), GWHE.

Then

$$T(x) = C^{st} 1 \exp\left(\frac{-x}{\dot{m} C_p R_{th}}\right) + C^{st} 2 \quad (V-42)$$

By considering boundary conditions, we find the constants A and B:

- For $x \rightarrow \infty$, $T(x) = T_s \rightarrow C^{st} 2 = T_s$;
- For $x \rightarrow 0$, $T(x) = T_0 \rightarrow A = T_0 - T_s$;

$$T(x) = (T_0 - T_s) \exp\left(\frac{-x}{\dot{m} C_p R_{th}}\right) + T_s \quad (V-43)$$

Also, we can write the equation (V-43) as:

CHAPTER V: New evaporative hybrid cooling tower coupled with a ground heat exchanger

$$T(x) = (T_0 - T_s) \exp\left(\frac{-x}{\rho C_p S V R_{th}}\right) + T_s \quad (V-44)$$

The equation (V-45) represents the pressure drop across the full length of the heat exchanger. And this is based on the total of the exchanger's linear, singular, and pressure losses between the input and outflow [106].

$$\Delta P_t = \Delta P_{lin} + \Delta P_{sin g} + \Delta P_{i-o} \quad (V-45)$$

To determine the linear pressure losses, use equation (V-46).

$$\Delta P_{lin} = \Lambda \rho_w L_t \frac{v_w^2}{2d} \quad (V-46)$$

Laminar or turbulent flow characteristics affect how the loss ratio of load Λ is calculated in the equation (V-47), [106].

For $2100 < Re < 10^5$, the BLASUIS formula is used

$$\Lambda = 0.3164 Re^{-0.25} \quad (V-47)$$

The singular pressure loss is defined by equation (V-48):

$$\Delta P_{sin g} = \xi \rho_w \frac{v_w^2}{2} \quad (V-48)$$

The following formula is used to calculate pressure losses at the heat exchanger's inlet and outlet [106]:

$$\Delta P_{i-o} = \frac{3}{4} \rho_w v_w^2 \quad (V-49)$$

V.4.5 Solving procedure

The governing equations (V-15), with the boundary conditions (V-16), are used to estimate heat and mass transfer of the SWS zone. These equations are solved numerically in the literature [87, 107] by using Range Kutta 4th order integration method. The analytical method is used to predict the temperature distribution in the tube rows of the HCT, as shown in Figure V-5.

Where ε is the convergence criterion of the calculation, it becomes as follows;

$$\varepsilon_1 = \frac{\Delta \omega}{\omega}, \quad \varepsilon_2 = \frac{\Delta T_a}{T_a}, \quad \varepsilon_3 = \frac{\Delta T_w}{T_w}, \quad \varepsilon_4 = \frac{\Delta T_f}{T_f} \quad (V-50)$$

CHAPTER V: New evaporative hybrid cooling tower coupled with a ground heat exchanger

For $i=1,4$ then $\varepsilon = \min(\varepsilon_i)$

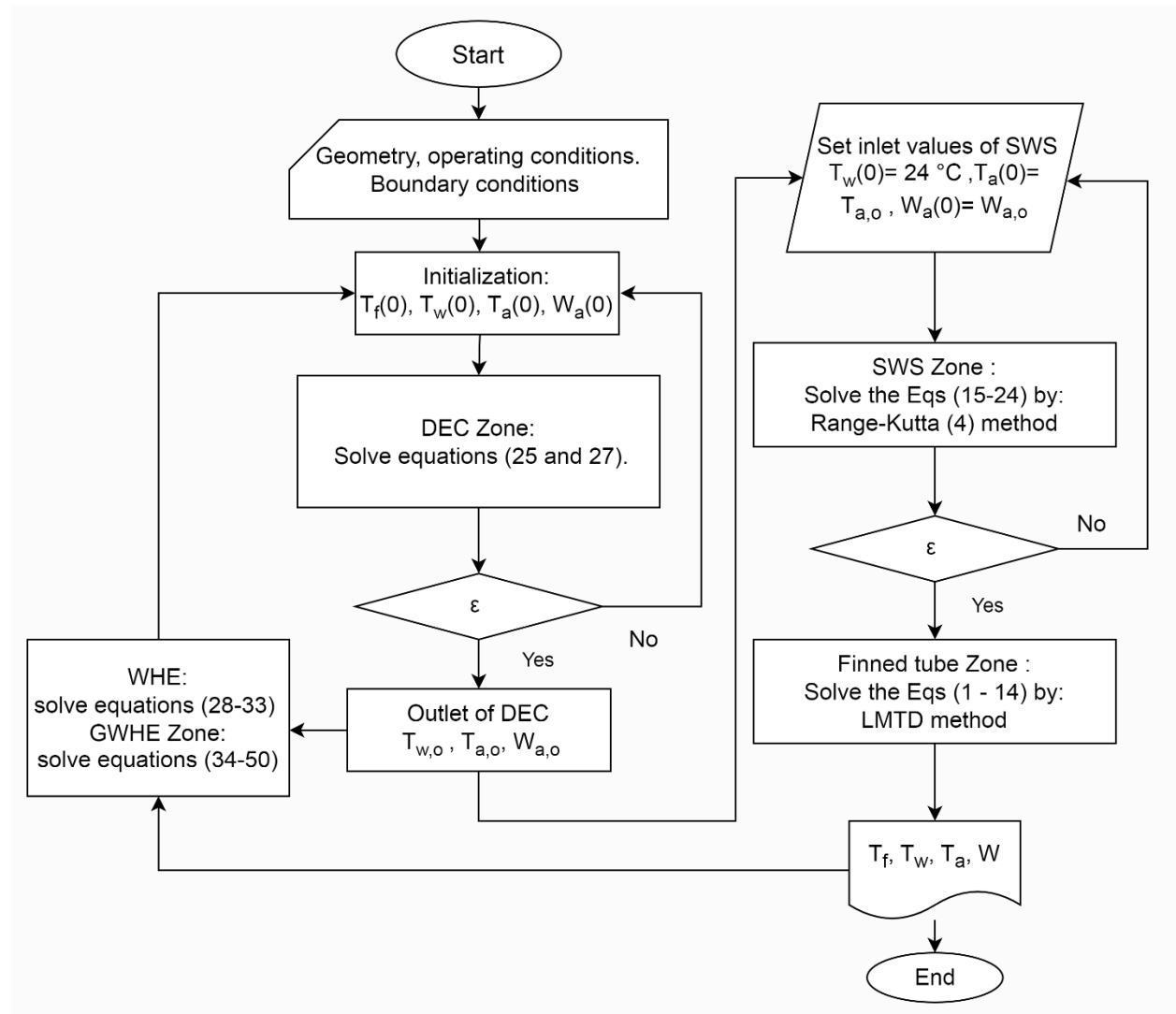


Figure V-4 flowchart of calculation program.

V.5 Comparison and validation model

V.5.1 DEC zone

Table V-2 shows the geometric characteristics of the porous material of the type (GLASdek 7090), the same characteristics used as data in the developed semi-analytical calculation code to produce a lower humid air temperature of 35°C.

CHAPTER V: New evaporative hybrid cooling tower coupled with a ground heat exchanger

Using heat and mass conversion equations, it is discovered that there is a good agreement between the air outlet temperatures after applying the total conservation equation between the water sprinkled on the top edges of the pad and the dry air through the pores. The results obtained are shown in Table V-4.

Table V-4 Comparisons between current results and experimental ones.

Inlet temperature	Outlet temperature			
Ta (dry bulb/ °C)	Ta (wet bulb/ °C)	Ta (wet bulb/ °C)	Ta (wet bulb/ °C)	Ta (saturated °C)
	Present calculation	Comparison [115]	Experimental [115]	
27.21	22.8152	22.76	22.9	20.15
27.84	22.3745	22.32	22.66	19.06
28.54	23.5662	23.51	23.5	20.55
28.9	23.7644	23.71	23.81	20.65
29.32	22.6717	22.6	22.37	18.64
29.91	23.7971	23.74	23.78	20.09
30.5	23.2541	23.18	22.77	18.86
30.83	23.9452	23.87	24.1	19.77
31.5	27.2608	27.22	27.6	24.69
31.86	25.8778	25.82	25.49	22.25
32.31	24.1802	24.1	23.94	19.25
32.86	23.8587	23.76	24.01	18.4
33.09	25.9935	25.92	25.49	21.69
33.73	27.1004	27.03	27.1	23.08
34.06	25.6127	25.52	25.73	20.49
34.46	27.4445	27.37	27.31	23.19
35.01	25.8904	25.8	25.9	20.36
35.81	28.2965	28.22	27.84	23.74
36.8	30.3572	30.29	30.4	26.45
37.06	28.5691	28.48	28.01	23.42

The continuous repetition of the water misting process on the pad produces a heat exchange between the water and the hot air, directly leading to a high temperature of the water. As a result, the amount of residual water has decreased. In other words, which involved an increase in water temperature as a cause of an increase in water consumption as experimentally proven in the literature by [119, 120].

CHAPTER V: New evaporative hybrid cooling tower coupled with a ground heat exchanger

V.5.2 SWS zone

In order to evaluate the accuracy of the present model, calculations were performed using the same experimental conditions as in the previous study. The outlet water temperatures obtained from the calculations were then compared with the experimental data [126].

To further assess the performance of the present model, a comparison was made with the model presented in Ref. [121]. The calculation results of the two models were presented side by side in Table 5, which also included the experimental conditions and results for reference.

The validation revealed that the present model produced more precise results than the reference model, with a maximum relative error of approximately 2.44% in the water temperature leaving the tower. This suggests that the present model is more reliable and accurate in describing the operation of the spray and rain zones in the tower.

Overall, the findings of this study suggest that the present model is a suitable tool for accurately predicting the performance of cooling towers. The model can be used to optimize the operation and design of cooling towers, which can help reduce energy consumption and costs associated with cooling systems. Furthermore, the present study can serve as a reference for future research in this field.

Table V-5 Experimental and calculation results for SWS zone.

Input		Experimental value [126].	Numerical value of Ref [121].	Present study
Inlet water temperature T_w (°C)	Inlet air temperature T_a (°C)	Outlet water temperature T_w (°C)	Outlet water temperature T_w (°C)	Outlet water temperature T_w (°C)
44	33	37.80	39.04	37.82
50	34	43.70	42.69	42.63
42	33	36.20	37.97	36.47

V.6 Results and discussions

V.6.1 Climatically conditions of this study

Since the objective of this study is the adaptation of an adsorption cooling system to hot and arid climates especially Biskra city in the summer, it's necessary to choose the hottest day in the year when the air temperature reaches 48°C.

From the Biskra's infoclimat website [76], it's found that the hottest typical day is July 1st 2021. The evolution of the hourly air ambient temperature and relative humidity of the chosen day are presented in figure V-5.

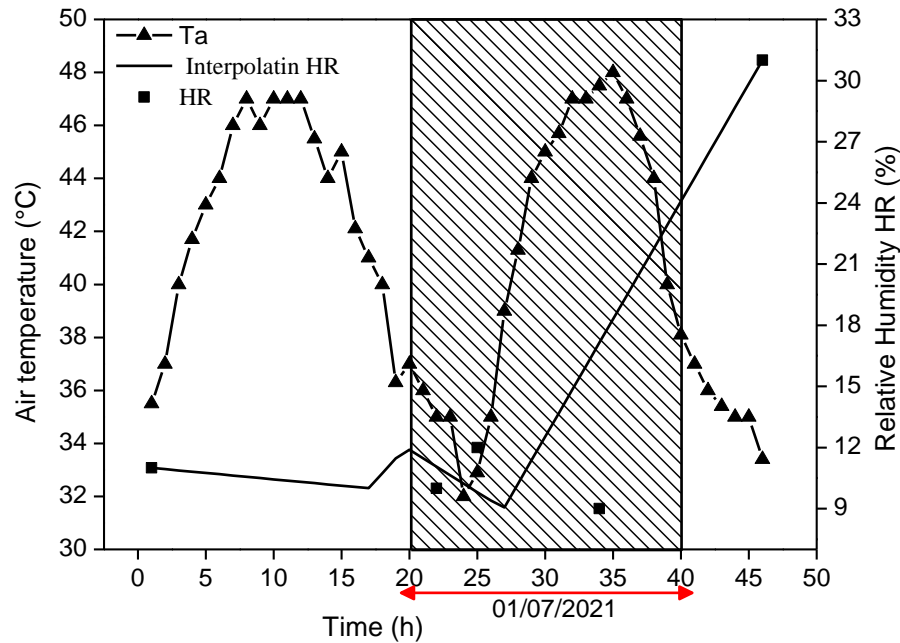


Figure V-5 The temperature and relative humidity variations of the hottest day in Biskra city in 2021.

V.6.2 GWHE thermal design

Table V-3 shows the different parameters of the GWHE. Using Eq. (V-44), the ground water heat exchanger dimensions required to cool the water for re-injection within the pad and SWS are calculated based on the temperature of the inlet water and the mass flow of the water.

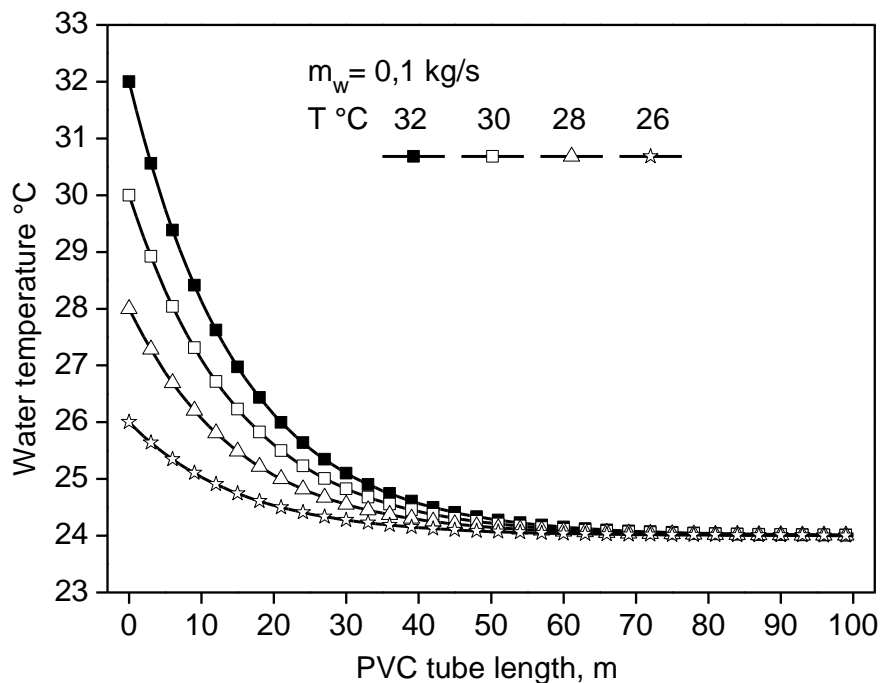
The present application was conducted in Biskra region. To simplify our analysis, we assumed that the temperature of the water in the HCT-GWHE tank was equal to the temperature

CHAPTER V: New evaporative hybrid cooling tower coupled with a ground heat exchanger

of the surrounding ground. As the leaving temperature of the pad and SWS rose by a few degrees at the outlet, we observed that the submerged WHE in the tank maintained a constant water temperature, and the temperature of the water reintroduced into the pad and SWS matched that of the ground.

The temperature of the water leaving the pad and SWS has been estimated as the critical temperature of the system for four different water temperatures. In addition, it should be noted that the temperature of the ground beyond 3 m was almost constant, varying between 22 and 24 °C. From the results of figure V-6, a decrease in the water outlet temperature is observed with the increase in the PVC tube length, which reaches its minimum length at 60 m with a small mass flow rate circulating in the PVC tube, such as in a closed loop.

The increase in water velocity causes an increase in the outlet water temperature due to the decrease in the residence time of the water in the GWHE tubes. By the way, if there is a need to increase the water flow within GWHE to a higher value, it is simple. It is possible to pick an acceptable low flow rate and increase the number of GWHEs to achieve the desired low temperature and high-water flow.



CHAPTER V: New evaporative hybrid cooling tower coupled with a ground heat exchanger

Figure V-6 Variation of water temperature along the geothermal heat exchanger with different inlet water temperature, $m_w=0.1$ kg/s.

V.6.3 WHE thermal design

The horizontal tube in the WHE zone emerges from a water tank and is connected to the outlet of GWHE at its inlet, forming a closed loop. The objective of this system is to cool the water in the tank. As water flows around the tube, it creates a boundary layer of stagnant water that affects the heat transfer process. Due to the temperature difference between the cold water inside the tube and the hot water in the bulk of the tank, a buoyancy-driven flow pattern known as a buoyant plume is created. This flow pattern enhances the heat transfer between the tube and the water by facilitating the exchange of heat between the stagnant boundary layer and the bulk water. The stagnant boundary layer is cooled by the cold water inside the tube, making it denser and causing it to sink, while the hot water from the bulk of the tank flows in to replace it. This process of fluid displacement creates a continuous flow that can efficiently cool the water in the tank.

To determine the optimal tube length for efficient heat transfer, a mathematical model (Eqs. V-28 and V-33) can be used to simulate the heat transfer and fluid flow behaviour in the system for different tube lengths. The simulations enable the calculation of the heat transfer rate and pressure drop for each tube length, which can then be used to identify the optimal tube length. By varying the tube length while keeping other parameters such as diameter, flow rate and temperature differential constant, a parametric study can be conducted to identify the tube length that provides the maximum heat transfer rate with minimal pressure drop or cost. It is important to consider the physical properties of the fluid, such as density, viscosity, and thermal conductivity, as well as the tube geometry and flow conditions in order to determine the optimal tube length.

Table V-6 The different parameters of WHE.

Tubes material, -	Copper
Water temperature tank, °C	26 - 24
Width of tank, m	1
Length of tank, m	2
Inlet water temperature of tube, °C	≤ 24
Outlet water temperature from tube, °C	25,7
Water mass flow rate inside tube, kg/s	0.1

CHAPTER V: New evaporative hybrid cooling tower coupled with a ground heat exchanger

Tube length, m	32
Tube diameter, m	0.02

Figure V-7 shows the calculated outlet air temperature from the DEC system compared with the ambient inlet temperature. As seen, the outlet air temperature is always lower than the inlet temperature and the difference between the two increases with the increasing of the ambient temperature. This can be explained by that the high ambient air temperature leads to more water evaporation and then high performance. From the results obtained from figure V-7, it's clear that the proposed system (GWHE coupled to DEC system) can maintain the temperature of the air below the functioning limits of DCT in hot and dry climates.

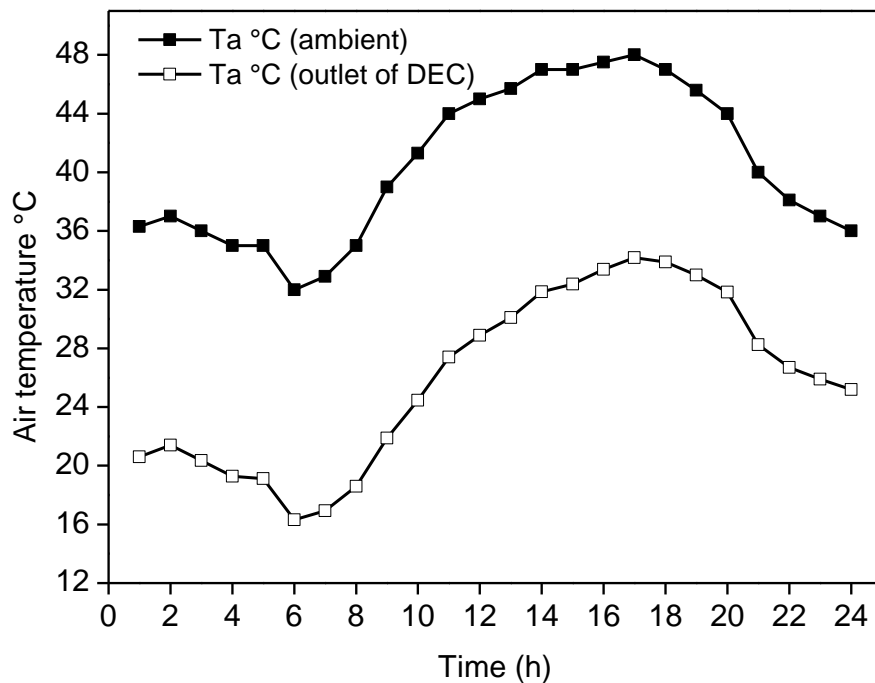


Figure V-7 The effect of the DEC zone at ambient air temperature for 24 hours of a hot day in Biskra city, $T_w = 24^\circ\text{C}$.

Figure V-8 depicts the temperature profile of the air as it travels through the DEC and SWS zones. In the DEC zone, the air enters at a high temperature of 48°C and exits at a lower temperature of 31°C . This temperature reduction is attributed to convective and mass transfer mechanisms, including heat transfer to the cooling water and evaporative cooling, where water

CHAPTER V: New evaporative hybrid cooling tower coupled with a ground heat exchanger

droplets evaporate into the air stream. The air then moves to the SWS zone, where its temperature further decreases to a final value of 26°C. This temperature reduction is primarily due to evaporative cooling, as water droplets are sprayed into the air stream, and heat is absorbed as the water droplets evaporate. As water evaporates, it also increases the moisture content of the air, which may cause supersaturation if the air is sufficiently cooled. In this application, $T_w=24^\circ\text{C}$, which is the same temperature as the ground. Understanding the temperature and moisture changes that occur in these zones is crucial for numerous industrial and environmental applications, particularly for hybrid cooling tower (HCT) systems.

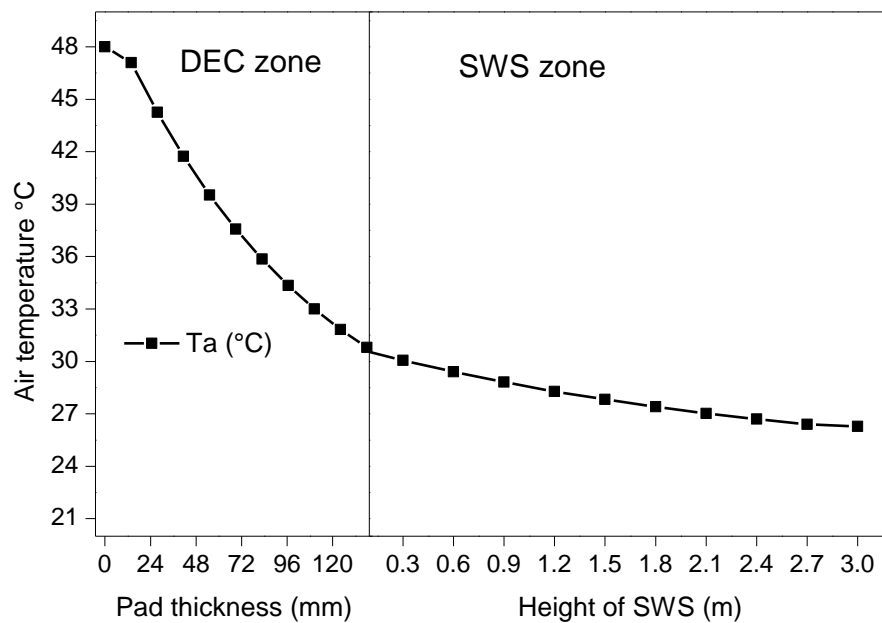


Figure V-8 Depicts the ambient air temperature as it varies within the DEC and SWS zones, $T_w = 24^\circ\text{C}$.

Figure V-9 presents the temperature changes of finned tube zone by two modes. Immediately, we note an increase in the temperature of the process fluid. On the other hand, the air temperature drops from 48°C to 46°C, which means poor functioning of the cooling tower system.

CHAPTER V: New evaporative hybrid cooling tower coupled with a ground heat exchanger

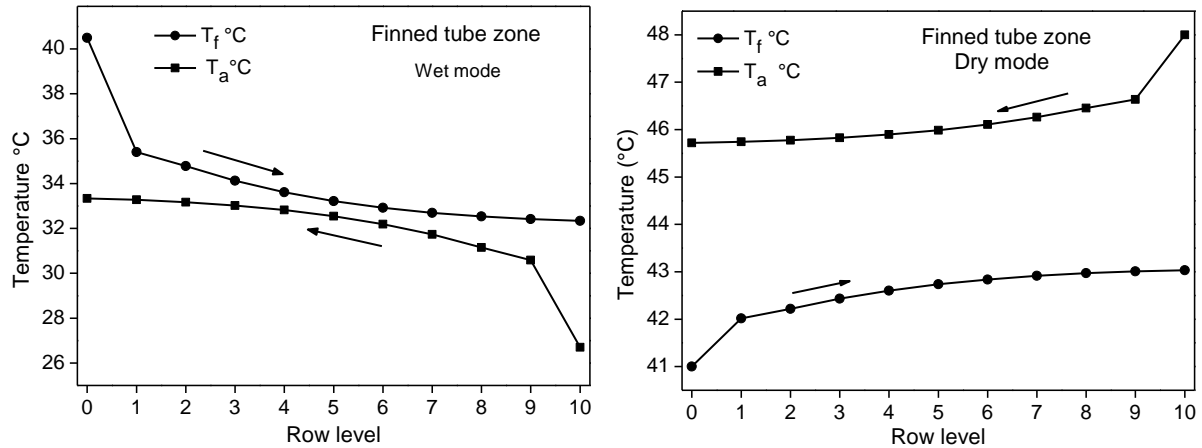


Figure V-9 The comparison between wet and dry modes on a finned tube heat exchanger zone.

V.7 Conclusion

- The use of supersaturated air can result in higher cooling performance due to the increased heat transfer coefficient, which is related to the increased mass transfer rate between the air and the cooling fluid.
- Wet mode cooling can be particularly effective in applications where the ambient air temperature and humidity are high, as the production of supersaturated air can result in significant cooling of the fluid being circulated through the finned tubes.
- The effectiveness of wet mode cooling can be improved by optimizing the design and operation of the cooling tower, such as by increasing the airflow rate over the tubes, using counterflow or crossflow configurations, or installing drift eliminators to minimize water loss.

GENERAL CONCLUSION

According to research on the optimization of solar cooling performance, the major categories of adsorption cooling systems are silica gel-water, zeolite-water, and activated carbon-ammonia systems. These systems operate within limited conditions, with ambient air temperatures typically ranging from less than 34°C to exceeding 45°C on hot days.

To adapt an adsorption cooling machine, specifically the Sortech ACS 08, to the Biskra region, researchers have made improvements to the cooling tower. By modifying the cooling tower configurations from dry cooling mode to wet mode and from dry mode to evaporative mode, in addition to combining with a ground heat exchanger, the use of these improved cooling tower configurations has allowed for more efficient and effective cooling in the Biskra region. This has the potential to further improve the efficiency and sustainability of the cooling system in the region.

The results of the present research make the improvement applicable, as shown in the following:

- The use of supersaturated air can result in higher cooling performance due to the increased heat transfer coefficient, which is related to the increased mass transfer rate between the air and the cooling fluid.
- Wet mode cooling can be particularly effective in applications where the ambient air temperature and humidity are high, as the production of supersaturated air can result in significant cooling of the fluid being circulated through the finned tubes.
- The effectiveness of wet mode cooling can be improved by optimizing the design and operation of the cooling tower, such as by increasing the airflow rate over the tubes, using counterflow or crossflow configurations, or installing drift eliminators to minimize water loss.

REFERENCES

1. Hassan, H., A.J.R. Mohamad, and S.E. Reviews, *A review on solar-powered closed physisorption cooling systems*. 2012. **16**(5): p. 2516-2538.
2. Fernandes, M., G. Brites, J. Costa, A. Gaspar, V.J.R. Costa, and S.E. Reviews, *Review and future trends of solar adsorption refrigeration systems*. 2014. **39**: p. 102-123.
3. Ullah, K., R. Saidur, H. Ping, R. Akikur, N.J.R. Shuvo, and S.E. Reviews, *A review of solar thermal refrigeration and cooling methods*. 2013. **24**: p. 499-513.
4. Colesca, S.E., C.N.J.R. Ciocoiu, and s.e. reviews, *An overview of the Romanian renewable energy sector*. 2013. **24**: p. 149-158.
5. Lucas, T. and A.J.I.J.o.R. Raoult-Wack, *Immersion chilling and freezing in aqueous refrigerating media: review and future trends: Réfrigération et congélation par immersion dans des milieux réfrigérants: revue et tendances futures*. 1998. **21**(6): p. 419-429.
6. Hamdeh, N.H.A., A.J.E.C. Mu'Taz, and Management, *Optimization of solar adsorption refrigeration system using experimental and statistical techniques*. 2010. **51**(8): p. 1610-1615.
7. Li, Z., K.J.R. Sumathy, and s.e. reviews, *Technology development in the solar absorption air-conditioning systems*. 2000. **4**(3): p. 267-293.
8. GOVERNORS, B.O.J.O., *European Bank for Reconstruction and Development—EBRD*. 2020.
9. Kalkan, N., E. Young, A.J.R. Celiktas, and s.e. reviews, *Solar thermal air conditioning technology reducing the footprint of solar thermal air conditioning*. 2012. **16**(8): p. 6352-6383.
10. Balaras, C.A., G. Grossman, H.-M. Henning, C.A.I. Ferreira, E. Podesser, L. Wang, E.J.R. Wiemken, and s.e. reviews, *Solar air conditioning in Europe—an overview*. 2007. **11**(2): p. 299-314.
11. Abdul-Wahab, S.A., A. Elkamel, A.M. Al-Damkhi, A. Is' haq, H.S. Al-Rubai'ey, A.K. Al-Battashi, A.R. Al-Tamimi, K.H. Al-Mamari, and M.U.J.R.E. Chutani, *Design and experimental investigation of portable solar thermoelectric refrigerator*. 2009. **34**(1): p. 30-34.
12. Yeo, T., I. Tan, M.J.R. Abdullah, and S.E. Reviews, *Development of adsorption air-conditioning technology using modified activated carbon—A review*. 2012. **16**(5): p. 3355-3363.
13. Otanicar, T., R.A. Taylor, and P.E.J.S.e. Phelan, *Prospects for solar cooling—An economic and environmental assessment*. 2012. **86**(5): p. 1287-1299.
14. Sarbu, I., C.J.E. Sebarchievici, and buildings, *Review of solar refrigeration and cooling systems*. 2013. **67**: p. 286-297.
15. Sarbu, I., E. Valea, and C. Sebarchievici. *Solar refrigerating systems*. in *Advanced Materials Research*. 2013. Trans Tech Publ.
16. Zeyghami, M., D.Y. Goswami, E.J.R. Stefanakos, and S.E. Reviews, *A review of solar thermo-mechanical refrigeration and cooling methods*. 2015. **51**: p. 1428-1445.
17. Hwang, Y., R. Radermacher, A.A. Alili, I.J.H. Kubo, and R. Research, *Review of solar cooling technologies*. 2008. **14**(3): p. 507-528.
18. Almasri, R.A., N.H. Abu-Hamdeh, K.K. Esmail, and S.J.A.E.J. Suyambazhahan, *Thermal solar sorption cooling systems, a review of principle, technology, and applications*. 2021.
19. Ayaz, H., V. Chinnasamy, J. Yong, and H.J.E. Cho, *Review of Technologies and Recent Advances in Low-Temperature Sorption Thermal Storage Systems*. 2021. **14**(19): p. 6052.
20. Henninger, S.K., F. Jeremias, H. Kummer, P. Schossig, and H.-M.J.E.P. Henning, *Novel sorption materials for solar heating and cooling*. 2012. **30**: p. 279-288.

REFERENCES

21. Allouhi, A., T. Kousksou, A. Jamil, T. El Rhafiki, Y. Mourad, Y.J.R. Zeraouli, and S.E. Reviews, *Economic and environmental assessment of solar air-conditioning systems in Morocco*. 2015. **50**: p. 770-781.
22. Jani, D., M. Mishra, P.J.R. Sahoo, and S.E. Reviews, *Solid desiccant air conditioning—A state of the art review*. 2016. **60**: p. 1451-1469.
23. Labed, A., A. Rouag, A. Benchabane, N. Moumami, M.J.J.o.A.E.S. Zerouali, and Technology, *Applicability of solar desiccant cooling systems in Algerian Sahara: Experimental investigation of flat plate collectors*. 2015. **1(2)**: p. 61-69.
24. Sarbu, I. and C. Sebarchievici, *Solar heating and cooling systems: Fundamentals, experiments and applications*. 2016: Academic Press.
25. Hassan, H. and A. Mohamad, *A review on solar cold production through absorption technology*. Renewable Sustainable Energy Reviews, 2012. **16(7)**: p. 5331-5348.
26. Stanciu, C., D. Stanciu, and A.-T.J.E. Gheorghian, *Thermal analysis of a solar powered absorption cooling system with fully mixed thermal storage at startup*. 2017. **10(1)**: p. 72.
27. Sriksirin, P., S. Aphornratana, S.J.R. Chungpaibulpatana, and s.e. reviews, *A review of absorption refrigeration technologies*. 2001. **5(4)**: p. 343-372.
28. Zohar, A., M. Jelinek, A. Levy, and I.J.A.t.e. Borde, *The influence of diffusion absorption refrigeration cycle configuration on the performance*. 2007. **27(13)**: p. 2213-2219.
29. Zhai, X., M. Qu, Y. Li, R.J.R. Wang, and s.e. reviews, *A review for research and new design options of solar absorption cooling systems*. 2011. **15(9)**: p. 4416-4423.
30. Chidambaram, L., A. Ramana, G. Kamaraj, R.J.R. Velraj, and s.e. reviews, *Review of solar cooling methods and thermal storage options*. 2011. **15(6)**: p. 3220-3228.
31. <Ruzhu Wang, Liwei Wang, Jingyi Wu - Adsorption Refrigeration Technology_ Theory and Application (2014, Wiley) - libgen.lc.pdf>.
32. Saravanan, N., M.J.J.o.R. Edwin, and S. Energy, *Optimization and experimental analysis of a solar-powered adsorption refrigeration system using selective adsorbent/adsorbate pairs*. 2022.
33. Sapienza, A., S. Santamaria, A. Frazzica, and A.J.E. Freni, *Influence of the management strategy and operating conditions on the performance of an adsorption chiller*. 2011. **36(9)**: p. 5532-5538.
34. WANG, D.C., LI, Y. H., LI, D., et al. , *A review on adsorption refrigeration technology and adsorption deterioration in physical adsorption systems*. Renewable and Sustainable Energy Reviews, 2010. **vol. 14(no 1)**: p. p. 344-353.
35. WANG, R.Z., LI, Ming, XU, Y. X., et al, *An energy efficient hybrid system of solar powered water heater and adsorption ice maker*. Solar energy, 2000. **vol. 68(no 2)**: p. p. 189-195.
36. Liu YL, W.R., Xia ZZ, *Experimental study on a continuous adsorption water chiller with novel design*. International Journal of Refrigeration, 2005. **28**: p. 218-30.
37. Wang RZ, O.R., *Adsorption refrigeration e an efficient way to make good use of waste heat and solar energy*. In: Proceedings of International Sorption Heat Pump Conference, 2005.
38. Erhard, A., K. Spindler, and E.J.I.j.o.r. Hahne, *Test and simulation of a solar powered solid sorption cooling machine*. 1998. **21(2)**: p. 133-141.
39. Maggio, G., L. Gordeeva, A. Freni, Y.I. Aristov, G. Santori, F. Polonara, and G.J.A.T.E. Restuccia, *Simulation of a solid sorption ice-maker based on the novel composite sorbent "lithium chloride in silica gel pores"*. 2009. **29(8-9)**: p. 1714-1720.
40. Gopal, M.R. and S.S.J.I.j.o.R. Murthy, *Performance of a metal hydride cooling system*. 1995. **18(6)**: p. 413-420.

REFERENCES

41. Sharafian, A., M.J.R. Bahrami, and S.E. Reviews, *Assessment of adsorber bed designs in waste-heat driven adsorption cooling systems for vehicle air conditioning and refrigeration*. 2014. **30**: p. 440-451.
 42. Zhang, L.J.A.t.e., *Design and testing of an automobile waste heat adsorption cooling system*. 2000. **20**(1): p. 103-114.
 43. Wang, R., J. Wu, Y. Xu, W.J.E.c. Wang, and management, *Performance researches and improvements on heat regenerative adsorption refrigerator and heat pump*. 2001. **42**(2): p. 233-249.
 44. Li, M., R. Wang, Y. Xu, J. Wu, and A.J.R.e. Dieng, *Experimental study on dynamic performance analysis of a flat-plate solar solid-adsorption refrigeration for ice maker*. 2002. **27**(2): p. 211-221.
 45. Wang, L., R. Wang, Z. Lu, C. Chen, K. Wang, and J.J.C. Wu, *The performance of two adsorption ice making test units using activated carbon and a carbon composite as adsorbents*. 2006. **44**(13): p. 2671-2680.
 46. Hassan, H., A. Mohamad, and R.J.E. Bennacer, *Simulation of an adsorption solar cooling system*. 2011. **36**(1): p. 530-537.
 47. Tso, C.Y., S.C. Fu, and C.Y. Chao. *Modeling a solar-powered double bed novel composite adsorbent (silica activated carbon/CaCl₂)-water adsorption chiller*. in *Building Simulation*. 2014. Springer.
 48. Tso, C.Y., K.C. Chan, C.Y. Chao, C.J.I.j.o.h. Wu, and m. transfer, *Experimental performance analysis on an adsorption cooling system using zeolite 13X/CaCl₂ adsorbent with various operation sequences*. 2015. **85**: p. 343-355.
 49. Chan, K.C., C.Y. Tso, C. Wu, C.Y.J.E. Chao, and Buildings, *Enhancing the performance of a zeolite 13X/CaCl₂-water adsorption cooling system by improving adsorber design and operation sequence*. 2018. **158**: p. 1368-1378.
 50. Zhu, L., C.Y. Tso, K.C. Chan, C. Wu, C.Y. Chao, J. Chen, W. He, and S.J.A.T.E. Luo, *Experimental investigation on composite adsorbent-Water pair for a solar-powered adsorption cooling system*. 2018. **131**: p. 649-659.
 51. Wang, D., Z. Xia, J. Wu, R. Wang, H. Zhai, and W.J.I.j.o.r. Dou, *Study of a novel silica gel-water adsorption chiller. Part I. Design and performance prediction*. 2005. **28**(7): p. 1073-1083.
 52. Sah, R.P., B. Choudhury, and R.K.J.I.J.o.S.E. Das, *Study of a two-bed silica gel-water adsorption chiller: performance analysis*. 2018. **37**(1): p. 30-46.
 53. Wang, D., J. Wu, Z. Xia, H. Zhai, R. Wang, and W.J.I.j.o.r. Dou, *Study of a novel silica gel-water adsorption chiller. Part II. Experimental study*. 2005. **28**(7): p. 1084-1091.
 54. Alahmer, A., X. Wang, R. Al-Rbaihat, K.A. Alam, and B.B.J.A.E. Saha, *Performance evaluation of a solar adsorption chiller under different climatic conditions*. 2016. **175**: p. 293-304.
 55. Wang, R., L. Wang, and J. Wu, *Adsorption refrigeration technology: theory and application*. 2014: John Wiley & Sons.
 56. Daßler, I. and W.J.E.P. Mittelbach, *Solar cooling with adsorption chillers*. 2012. **30**: p. 921-929.
 57. Jakob, U. and W. Mittelbach. *Development and investigation of a compact silica gel/water adsorption chiller integrated in solar cooling systems*. in *VII Minsk international seminar "heat pipes, heat pumps, refrigerators, power sources"*, Minsk, Belarus. 2008.
 58. ; Available from: <https://www.infoclimat.fr/observations-meteo/temps-reel/biskra/60525.html>.
 59. Rouag, A., A. Benchabane, C.-E. Mehdid, M.-A. Melhegueg, N. Boulouf, S.-H. Sellam, A.J.E.S. Labeled, Part A: Recovery, Utilization,, and E. Effects, *Technical solution for malfunction of air coolers and condensers in hot climates: thermal design of a Geothermal Air-Cooler*. 2020: p. 1-14.
 60. Al-Khoury, R., *Computational modeling of shallow geothermal systems*. 2011: CRC press.
-

REFERENCES

61. Bergougnoux, J.J.R.e.d., *Des technologies compétitives au service du développement durable*. 2012. **10**.
62. De Kerorguen, Y., *Energoscope: guide de toutes les énergies, connues et inconnues*. 2009: Editions TECHNIP.
63. Haehnlein, S., P. Bayer, P.J.R. Blum, and S.E. Reviews, *International legal status of the use of shallow geothermal energy*. 2010. **14**(9): p. 2611-2625.
64. Hähnlein, S., P. Bayer, G. Ferguson, and P.J.E.P. Blum, *Sustainability and policy for the thermal use of shallow geothermal energy*. 2013. **59**: p. 914-925.
65. Boukli Hacene, M.E.A., R. Laroui, H. Rozale, A.J.E.S. Chahed, Part A: Recovery, Utilization,, and E. Effects, *Thermal simulation of the ground source heat pump used for energy needs of a bioclimatic house in Tlemcen City (western ALGERIA)*. 2019: p. 1-15.
66. Karabacak, R., Ş.G.J.E.S. Acar, Part A: Recovery, Utilization,, and E. Effects, *The experimental thermal performance analysis of the ground source heat pump system dependent on environmental conditions*. 2010. **32**(12): p. 1142-1158.
67. Rouag, A., A. Benchabane, A. Labeled, K. Belhadj, and N. Boultif, *Applicability of a Solar Adsorption Cooling Machine in Semiarid Regions: Proposal of Supplementary Cooler Using Earth-Water Heat Exchanger*. International Journal of Heat and Technology, 2016. **34**(2): p. 281-286.
68. Ounis, H., A. Benchabane, and A.J.D.P.A. Rouag, *Accessory of humidified grid to improve the efficiency of air heat exchangers: Proposal of a mechanism for the aircoolers and condensers*. 2016. **160057**: p. 01-02.
69. Rouag, A., A. Benchabane, A. Labeled, and N.J.D.P.A. Boultif, *Use of shallow geothermal energy to improve the efficiency of air heat exchangers: Proposal of a Geothermal Air-Cooler (GAC)*. 2014. **140719**: p. 04-12.
70. Soni, S.K., M. Pandey, V.N.J.E. Bartaria, and Buildings, *Energy metrics of a hybrid earth air heat exchanger system for summer cooling requirements*. 2016. **129**: p. 1-8.
71. Benhamza, M.E., A. Brima, S. Houda, and N.J.H.T.A.R. Moumami, *Contribution to the Study of the Reduction of Energy Consumption through the Exchanger Coupled Conventional Air-Ground-Air Conditioner. Application to the Building*. 2017. **46**(8): p. 1104-1118.
72. Zapałowicz, Z., A.J.S.C. Opiela, and Society, *Boundary value of the air distribution coefficient that ensures working effectivity of the air-condition system connected with ground heat exchanger and with PV installation*. 2018. **42**: p. 93-99.
73. Habibi, M. and A.J.I.J.o.R. Hakkaki-Fard, *Long-term energy and exergy analysis of heat pumps with different types of ground and air heat exchangers*. 2019. **100**: p. 414-433.
74. Melhegueg, A. Benchabane, and A. Rouag, *Dispositif de couplage 'machine frigorifique à adsorption / aéro-refroidisseur géothermal' avec de nouveaux éléments assurant le refroidissement de l'adsorbeur*. p. DZPatent. App. N° 210383 (2021).
75. Kheireddine, M.-A. and A. Benchabane, *Dispositif d'amélioration de l'efficacité des échangeurs de chaleur à air avec nouveaux éléments couplant trois systèmes de refroidissement basés sur l'évaporation directe de l'eau et la géothermie*, in DZ Patent. 2022
76. Infoclimat.fr, *Climatology of the year 2020 in Biskra*. Date accessed 08/02/2023 in <https://www.infoclimat.fr/climatologie/annee/2020/biskra/valeurs/60525.html>. 2023.
77. Mehrabian, M. and B. Samadi, *Heat-transfer characteristics of wet heat exchangers in parallel-flow and counter-flow arrangements*. International Journal of Low-Carbon Technologies, 2010. **5**(4): p. 256-263.
78. Dreyer, A.A., D.E. Kriel, and P.J. Erens, *Analysis of Spray-Cooled Finned-Tube Heat Exchangers*. Heat Transfer Engineering, 1992. **13**(4): p. 53-71.

REFERENCES

79. Kheireddine, M.-A., A. Rouag, A. Benchabane, N. Boutif, and A. Labeled, *Hybrid Cooling Tower for a Solar Adsorption Cooling System: Comparative Study Between Dry and Wet Modes in Hot Working Conditions*, in *Green Energy and Technology: Environmentally-Benign Energy Solutions*, B. Dincer, C.O. Colpan, and M.A. Ezan, Editors. 2020, Springer. p. 293-308.
80. Kalantari, H., S.A. Ghoreishi-Madiseh, J.C. Kurnia, and A.P. Sasmito, *An analytical correlation for conjugate heat transfer in fin and tube heat exchangers*. International Journal of Thermal Sciences, 2021. **164**: p. 106915.
81. Biyanto, T.R., E.K. Gonawan, G. Nugroho, R. Hantoro, H. Cordova, and K. Indrawati, *Heat exchanger network retrofit throughout overall heat transfer coefficient by using genetic algorithm*. Applied Thermal Engineering, 2016. **94**: p. 274-281.
82. Wang, C.-C. and K.-Y. Chi, *Heat transfer and friction characteristics of plain fin-and-tube heat exchangers, part I: new experimental data*. International Journal of Heat and Mass Transfer, 2000. **43**(15): p. 2681-2691.
83. Bougriou, C., *Calcul et technologie des échangeurs de chaleur, cours de technologie et calcul des échangeurs de chaleur*. 2002: University of Batna (Algeria).
84. Gnielinski, V., *New equations for heat and mass transfer in turbulent pipe and channel flow*. International Chemistry Engineering, 1976. **16**(2): p. 359-368.
85. Fallahsohi, H., *Modélisation dynamique des échangeurs diphasiques, appliquée aux groupes frigorifiques contrôlés par une commande avancée*. 2011, INSA de Lyon.
86. Saravanan, M., R. Saravanan, and S. Renganarayanan, *Energy and exergy analysis of counter flow wet cooling towers*. Thermal Science, 2008. **12**(2): p. 69-78.
87. Papaefthimiou, V., E. Rogdakis, I. Koronaki, and T. Zannis, *Thermodynamic study of the effects of ambient air conditions on the thermal performance characteristics of a closed wet cooling tower*. Applied thermal engineering, 2012. **33**: p. 199-207.
88. Sharqawy, M.H., J.H. Lienhard, and S.M. Zubair, *Thermophysical properties of seawater: a review of existing correlations and data*. Desalination and water Treatment, 2010. **16**(1-3): p. 354-380.
89. Mehrabian, M.A. and B. Samadi, *Heat-transfer characteristics of wet heat exchangers in parallel-flow and counter-flow arrangements*. International Journal of Low-Carbon Technologies, 2010. **5**(4): p. 256-263.
90. Halasz, B., *A general mathematical model of evaporative cooling devices*. Revue générale de thermique, 1998. **37**(4): p. 245-255.
91. Zheng, W.-Y., D.-S. Zhu, G.-Y. Zhou, J.-F. Wu, and Y.-Y. Shi, *Thermal performance analysis of closed wet cooling towers under both unsaturated and supersaturated conditions*. International Journal of Heat and Mass Transfer, 2012. **55**(25-26): p. 7803-7811.
92. Papaefthimiou, V., T. Zannis, and E. Rogdakis, *Thermodynamic study of wet cooling tower performance*. International journal of energy research, 2006. **30**(6): p. 411-426.
93. Fouda, A. and Z. Melikyan, *A simplified model for analysis of heat and mass transfer in a direct evaporative cooler*. Applied Thermal Engineering, 2011. **31**(5): p. 932-936.
94. Webb, R. and A. Villacres, *Algorithms for performance simulation of cooling towers, evaporative condensers, and fluid coolers*. ASHRAE transactions, 1984. **90**(2): p. 416-458.
95. Qureshi, B.A. and S.M. Zubair, *Second-law-based performance evaluation of cooling towers and evaporative heat exchangers*. International Journal of Thermal Sciences, 2007. **46**(2): p. 188-198.
96. Bergman, T.L., T.L. Bergman, F.P. Incropera, D.P. Dewitt, and A.S. Lavine, *Fundamentals of heat and mass transfer*. 2011: John Wiley & Sons.
97. Starace, G., M. Fiorentino, B. Meleleo, and C. Risolo, *The hybrid method applied to the plate-finned tube evaporator geometry*. International Journal of Refrigeration, 2018. **88**: p. 67-77.

REFERENCES

98. Kim, N.-H., J.-H. Yun, and R. Webb, *Heat transfer and friction correlations for wavy plate fin-and-tube heat exchangers*. 1997.
99. Mehdid, C.-E., A. Benchabane, A. Rouag, N. Moumami, M.-A. Melhegueg, A. Moumami, M.-L. Benabdi, and A. Brima, *Thermal design of Earth-to-air heat exchanger. Part II a new transient semi-analytical model and experimental validation for estimating air temperature*. Journal of Cleaner Production, 2018. **198**: p. 1536-1544.
100. Rouag, A., A. Benchabane, and C.-E. Mehdid, *Thermal design of Earth-to-Air Heat Exchanger. Part I a new transient semi-analytical model for determining soil temperature*. Journal of cleaner production, 2018. **182**: p. 538-544.
101. Hadjadj, A., B. Benhaoua, A. Atia, A. Khechekhouche, N. Lebbihiat, and A. Rouag, *Air velocity effect on the performance of geothermal helicoidally water-air heat exchanger under El Oued climate, Algeria*. Thermal Science and Engineering Progress, 2020. **20**: p. 100548.
102. Ozgener, O., L. Ozgener, and D.Y. Goswami, *Experimental prediction of total thermal resistance of a closed loop EAHE for greenhouse cooling system*. International Communications in Heat and Mass Transfer, 2011. **38**(6): p. 711-716.
103. Scott, N. *Analysis and performance of an earth-air heat exchanger*. in *Presented at the 1965 Winter meeting*. 1965. Chicago, Illinois.
104. Zapałowicz, Z. and A. Opiela, *Boundary value of the air distribution coefficient that ensures working effectivity of the air-condition system connected with ground heat exchanger and with PV installation*. Sustainable Cities and Society, 2018. **42**: p. 93-99.
105. Elmer, D. and G. Schiller. *A Preliminary Examination of the Dehumidification Potential of Earth to Air Heat Exchangers*. in *Proceedings of the International passive cooling conference*. 1981. Miami, Florida.
106. Idelchik, I.E., *Memento des pertes de charge-coefficients de pertes de charge singulières et de pertes de charge par frottement*. Editions Eyrolles ed. 1969, Saint-Germain, Paris: Eyrolles. 496p.
107. Zheng, W.-Y., D.-S. Zhu, J. Song, L.-D. Zeng, and H.-j. Zhou, *Experimental and computational analysis of thermal performance of the oval tube closed wet cooling tower*. Applied Thermal Engineering, 2012. **35**: p. 233-239.
108. Wiksten, R. and M.E.H. Assad, *Heat and mass transfer analysis of a wavy fin-and-tube heat exchanger under fully and partially wet surface conditions*. International Journal of Thermal Sciences, 2010. **49**(2): p. 349-355.
109. Kabeel, A. and M. Bassuoni, *A simplified experimentally tested theoretical model to reduce water consumption of a direct evaporative cooler for dry climates*. International Journal of Refrigeration, 2017. **82**: p. 487-494.
110. Melhegueg, M.-A., A. Benchabane, A. Rouag, C.-E. Mehdid, H. Demir, M.K. Sevindir, and M.-A. Kheireddine, *Thermal design of Earth-to-Air Heat Exchanger: Performance analysis of new transient semi-analytical model for short period of continuous operation*. Case Studies in Thermal Engineering, 2022. **40**: p. 102580.
111. Melhegueg, M.-A., A. Benchabane, A. Rouag, C.-E. Mehdid, H. Demir, and M.K.J.C.S.i.T.E. Sevindir, *Thermal design of Earth-to-Air Heat Exchanger: Performance analysis of new transient semi-analytical model for short period of continuous operation*. 2022. **40**: p. 102580.
112. Butcher, J.C., *Numerical methods for ordinary differential equations*. 2016: John Wiley & Sons.
113. SorTech, *SorTech Adsorption Chiller ACS 08/ACS 15, Design manual*. Version 2.2 ed. 2009: SorTech, Halle.
114. Kovačević, I. and M. Sourbron, *The numerical model for direct evaporative cooler*. Applied Thermal Engineering, 2017. **113**: p. 8-19.

REFERENCES

115. Wu, J., X. Huang, and H. Zhang, *Theoretical analysis on heat and mass transfer in a direct evaporative cooler*. Applied Thermal Engineering, 2009. **29**(5-6): p. 980-984.
116. Fallahsohi, H., *Modélisation dynamique des échangeurs diphasiques, appliquée aux groupes frigorifiques contrôlés par une commande avancée*, in *Laboratoire d'Energétique de l'ECAM de LYON*. 2011, INSA de Lyon: Lyon. p. 161.
117. Zoellick, B. *Predicted and observed performance of a buried earth-air heat exchanger cooling system*. in *Proc. Annu. Meet.-Am. Sect. Int. Sol. Energy Soc.* 1981. United States: Sunspace, Inc., Ada, OK.
118. Elmer, D. and G. Schiller. *A Preliminary Examination of the Dehumidification Potential of Earth to Air Heat Exchangers*. in *Proceedings of the International passive cooling conference*. 1981. Miami, Florida.
119. Kabeel, A. and M. Bassuoni, *A simplified experimentally tested theoretical model to reduce water consumption of a direct evaporative cooler for dry climates*. International Journal of Refrigeration, 2017. **82**: p. 487-494.
120. Sellam, S.-H., A. Moumimi, C.-E. Mehdid, A. Rouag, A.-H. Benmachiche, M.-A. Melhegueg, and A. Benchabane, *Experimental performance evaluation of date palm fibers for a direct evaporative cooler operating in hot and arid climate*. Case Studies in Thermal Engineering, 2022. **35**: p. 102119.
121. Yu, J., Z. Qu, J. Zhang, S. Hu, and J.J.E. Guan, *Comprehensive coupling model of counter-flow wet cooling tower and its thermal performance analysis*. 2022. **238**: p. 121726.
122. Qureshi, B.A. and S.M.J.A.t.e. Zubair, *A complete model of wet cooling towers with fouling in fills*. 2006. **26**(16): p. 1982-1989.
123. Yuge, T.J.J.o.H.T., *Experiments on heat transfer from spheres including combined natural and forced convection*. 1960. **82**.
124. Levich, V., , *Physicochemical Hydrodynamics*. Prentice Hall, Englewood Cliffs, New Jersey. 1962, Pages.
125. Yener, Y. and S. Kakac, *Heat conduction*. 2018: CRC Press.
126. Qi, X., Y. Liu, and Z.J.J.o.M.E. Liu, *Exergy based performance analysis of a shower cooling tower*. 2013. **59**(4): p. 251-259.

APPENDIX I

ENERGY SOURCES, PART A: RECOVERY, UTILIZATION, AND ENVIRONMENTAL EFFECTS
<https://doi.org/10.1080/15567036.2023.2231883>



Adaptation of adsorption cooling system for hot and dry climates: Use of ground water heat exchanger coupled to direct evaporative cooling tower

Q1 Mohamed-Abdelbassit Kheireddine^a, Adel Benchabane ^a, Amar Rouag^{b,a}, I.M. Mahbul ^c,
 Q2 Müslüm Arıcı ^d, Hakan Demir ^e, and Mustafa Kemal Sevindir^c 5
 Q3

^aLaboratoire de Génie Energétique Et Matériaux, Université de Biskra, LGEM, Biskra, Algeria; ^bDépartement des Energies Renouvelables, Université de Ouargla, Faculté des Hydrocarbures, des Energies Renouvelables, des Sciences de la Terre Et de l'Univers, Ouargla, Algeria; ^cInstitute of Energy Engineering, Dhaka University of Engineering & Technology, Gazipur, Bangladesh; ^dMechanical Engineering Department, Engineering Faculty, Kocaeli University, Kocaeli, Turkey; ^eDepartment of Mechanical Engineering, Yildiz Technical University, Istanbul, Turkey 10

ABSTRACT

The current study focused on the adaptation of adsorption cooling systems to hot and arid climates. A new combination is proposed to improve the performance of the direct evaporative cooler (DEC). This combined system consists in coupling Ground-Water Heat Exchanger (GWHE) with a DEC of a hybrid cooling tower. A mathematical model has been developed and validated to depict the heat and mass transfer that occurs in the DEC between the air and water, as well as between the ground and water in the geothermal heat exchanger. The key variables taken into consideration are the outdoor air temperature and the mass flow rate and the temperature of water. The effect of the inlet hot air velocity and temperature, and water mass flow rate, on the evaporated water is investigated. The findings indicate that the mathematical model of a DEC coupled to GWHE predicts optimal characteristics, leading to a reduction in the air temperature from 48°C to 32°C at the heat exchanger inlet of the cooling tower. 15

ARTICLE HISTORY

Received 24 April 2023
 Revised 26 June 2023
 Accepted 28 June 2023 20

KEYWORDS

Solar adsorption system;
 ground water heat
 exchanger; direct
 evaporative cooling tower;
 thermal analysis; hot and dry
 climate 25

Introduction

Commercial solar adsorption machines often operate at maximum outdoor air temperatures of around 35°C (Bouzeffour, Khelidj, and Tahar Abbes 2016; Sarbu and Sebarchievici 2013). The Dry Cooling Towers (DCT), used as the air cooling system of these machines, are responsible for the deterioration of the performance of these refrigeration systems in hot climates (Kheireddine et al. 2020; Khodakaram-Tafti and Golneshan 2020; Rouag et al. 2016). This is due to DCT sensitivity to external factors, especially outdoor air temperature. However, hot air temperatures in sub-Saharan regions such as in the Biskra region can exceed 48°C, especially in summer. Hence, it is essential to appeal to technical solutions to adapt solar refrigeration systems to these hot and dry regions by lowering the inlet air temperature of the cooling tower (CT). Previous studies have been carried out in the LGEM laboratory to locate technical solutions to the malfunction of adsorption devices, particularly when temperatures are at their maximum limits (Rouag et al. 2016, 2020). The proposed solutions are based on the coupling of CTs to (i) Ground-Air Heat Exchanger (GAHE) (Belloufi et al. 2022), (ii) Ground - Water Heat Exchanger (GWHE) (Rouag et al. 2016), or (iii) a direct or indirect evaporative cooler (Kheireddine et al. 2020; Sellam et al. 2022). 30
 35
 40

Q4 CONTACT Adel Benchabane adel.benchabane@gmail.com Laboratoire de Génie Energétique et Matériaux, Université de Biskra, LGEM, Biskra 0700, Algeria

© 2023 Taylor & Francis Group, LLC

APPENDIX II

ORAL AND POSTER PRESENTATIONS

Participation in the conference “First Arab Conference on Mechanical Engineering” ARCME’17 by a poster in Biskra, Algiers entitled “**Study of the effect of wet temperature on the efficiency of hybrid cooling towers**”

Participation in the conference ‘7th GLOBAL CONFERENCE ON GLOBAL WARMING, GCGW-2018" in Istanbul, (Turkey) with a paper entitled “*Comparative study between Dry and wet modes in a hybrid cooling tower for a solar adsorption cooling System*”

Participation in the conference “The first International Conference on Energy, Thermofluids and Materials Engineering 1st ICETME 2021 in Biskra, Algeria with a paper entitled “*Thermal analysis of the performance of a direct evaporative cooler coupled with water-air heat exchanger. Application for the farmer's house in Biskra region*”

Participation in the conference “1st International Seminar on Chemical Process and Environment, 2023 by a poster in Biskra, Algiers entitled “*Parametric study and performance analysis of A shower cooling tower for the Biskra region in summer season*”

APPENDIX III

LIST OF PUBLICATIONS

Book chapter: Kheireddine, M.-A., A. Rouag, A. Benchabane, N. Boutif, and A. Labeled, *Hybrid Cooling Tower for a Solar Adsorption Cooling System: Comparative Study Between Dry and Wet Modes in Hot Working Conditions*, in *Green Energy and Technology: Environmentally-Benign Energy Solutions*, B. Dincer, C.O. Colpan, and M.A. Ezan, Editors. 2020, Springer. p. 293-308.

Article: Kheireddine, M.-A., A. Benchabane, A. Rouag, I. Mahbubul, M. Arıcı, H. Demir, M.K.J.E.S. Sevindir, Part A: Recovery, Utilization,, and E. Effects, Adaptation of adsorption cooling system for hot and dry climates: Use of ground water heat exchanger coupled to direct evaporative cooling tower. 2023. 45(3): p. 9133-9148.

Patent : Kheireddine, M.-A. and A. Benchabane, Dispositif d'amélioration de l'efficacité des échangeurs de chaleur à air avec nouveaux éléments couplant trois systèmes de refroidissement basés sur l'évaporation directe de l'eau et la géothermie, in DZ Patent. 2023.